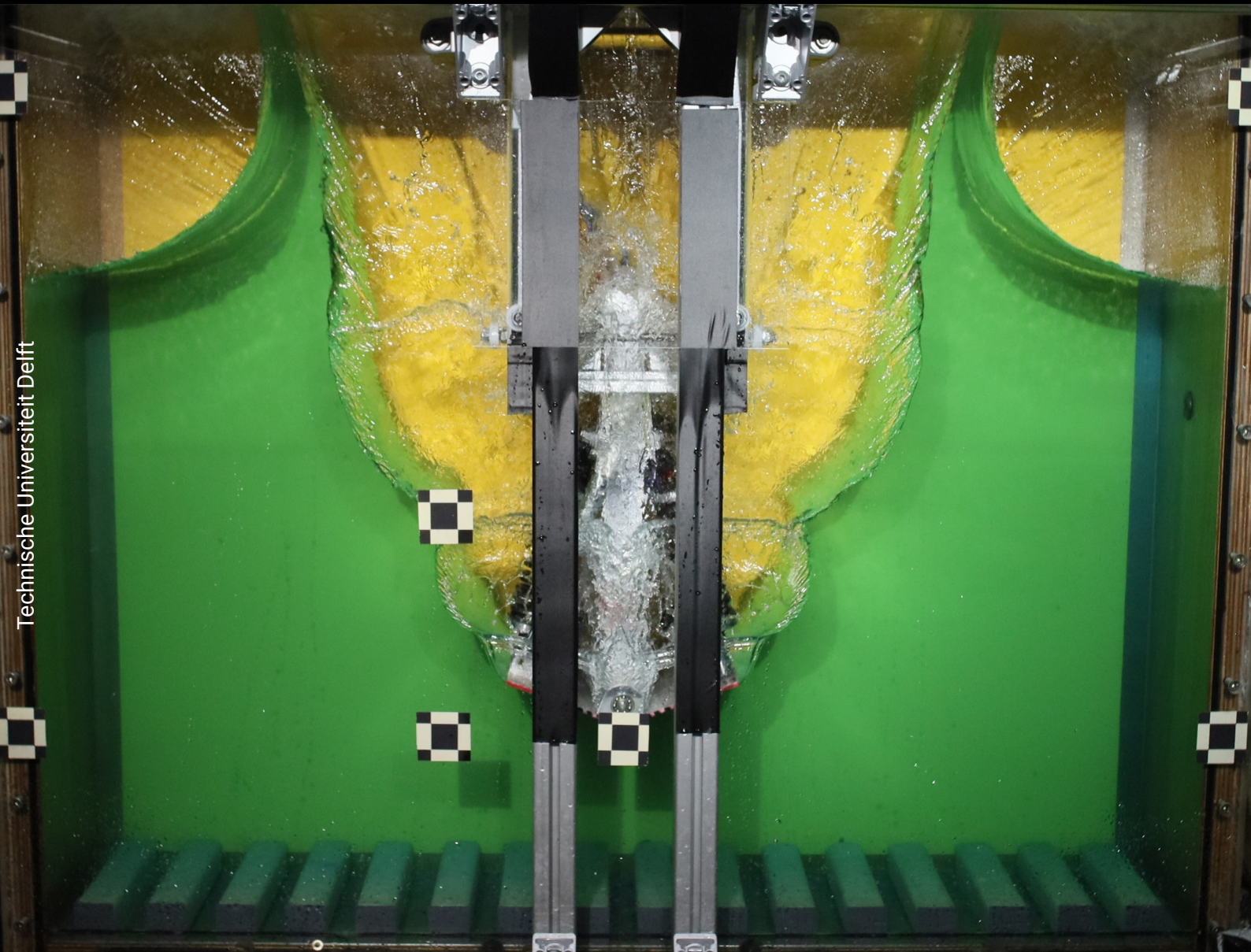


Deformation of structures upon impact with a liquid free surface

Elon Hendriksen | December 2022



Technische Universiteit Delft

Deformation of structures upon impact with a liquid free surface

Elon Hendriksen

to obtain the degree of Master of Science

at the *Delft University of Technology*,

to be defended publicly on December 14, 2022

Student number: 4966732
Project duration: April 24, 2022 – December 14, 2022
Thesis committee: Dr. ir. P. R. Wellens, TU Delft, Chair
Dr. ir. P. R. Wellens, TU Delft, Supervisor
ir. M. van der Eijk, TU Delft, Second reader
Dr. ir. G. H. Keetels, TU Delft, Third reader

An electronic version of this thesis is available at <http://repository.tudelft.nl/>.



Abstract

This thesis study is intended to research the effects on peak pressure during impact of a deformable structure with a liquid. To find an answer to this question, a novel wedge was designed to perform free fall wedge experiments at the TU Delft. This report describes the progress that lead to answering the research question:

What is the effect of dynamic deformation of a structure on the maximum pressure at the wedge surface during impact?

To create an overview of the problem, the various systems and knowledge required to answer the research question are discussed. Among others, a decision on wedge deformation type is made, the importance of multiple impact velocities and the sensors required to measure data of the impact are discussed. The proposed concept to perform experiments is with a deformable wedge that is allowed to fold around the keel upon impact with the free surface. Hypothesis is that the deformation on impact could lead to initial lower impact pressure but dynamic response could lead to higher peak pressures at later stage of impact.

In the next phase, estimations of impact pressures, forces and accelerations are used to finalize the design of the wedge. Strength calculations were performed on the critical parts of the wedge. It is concluded that the analysed parts are strong enough to withstand repeated loading of the structure. Also during this phase, an extra experiment into dynamic calibration of the accelerometer was performed. By curve fitting the expected acceleration to the experiment data, the error of the accelerometer is determined. The accelerometer used in this experiment has an error of 0.48% which is within the limits of the manufacturers requirement of $\leq 1\%$. Before the start of the experiments the limitations of the setup are discussed and an uncertainty analysis is performed on the sensors.

The experiment consists of a series of free falls with various wedge setups, either rigid or deformable. A rigid setup of the wedge is tested at impact velocities of 2, 4 and 6m/s and deadrise angles of 10 and 20 degrees to create a base line for maximum impact pressures. The results of the rigid experiment are compared against previously tested rigid wedges. It is concluded that the novel wedge showed similar peak pressures compared to previously tested rigid wedges. The deformable wedge is dropped at all impact velocities and deadrise angles with three different springs, varying in stiffness.

Deformation of the wedge during impact resulted in decrease in peak pressure. Decreasing spring stiffness and increasing impact velocity resulted in increasing deformation of the wedge. With these results the research question set in the first chapter of the report is answered.

The answer to the research question is that impact induced deformation of the structure leads to lower peak pressures. Dynamic effects were observed but did not lead to higher pressure than the rigid experiments. While further research into the matter is required, this result may already lead to improved ship design which could lead to lower manufacturing costs and lower emissions.

Preface

Ever since I could walk I have been busy building. Building physical things, but also myself. With this report I have finished building something I sometimes could not have imagined building. The setbacks I have had along the way to get where I am today make me incredibly proud to reach this finish line. I could not have made it this far without all the wonderful people that I have come to meet during this journey. Especially the last four years. This might be unconventional but I would first like to thank my house mates with whom I spend long hours absorbing dry mathematics such as differential equations and the tough physics problems of Advanced Dynamics during my pre-master. It was with these boys the uncertain times of the pandemic were made to feel like a holiday at home. Thanks. Also a special thanks to the friends around me with whom I did not live under the same roof but still were always there for me and my silly questions or debates.

During the realisation of this specific report I got to meet a new group of people that helped me out in the most diverse ways. First of all, my supervisor Peter Wellens, who somehow always had 15 spare minutes to discuss some minor issues that lead to discussions sometimes lasting for over an hour. Martin van der Eijk, who found the time next to writing his own papers to read all my endless drafts. Carey Walters, without which I would not have had the amazing footage in high speed that led to better analysis of the impacts.

Then second, everyone located at the towing tank facility. Frits Sterk, Jasper den Ouden, Jennifer Rodrigues Moneiro, Peter Poot, Pascal Taudin Chabot and Sebastian Schreier. Who not only helped me with my thesis but also allowed me to have a temporary office space of my own, which allowed me to run my experiment with much more ease.

The people at the employees workshop and IWS of the TU Delft; Damian de Nijs, Jorgen Blok and Nisse Linskens, who, during my manufacturing stage must have gone crazy of all the difficult requests I had but were always helpful.

From the materials science department, Kevork Perez, who allowed me to use equipment from his department to use in unconventional ways without any questions asked.

And finally, but most importantly, my parents, who somehow managed to raise me to be the person I am today and who during a minor health setback amid the experiment period, supported me so much that I basically would like them to receive a part of my masters degree themselves.

Thank you all.

*Elon Hendriksen
Delft, December 2022*

Glossary & Acronyms

Word/Acronym	Explanation
Chine	Edge of wedge that enters the water last
Deadrise angle	Angle of wedge relative to free surface of water
EVA	Enhanced Volume of fluid with Aeration
Free surface	Water surface in contact with air
FSI	Fluid Structure Interaction
g	Acceleration relative to free-fall: $9.81 m/s^2$
Item [®]	Aluminium extruded bar specially designed to quickly build frames and structures
Keel	Edge of the wedge that enters the water first
SF	Safety factor
Wedge	Object that is build to penetrate a liquid free surface for research purposes

Contents

Figures	1
Tables	4
1 Background	5
1.1 Literature review	5
1.1.1 Foundation of slamming research.	5
1.1.2 More advanced simulations and experiments	6
1.1.3 Most recent developments.	7
1.1.4 Reflection	8
1.2 Knowledge gap	10
1.3 Novelty statement	10
1.4 Research question	10
2 Methodology	11
2.1 Experiment motivation	11
2.2 Novel wedge design	11
2.3 Deformation options.	11
2.3.1 Elastic deformation.	12
2.3.2 Rotational deformation	12
2.3.3 Deformation used in this experiment.	12
2.4 Importance of variable impact velocity, spring stiffness and deadrise angles	13
2.4.1 Impact velocity	13
2.4.2 Spring stiffness	14
2.4.3 Deadrise angles.	15
2.5 Sensors	15
2.5.1 Accelerometer	15
2.5.2 Pressure sensor	15
2.5.3 Linear position sensors.	15
2.6 Wedge stiffness and sensor placement	15
2.7 Drop tower	16
3 Experiment Preparation	17
3.1 Hand Calculations and Detailed Hypothesis	17
3.1.1 Wagner theory	17
3.1.2 Maximum pressure from experiment runs in previous tests	18
3.1.3 Expected pressures for impact velocities and deadrise used in this experiment	18
3.1.4 Numerical analysis of wedge impact	19
3.1.5 Expected response of wedge impact	19
3.1.6 Release height required to achieve required impact velocity	20

3.2	Sensor Selection and Calibration	20
3.2.1	Accelerometer	20
3.2.2	Pressure sensor	25
3.2.3	Light gate	26
3.2.4	Linear displacement sensor	26
3.2.5	High Speed Camera	26
3.2.6	Overview of all parts used in experiment	26
3.3	Wedge Design.	27
3.3.1	Design process	27
3.3.2	Build process	28
3.3.3	Wedge design explanation	29
3.3.4	Strength calculations.	30
3.3.5	Dimensions	35
3.4	Pressure sensor placement	35
3.5	Springs	36
3.5.1	Spring stiffness test.	39
3.6	R-ratio of wedge plate/spring system.	40
3.7	Drop tower	42
3.8	Water tank	42
3.9	Limitations of setup	43
3.9.1	Wedge	43
3.9.2	Tower	45
3.9.3	Tank	45
3.9.4	Measurements	46
3.10	Test plan	47
4	Experiments	49
4.1	Uncertainty analysis	49
4.1.1	Accelerometer	50
4.1.2	Pressure sensors	50
4.1.3	Potentiometer.	50
4.2	Hammer test analysis	50
4.2.1	Emerged hammer test	50
4.2.2	Submerged hammer test.	51
4.3	Impact velocities	52
4.3.1	2m/s.	52
4.3.2	4m/s.	52
4.3.3	6m/s.	53
4.3.4	Overview of all rigid impact velocities	53
4.3.5	Overview of all deformable impact velocities.	53
4.4	Impact rigid wedge.	54
4.4.1	Pressure analysis	54
4.4.2	Acceleration analysis.	55
4.4.3	Comparison with previous drop test experiment	56
4.5	Impact deformable wedge.	57
4.5.1	Preload springs	57
4.5.2	Pressure analysis	57
4.5.3	Acceleration analysis.	58
4.5.4	Deformation analysis.	58

4.6	Post-impact rigid wedge	59
4.6.1	Pressure analysis	59
4.6.2	Acceleration analysis	60
4.7	Post-impact deformable wedge	60
4.7.1	Pressure analysis	60
4.7.2	Acceleration analysis	60
4.7.3	Deformation analysis.	60
4.8	Comparison deformable and rigid impacts	63
4.8.1	Rigid compared to deformable with 3.82N/mm spring and 10 degree deadrise	63
4.8.2	Rigid compared to deformable with 3.82N/mm spring and 20 degree deadrise	66
4.9	Free fall of all drops	67
4.9.1	Acceleration analysis	67
4.10	g-stickers	69
4.11	Conclusions.	69
5	Conclusion and recommendations	71
5.1	Conclusions.	71
5.2	Recommendations	74
5.2.1	Recommendations for improved scientific results	74
5.2.2	Recommendations for improved comfort	75
A	Appendix A	81
A.1	Calculations	81
A.1.1	Accelerations on impact	81
A.1.2	Okada empirical formula for flat plate maximum pressure	81
B	Appendix B	83
C	Appendix C - Experiment graphs	93
C.1	Acceleration	93
C.1.1	Free fall rigid	93
C.1.2	Impact rigid	95
C.2	Pressure	96
C.2.1	Impact rigid	96
C.3	Deformation/Pressure	97
C.3.1	Post impact	97

Figures

2.1	FLTR: Classic rigid wedges and plate used in most research, elastic wedges to deform on impact, rotational type wedges to rotate on impact.	12
2.2	Keel of elastic deformation magnified that showw rotational deformation at keel	13
2.3	SolidWorks Render of drop tower setup.	14
3.1	Wagner impact maximum pressure with 7m/s impact velocity and variable deadrise angle β	18
3.2	Pendulum acceleration calibration setup.	22
3.3	Matlab simulation of expected g force. Red line represents earth acceleration in g, blue line represents centripetal acceleration in g, purple line represents total acceleration in g.	23
3.4	Matlab simulation of expected g force. The green line represents measured data from accelerometer in g.	24
3.5	Matlab graph of curve fit, time is shown on x axis, acceleration shown on y axis.	25
3.6	Early render of wedge design. Front plate removed for clear view of components.	27
3.7	SolidWorks render of wedge design, left: Isometric view, Middle: Front view , Right: Side view.	30
3.8	Complete wedge with carriage, front corner from carriage removed for better view of components.	31
3.9	Sketch of specified corner that is analyzed for bending stress and deflection. The red line indicates the specific bending line.	34
3.10	Simplified approach on distributed load on plate.	34
3.11	Full wedge dimensions in mm.	36
3.15	Left:Pressure distribution on symmetric wedges during water entry with constant vertical velocity. (c)=10 degrees deadrise angle (e)=20 degrees deadrise angle. (figure from: Zhao and Faltinsen (1993) [53]) Right: Drawing of wedge plate with position of pressure sensors from keel in mm.	36
3.12	Wedge plate 1 dimensions in mm. Accelerometer housing on bottom left of plate, three pressure sensor housings in the middle of the plate.	37
3.13	Wedge plate 2 dimensions in mm. Accelerometer on bottom left of plate, single pressure sensor housing in middle of plate. The two other cylinders are there to create equal inertia on both plates.	37
3.14	The three angles of the adjustable deformable wedge, please note that in this figure the solid rods are installed instead of the springs. All dimensions in mm.	38
3.16	Simplified view of wedge to show forces during impact at 10 degree deadrise angle. $\alpha = 18.1degrees$, $\beta = 80degrees$, $\gamma = 8.1degrees$	39

3.17	Top view of tower and carriage. The axles and bearings are highlighted in red. In the corners the Item [®] beams are visible and on the Item [®] profiles, in light blue, four beams of plastic are placed to provide smooth transition between tower and water tank.	42
3.18	Overview of test plan that is used during the experiments.	48
4.1	Graph of isolated single impact of emerged hammer test.	51
4.2	Fast Fourier transform analysis of emerged hammer test	51
4.3	Fast Fourier transform analysis of emerged hammer test.	52
4.4	Overview of all pressure and deformation graphs, focused on the initial impact period.	59
4.5	Pressure and deformation of wedge impact with following setup: 6m/s, 10 degree deadrise angle and 29.5N/mm spring.	60
4.6	Progression of deformation with varying deadrise and impact velocity.	61
4.7	Progression of deformation with varying deadrise and spring stiffness.	62
4.8	Progression of deformation with varying deadrise and spring stiffness, for constant impact velocity.	62
4.9	Overview of all pressure graphs from the rigid tests.	63
4.10	Pressure sensor 3 time-history for rigid and deformable impact.	64
4.11	Pressure sensor 2 time history for rigid and deformable impact.	64
4.12	Pressure sensor 1 time history for rigid and deformable impact.	65
4.13	Overview of all pressure graphs from the rigid tests.	66
4.14	Rigid, 2m/s, 10(top) and 20(bottom) degree deadrise acceleration during free fall.	68
B.1	Using a special tool to make sure tapping the thread in the part is exactly centered.	83
B.2	Difference in outer diameter with thread cutting tool inside part.	84
B.3	CNC milling of spine in progress	85
B.4	Four holes reamed and the other 4 still in their original shape in the cylinder of the shock absorber	86
B.5	Before and after of ball bearing joint.	87
B.6	Milling of hinge part	88
B.7	Cutting of hinge part	89
B.8	Centering of hinge part to prepare for milling	90
B.9	Wedge plates cut out of wood with laser to check dimensions and placing of sensors	91
C.1	Rigid, 4m/s, 10(top) and 20(bottom) degree deadrise acceleration during free fall	93
C.2	Rigid, 6m/s, 10(top) and 20(bottom) degree deadrise acceleration during free fall	94
C.3	Overview of all accelerometer graphs from the impact of the rigid tests	95
C.4	Overview of all pressure graphs from the rigid tests	96
C.5	Overview of all pressure and deformation graphs post for post impact analysis with the 3.82N/mm spring.	97
C.6	Overview of all pressure and deformation graphs post for post impact analysis with the remaining 4m/s impacts for 10.58 and 29.5N/mm spring.	98

C.7 Overview of all pressure and deformation graphs post for post impact analysis
with the remaining 6m/s impacts for 10.58 and 29.5N/mm spring. 98

Tables

1.1	Summary of most interesting conclusions from literature review	9
3.1	Expected maximum and average pressure for 15 and 30 degrees deadrise angle.	18
3.2	Measured maximum pressure on impact during experiments next to Wagner expected maximum pressure.	18
3.3	Wagner maximum impact pressure in bar for rigid wedge impact at various impact velocities and deadrise angles.	19
3.4	Release height for determined impact velocity.	20
3.5	Overview of all parts used in experiment.	26
3.6	Properties of materials used in experiment setup (SF= Safety factor).	31
3.7	Results of shear and bending stress calculation for main axle.	32
3.8	Results of shear and bending stress calculation for M4 bolts.	32
3.9	Bending stress for plate from keel to chine.	33
3.10	Bending stress for plate section.	35
3.11	Spring stiffness for each spring determined, values in N/mm.	40
3.12	R ratios for 10 degree deadrise angle.	41
3.13	R ratios for 20 degree deadrise angle.	41
3.14	Wet and dry weights of wedge.	43
3.15	Average deadrise in degrees calculated by rise over the run.	43
4.1	All sensors used in each experiment.	49
4.2	Uncertainty and linearity of all pressure sensors used in the experiment. . . .	50
4.3	All measured average velocities in rigid experiment. Indicated per velocity and deadrise combination.	53
4.4	All measured average maximum velocities, indicated per expected velocity and deadrise combination. In the third column the total wet mass of the wedge is provided	54
4.5	All measured average velocities and maximum values from average pressure of five runs in rigid experiment. Indicated per velocity and deadrise combination.	55
4.6	Preload in springs in N.	57
4.7	All measured average velocities and maximum values from average pressure of five runs in rigid and deformable experiment. Indicated per velocity and deadrise combination.	57
4.8	Maximum deformation in degrees on impact. Third value in experiment column is spring stiffness in N/mm.	61
4.9	Rigid and deformable maximum pressures.	67
4.10	Pressure reduction percentage for a series of impacts.	67
5.1	Results comparison with existing literature	73

Chapter 1

Background

Ships sailing in heavy weather conditions can emerge from the water due to a combination of forward speed of the hull and specific sea state. The reentering of the ship through the free surface of the water is called ship slamming. More general, ship slamming is the impact between any panel of a given ship and an incoming water surface. [15] This impact can vary from mild to severe depending on hull shape, wave size and speed of the vessel.

Depending on the impact, slamming can have consequences for its passengers and equipment onboard. Heavy accelerations brought on by slamming impacts can cause injuries to passengers [47] as well as damage to cargo and equipment. If the impacts become extreme, the hull might locally or completely fail, resulting in sinking of the ship [41]. Examples of structural damage as a result of slamming are shown in Yamamoto et al (1985) [52].

Currently slamming impacts are analysed with numerical algorithms as described in Ibrahim (2020) [22]. Both numerical and experimental research is conducted in order to improve resilience of the hull against slamming and increase safety on board. In order to effectively design ships for slamming impacts one must first comprehend the fundamentals of a wave collision. To accomplish this, research is designed such that it represents only simplified parts of a ship. Research into novel hull designs has led to the development of the "Axe Bow". A hull with a bow shape similar to the shape of an axe. According to research into the axe bow, the vertical accelerations in the wheelhouse have significantly decreased due to the novel hull shape [25].

A ship can be simplified by taking a 2D section of the hull and using only its outer perimeter. Shapes like this used in experiments are called wedges. The shapes of these wedges typically vary in shape and size. Most notably, the deadrise angle is varied for different wedges. The deadrise angle of a wedge is the angle between the free surface of the water and the wedge. A different deadrise angle changes the dynamics of the impact with the free surface.

Over the past century, extensive research has been conducted in the field of fluid structure interaction with wedges. To investigate the most recent developments in the field of study for this research, a literature review was conducted. Papers that had the closest relation to the subject of this research are summarized below.

1.1. Literature review

1.1.1. Foundation of slamming research

Von Karman (1928) [24] laid the foundation for fluid structure interaction (FSI) with his work on two dimensional hull-water impacts for landing seaplanes. Wagner (1932) [49]

then extended this research. He suggests a new formula that describes fluid dynamics of a wedge impact in more detail. Bisplinghoff and Doherty (1952) [5] are one of the first to publish a report that uses a drop test experiment in order to verify the theoretical calculation methods known up to that moment. In their experiment a set of wedges is used with a deadrise angle between 10 to 50 degrees. They find that for 20 and 30 degree deadrise there is good agreement between experiment and theory. In 1967 Verhagen [48] studied the impact of a flat plate on water surface and finds that for flat plates impact pressure is decreased on impact with free surface due to trapped air. He states in his discussion that the most crucial premise is that the body's elasticity and the water's compressibility won't be taken into account.

It can be assumed that due to lower impact pressure, the driving force behind structural deformation, the strain in the plate is lower as a result. In order to determine how much damage a ship's bottom plating will sustain during a slam, Jones (1973) [23] wanted to develop a relatively simple theoretical method. Jones succeeded in developing the theoretical method, but concludes that further experimental results are necessary to fully accept the theoretical approach. Early work on hydroelasticity was done by Bishop and Price (1979) [4]. Hydroelasticity was then studied by Faltinsen (1997) [12]. He found that *the maximum bending stress is proportional to the drop velocity*.

Korobkin (1998) [27] links his research to a real world problem in the form of liquid impact with the wetdeck of a catamaran and finds that fluid impact leads to high levels of stress on the elastic plates. All above stated research forms the early knowledge on slamming impacts on panels. Most work started with a hypothesis which was then worked out in mathematics. Some research was done in the form of experiments which could then validate or disprove the mathematical theories.

1.1.2. More advanced simulations and experiments

Okada and Sumi (2000) [39] focus their research on impacts at small deadrise angles, hereby focusing on the trapped air between the specimen and water. An empirical formula for trapped-air impact is proposed. It is also stated that *the average pressure at impact can be used to determine structural reaction*, which results in a novel design strategy for impacts with a small deadrise angle and ultimately to an empirical formula. This empirical formula is to be used for validation of carried out drop tests and their results. Faltinsen (2000) [14] researches the difference in deformation on impact by using 2 different plates, one steel, one aluminium. Two findings in his paper are of interest for this thesis. Firstly, Faltinsen finds that even *when maximum pressure varied significantly, the observed maximum stresses showed very low dispersion for a given impact velocity and plate*. This result contradicts the assumption that larger impact pressures equal larger deformations. Secondly, Faltinsen mentions that *"The results show that it is misleading from a structural point of view to measure pressures when hydroelasticity is important"*. This quote suggests that Faltinsen believes pressures are possibly influenced by hydroelasticity. Further research into this subject by means of an experiment might be of interest.

One of the first to describe the importance of ratio between duration of impact and first natural period of the structure is Bereznitski (2001) [3]. In his conclusion he states that hydroelasticity has no impact if the ratio is greater than 2.0. He thinks that this advice is essentially universal. But this needs to be justified. Stenius et al. (2007) [44] then presents a formula that describes the ratio (R) between loading period and first wet natural period for a slamming loaded panel. For $R > 1$, the loading can be considered quasi-static. For $R < 1$

dynamic effects can be expected. Faltinsen et al. (2004) [13] conclude in their paper on slamming that "...slamming should be considered in the framework of structural-dynamics response." According to Faltinsen, to validate the given statements, more experimental data is required to eventually compare results against computer simulations.

Tveitnes et al. (2008) [46] construct a setup in which wedges can be dropped into water at constant velocity. This is done because in numerical simulations of wedge impacts, constant velocity is assumed. They find that the initial stages of impact are modelled correctly but the added mass part often does not compare well. Battley et al. (2009) [2] perform a research in which a drop test experiment is performed with three plates with varying stiffness. They use the ratio R to determine the required impact velocities to find hydroelastic effects. Their results show that the rigid panel yields a classic pressure time trace. The moderately flexible panel shows a lower peak but longer duration of impact pressure. Finally the flexible panel shows a completely different time trace. The initial peak is smaller but a second peak is higher than expected based on experience with rigid wedge experiments. Also, significant pressure oscillations are recorded. Due to the deformation of the wedge the chine has a lower deadrise angle which results in higher peak pressures than a rigid plate would induce. A final interesting finding is that *increased impact pressure for decreasing panel stiffness did not result in increased panel deflection*. This is somewhat counter-intuitive.

1.1.3. Most recent developments

Following up on their own research, Stenius et al. (2011) [42] publish a paper that summarizes numerical and experimental results. They conclude with "*Where the hydroelastic interaction seems to have a significant effect, it is found both numerically and experimentally that the hydroelastic effects are amplifying the structural responses in comparison to the rigid/quasi-static solutions*" Luo et al. (2012) [31] perform tests with a large wedge with the purpose to study the impact response of a complex 3D structure. Measured and predicted results are compared. The conclusion mentions that the effect of elastic response on hydrodynamic pressure is not considered. This conclusion is recurring in multiple published articles and therefore asks for further investigation since the effect of hydroelasticity might be of importance to further enhance ship design. To eliminate noise in sensor data Kwon (2013) [29] uses a test setup to accelerate wedge shapes with a pneumatic cylinder. This test setup was already proposed by Kwon in 2003 [28] and proved to be a slight improvement regarding noise.

In 2020, Mai et al. [33] study the effect of linear deformation on impact pressure with a flat plate. Their conclusion is that *the hydrodynamic impact loading of the dropped plates is influenced by the elasticity of the system of springs and plates*. The scale of this effect is not further investigated. The research of Mai et al. focuses on linear movement of the plate on impact and leads to the conclusion that movement of the plate reduces impact pressures. This result could indicate that elastic or rotational deformation could also lead to lower impact pressures and accelerations. The experiment of Mai et al. was performed with a wedge released into a significantly larger tank. This leads to the conclusion that 3D effects were likely present during the impacts. Between 3D simulations and experiments where 3D effects are allowed slight discrepancies are always present. To cancel out these discrepancies it is preferable to design experiments in which 2D effects are the prevailing displacement of liquids. By doing so, better validation can be made with numerical models.

Wang and Guedes Soares (2018) [51] propose to model water impact of an elastic wedge by combining a modal analysis for the structural deflection and an analytical model for the

hydrodynamic pressure on a rigid body in FEM analysis. They find that “... *the structural deflection is not affected by the maximum pressure.*” The results also demonstrated that the hydroelastic effect significantly decreased with increasing plate thickness or decreasing impact velocity. The quote indicates that even though the maximum pressure varies, the deflection of the specimen was not affected.

Research of van der Eijk and Wellens (2022) [10] with drop tower impacts suggests that on impact, accelerometers rated up to 200g are necessary to measure acceleration of the specimen. Assuming an initial velocity of 7m/s at impact, a final velocity of 0m/s and a displacement of 20cm an average g-force of 12.5g is calculated [A.3]. Even if we assume that 90% of the deceleration happens in the first 5cm of the impact with the fluid, an average g-force of 40g is calculated [A.4]. This suggests that a accelerometer rated for 50g should suffice for tests with this drop tower while previous results declare otherwise. This asks for calibration of accelerometers and possibly further verification methods.

Okada and Sumi perform an experiment that includes impact velocities between 1.4 and 3.4m/s. For these velocities Okada and Sumi find different responses in pressures compared to Huera-Huarte et al. [21], which perform their experiment at high impact velocities, above 5m/s. This difference in results between similar tests but varying speeds highlights the importance of multiple impact velocities. Hence, it is of interest to experiment with multiple impact velocities and deadrise angles in drop test experiments to measure a broad spectrum of responses.

Bos and Wellens (2021) [6] [7] try to increase fundamental understanding of fluid structure interaction in extreme wave impacts with a physical experiment of a single degree of freedom pendulum. They find that the focal position and initial vertical clearance had a significant impact on the pendulum’s response. Wang et al. (2019) [50] investigate the unsteady hydrodynamic force on solid objects that enter the water vertically. In the work of Wang et al. the unsteady hydrodynamic force is decomposed exactly into three individual components, the acceleration, gravity and velocity term. The major goal of the work of Lugni 2006[30] is to compile a complete temporal history of pressure effects combined with an improved description of the interior flow kinematics. The large scale wave impacts on a vertical wall experiment by Kaminski et al. (2011) [19] shows that impacts on large structures can lead to forces in the order of MN.

1.1.4. Reflection

In the featured research of the past century, we see that the research started with a physics approach of a wedge penetrating the water. A drop tower experiment validates the mathematical approaches not long after. The first drop tower experiments show that the formulas devised earlier correspond well with reality. However, early research often concludes that there are research limitations related to ignoring the elasticity of the wedge plates which compromises the research. As more knowledge is gathered and more in-depth research is done, the research questions become more complex, and so do the physics and the simulations to test hypotheses. From the moment the computer software allows it, mathematical hypothesis are frequently tested with numerical models. From that moment on studies follow each other up in a pattern;

1. Mathematical proof for new theory;
2. Numerical simulation with software and then finally;
3. Validation with an experiment

Until recently, computers were not powerful enough to simulate models in which there was a dynamic interaction between liquid and solid. However, with today's computers this is possible and these simulations have been successfully performed. To date, these advanced simulations have not been validated extensively by means of an experiment. Hence the reason for the research question and the accompanying experiment.

A multitude of the reviewed papers describe the effects of hydroelasticity. Different situations are described with the word "hydroelasticity," hence a definition is given here to clear any confusion. In this thesis the definition of hydroelasticity can be defined as elastic deformation, e.g. bending, of a rigid structure as a result of fluid pressure. By setting this definition as such, for example the effects observed in the paper of Mai et al. (2020) [33] do not qualify for hydroelasticity. An example that does qualify is the research of Battley (2009) [2] and Stenius et al. [42].

Table 1.1: Summary of most interesting conclusions from literature review

Report/paper	Conclusion	Missing
Faltinsen 1997	Maximum bending stress is proportional to the drop velocity.	Only zero degree deadrise angle is used in the experiment.
Okada & Sumi 2000	Structural response can be estimated by using the average pressure at impact which leads to a new design approach for small impact angles.	Only small deadrise angle (0 to 4 degrees) and no high velocity impact (all $< 3.4 m/s$)
Faltinsen 2000	The results show that it is misleading from a structural point of view to measure pressures when hydroelasticity is important	Thorough review of the small scatter in strain with varying velocities.
Battley 2009	Increased impact pressure for decreasing panel stiffness did not result in increased panel deflection	The dimensions of the water tank were not described in detail in order to guarantee that only two-dimensional effects were present.
Stenius et al. 2011	Where the hydroelastic interaction seems to have a significant effect, it is found both numerically and experimentally that the hydroelastic effects are amplifying the structural responses in comparison to the rigid/quasi-static solutions.	The dimensions of the water tank were not described in detail in order to guarantee that only two-dimensional effects were present.
Wang & Guedes Soares 2018	The structural deflection is not affected by the maximum pressure.	Physical experiment to validate numerical analysis is missing
Mai et al. 2020	The hydrodynamic impact loading of the dropped plates is influenced by the elasticity of the system of springs and plates	Only 0 degree deadrise angle tested, deadrise angles are not tested.

1.2. Knowledge gap

Previously carried out research paved the way for this report. The relation between deformation and impact pressure has not been studied extensively by means of an experiment. More data is required to study the relation between deformation, speed of deformation and impact pressure. Computer simulations can help the research into wedge impacts but physical experiments are needed to acquire data for validation of software. It is interesting to fill the knowledge gap, which primarily consists of missing experimental data of deformable wedges, in part because of the high number of papers (Verhagen 1967, Luo 2012, Wang and Guedes Soares 2018) [48] [31] [51]) explicitly referring to the potential importance of the effects of hydroelasticity. Table 1.1 provides a summary of the most noteworthy findings from earlier research.

1.3. Novelty statement

The novelty of this research is a deformable wedge of our own design. This wedge design is proposed to study the effect of deformation, speed of deformation and impact pressure. The wedge is designed such that on impact with the free surface, the specimen is allowed to deform.

Deformation is measured together with pressure and acceleration. To compare the effect of deformation on impact a set of rigid wedges with similar deadrise angles is dropped and analyzed as a baseline experiment. Hence the focus of this study revolves around the results of the drop test results of the deformable wedge which will be verified and validated in multiple ways, described in chapter 2. The knowledge gap found is intended to be filled with the research question below.

1.4. Research question

Since the knowledge gap that arises from the literature review has been identified, the research question for this thesis is defined. The research question is as follows:

- What is the effect of dynamic deformation of a structure on the maximum pressure at the wedge surface during impact?

According to literature [43] [44], there is typically a discrepancy between experiments and numerical analysis of the same wedge impacts. Hence it is expedient to design an experiment to find a reliable answer to the research question. The different considerations that must be taken in order to correctly construct this experiment are discussed in the next chapter.

Chapter 2

Methodology

Now that a knowledge gap has been found and a research question has been stated, a plan to answer the research question and fill the knowledge gap has to be made. In the following chapter the key factors necessary to do so are introduced. The choices made in this chapter will define the design requirements that must be addressed in later stage during this thesis.

2.1. Experiment motivation

The knowledge gap shows that experimental data of deformable wedge impacts have seldom been performed in 2D, hence the drop tower experiment described in the sections below is designed. The acquired data from an experiment with a deformable wedge, and especially comparison with a rigid wedge, will provide a better insight in the effect of deformation on pressure during an impact.

2.2. Novel wedge design

To properly research the effects of deformation on impact a new type of wedge should be designed which is able to deform on impact. This is necessary to eventually validate numerical simulations in which this deformation is simulated. The design should be such that it can deform on impact with water but for comparison must also be able to be tested in rigid form. The impact with the water is created by means of a drop tower from which the wedge is released from a set height. The wedge should be designed such that it fits within the available drop tower which is discussed in more detail in section 2.7. With the use of this new wedge design, repetitive and controlled drop tests can be performed to investigate the effects of deformation with respect to peak pressure and acceleration. The hypothesis is that the deformable wedge will endure lower peak pressures on impact compared to the rigid wedge. Dynamic effects, however, could also lead to higher peak pressures.

2.3. Deformation options

For this experiment there are two ways the wedge can be compliant. Either elastic or hinged. Both have their advantages and disadvantages. Figure 2.1 shows the three different wedge designs that can be used for this experiment.

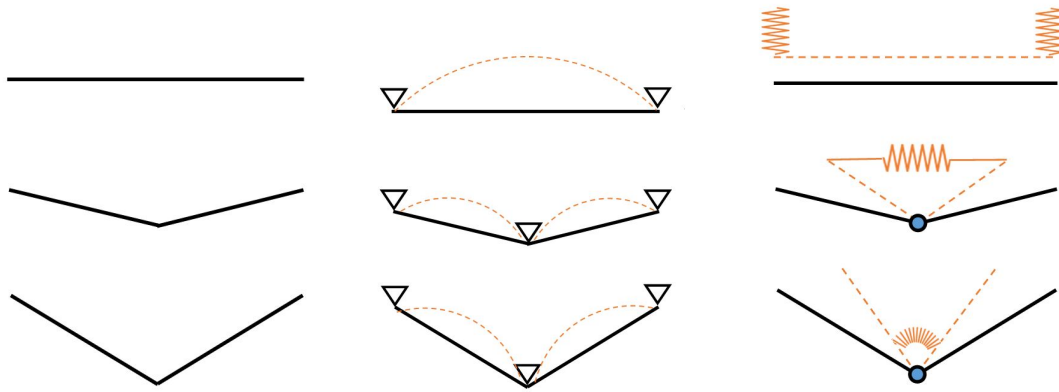


Figure 2.1: FLTR: Classic rigid wedges and plate used in most research, elastic wedges to deform on impact, rotational type wedges to rotate on impact.

2.3.1. Elastic deformation

Elastic deformation of the wedge is the most representative for actual ship response on impact. Hence it is the most interesting considering future application of the found results. Elastic deformations will most likely appear in high frequencies and small movement, this makes it harder to measure and find results. Due to high complexity of 3D fluid motions it is preferable to perform the drop tests in such a way that deformation of the plate specimens is of 2D form. This is accomplished by hinging the plates on two opposite ends, leaving the other two edges free. Due to the hinged edges, bending will mainly occur over the unhinged edge which can be analyzed as a 2D deformation. By doing this, validation of deformation with mathematical formulas is more feasible.

2.3.2. Rotational deformation

By connecting the two sides of the wedge in the middle by means of a hinging mechanism a compliant system is created. The system of hinged plates can be stiffened by torsional or compression springs that can be replaced to vary stiffness. With this system of varying spring stiffness the influence of deformation on impact pressure can be further examined. Springs with lower stiffness allow for larger deformation of the specimen on impact. This specific wedge design is harder to construct but probably easier to analyse due to larger deformation on impact. For validation of impacts without air cushioning effect, Wagner theory is used. For impacts with air cushioning effect Okada's empirical formula is used. With this type of wedge design, deformation is less representative for ship response, but deformation is easier to measure and stiffness is easier to change by the use of various springs with varying stiffness.

2.3.3. Deformation used in this experiment

For the experiment in this thesis the rotational deformation is selected on the assumption that deformations are easier to measure and analyze afterwards. Due to the high forces and many moving parts this design will likely bring some challenges regarding design and construction of the wedge. Please note that the rotational deformation is actually the linearization of the keel of the elastic deformation when zoomed in on the keel only.

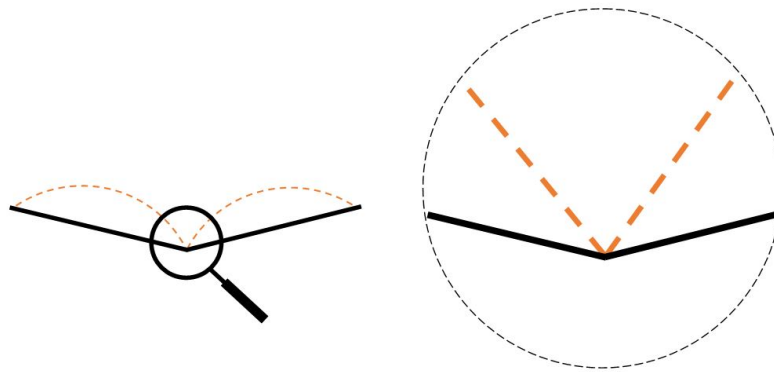


Figure 2.2: Keel of elastic deformation magnified that showw rotational deformation at keel

2.4. Importance of variable impact velocity, spring stiffness and deadrise angles

Okada and Sumi [38] find that higher pressures occur in wedge impacts compared to flat plate impacts due to the cushioning effect in wedge impacts, which initially lowers peak pressures, upon implosion of the air bubble the peak pressure is higher as a result. If this effect occurs it would suggest there is a chance that wedge impacts will cause larger deformations on the deformable wedge. The experiment of van der Zee (2022) [45] shows that a flat plate impact has a higher peak pressure compared to the wedges tested. Okada and Sumi dropped their specimen from a height of 0.1 to 0.6 meter. Van der Zee used a larger drop tower with a maximum free fall of 2.8 meter. This is reason to assume that the impact velocity influences the FSI and therefore also peak pressures. The use of varying drop heights, spring stiffness and deadrise angles is expected to give different results on peak pressure, deformation and acceleration.

2.4.1. Impact velocity

Research of Nikfarjam et al. (2017) [37] finds that higher impact velocities result in larger peak pressure on impact. Varying impact velocities are obtained by releasing the wedge from different heights. Due to the non-linear relation of velocity to pressure, quadratic increase in pressure with linear increasing velocity is expected. To verify the results the following conclusion from Okada (2000) [39] is used; “*Structural response can be estimated by using average pressure at impact.*” Following this conclusion from Okada it is expected that the increasing impact velocity will lead to an increased average pressure and therefore an increased structural response. To estimate the expected forces on the wedge during impact a numerical FVM analysis is used. In this numerical model a wedge is dropped into water with an impact velocity of $7m/s$. The output from the numerical model is pressure on the plate, this pressure is used to calculated to find the force on impact normal to the plate of the wedge. With the forces gathered from the FVM analysis the wedge can be designed accordingly. The results from the FVM analysis are also used for validation of the experiment results. The drop tower has a maximum drop height of 2.8 meters which results in a maximum theoretical impact velocity of $7,44m/s$. Previous experiments with the drop tower showed that due to frictional losses the maximum velocity will be around $7m/s$. The increments for impact velocity are set at 2, 4 and $6m/s$ because research of Chuang (1967) [8], among others, shows that impact velocity plays a big role in FSI. Impact velocity

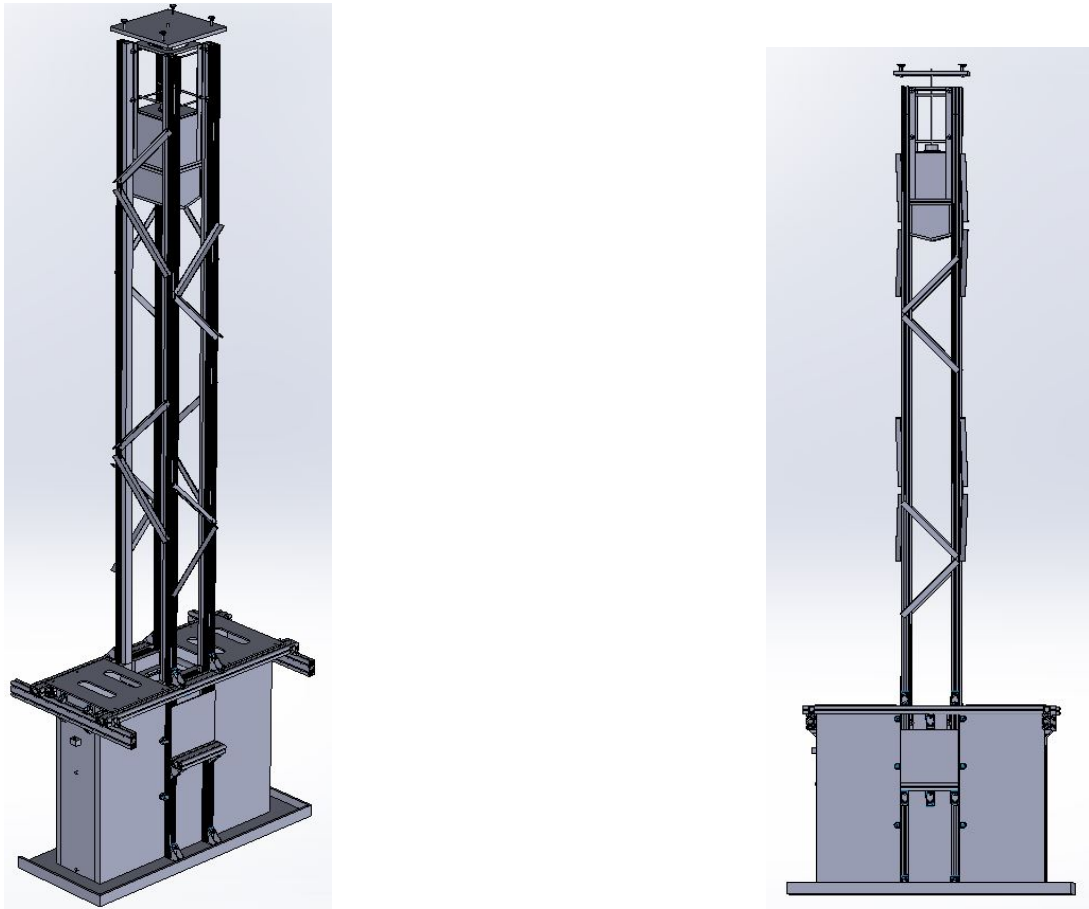


Figure 2.3: SolidWorks Render of drop tower setup.

and deadrise angle are increased incrementally. All drops are repeated 5 times and results are averaged to eliminate measurement uncertainty. Within the drop-tower a set of light gate sensors is placed. With the light gate sensors the velocity just before impact is derived. Although not perfect, the light sensor measurement gives an indication of whether the desired impact velocity is reached. Small discrepancies in final velocity are expected for each individual drop due to friction.

2.4.2. Spring stiffness

A rotational deformation for the wedge is chosen. To create a dynamic response between water pressure and wedge plate, springs are needed to temporarily store energy and prevent complete collapse of the wedge on impact. Springs come in different shapes and sizes and most importantly with varying properties. The main property is the spring stiffness k in N/m . The spring stiffness says something about the required force to compress or elongate the spring. The spring stiffness therefore should be chosen such that the varying pressures on the plates, resulting from varying impact velocities and deadrise angles, can be adequately dealt with. To select the right spring with required stiffness, calculations both by hand and numerical simulations are used. These calculations can be found in section 3.1.

2.4.3. Deadrise angles

As found by Zhao and Faltinsen (1993) [53], different pressure peaks and distributions occur for varying deadrise angles. To include a wide variety of impacts, multiple deadrise angles are required. Deadrise angles ranging from 0 to 20 degrees with 10 degree increments are chosen. Due to the hinged mechanism the deformable wedge can be set at any angle. By including a 0 degree drop, it is likely that effects of trapped air will occur which could lead to an air cushioning effect. Air cushioning is expected to have a dampening effect of the impact in the first stage of the impact. When the air bubble implodes the combined effect of the velocity of the water and the velocity of the wedge in opposite directions could cause a higher peak pressure on the wedge, possibly resulting in a higher deformation of the wedge. Research into the air cushioning effect does not fall within the scope of this research and is therefore not analyzed further. The effect might occur even though this is not the area of research and should therefore be taken into account in the analysis of the data.

2.5. Sensors

2.5.1. Accelerometer

Acceleration on impact changes with varying deadrise angles.[50] To Measure acceleration on impact an accelerometer is placed on the frame of the complete wedge. Because of the folding mechanism of the wedge the frontal area of the wedge is reduced in size during impact. This is likely to reduce deceleration of the wedge. Also, the two chines of the wedge are fitted with accelerometers in order to measure the acceleration normal to the rotation of the plates during impact. Any high frequency vibrations that might occur will be measured by the acceleration sensors located on the plate.

Verification of acceleration measurement is done with special stickers that can measure if a specific acceleration is reached for a certain time period. The g-stickers work as follows: The sticker is placed on or inside the subject of interest. If a g-force of more than its allowed value (ranging from 5 to 100g) is reached over a time period of at least 50ms the sticker changes color to indicate the event. With the use of multiple g-stickers the sensor measurements are verified.

2.5.2. Pressure sensor

To measure pressure on impact, pressure sensors need to be placed on the surface of the newly designed wedge. The pressure sensors used in earlier experiments can be reused in the deformable wedge design. Considering the research question the pressure sensor can be viewed as the most valuable sensor in this experiment.

2.5.3. Linear position sensors

Deformation of the wedge during impact with the free surface is the novel part of this research. Hence the deformation needs to be recorded as precise as possible. To measure the deformation of the plates during impact linear sensors are used. In the data analysis phase, the deformation in combination with pressure is used to answer the research question.

2.6. Wedge stiffness and sensor placement

This research requires the usage of pressure sensors, linear position sensors and accelerometers on the dropped plates. Because of this, adaptations to the plates are necessary to accommodate for the sensors which might result in variation of stiffness, mode shapes and eigenfrequency of the plates. An analysis is done to find the first natural frequency of the

plates separately and the plates connected to the springs. In the materials science lab at the TU Delft, the plate is mounted with all sensors. With the accelerometer recording the plate is bend slightly to be released and brought to vibration. The measured frequency is the first natural frequency of the plate.

To record acceleration, accelerometers are installed inside the setup. Two accelerometers are placed on either side of the wedge to record the acceleration of the wedge plates. A third accelerometer is placed within the carriage of the system to measure the acceleration of the complete system.

The linear displacement sensors are placed at the end of the wedge plates. They record the displacement which can be translated to rotation of the wedge. The measurement of rotation of the plates on impact is of importance for this research because it is exactly this movement of the wedge that might have a correlation with surface pressure on the wedge. With the aforementioned set of sensors, all individual drops produce multiple graphs per drop; acceleration-, deformation- and pressure time history. The data from all drops is then used to analyse and possibly answer the research question stated in section 1.4. The placement of the pressure sensors is of importance to find the maximum pressures on impact. This is described further in section 3.4

2.7. Drop tower

With the drop tower located at the towing tank at the TU Delft, experiments with various wedge shapes are tested. With this tower, experiments can be carried out repeatedly and various parameters can be controlled. The tower consists of a guide rail of fixed dimensions. At the bottom of the rail a water tank is placed. The water tank has dimensions such that the width of the previous wedges corresponded to the width of the tank with a few mm clearance. This perfect fit was created in order to eliminate 3D effects of water. 3D effects are challenging to model in computer simulations, 2D simulations on the other hand are less challenging. At the TU Delft, 2D simulation software is available which can be used for validation of the experiment.

Specimen of different shapes and sizes can be attached to the carriage which is guided by the rail. The carriage is hoisted up with a pulley, connected to the ceiling, to the specific release height, where an electromagnet holds the carriage in place until it is released when the system is triggered. Figure 2.3 shows a render of the drop tower. Inside the structure in the top of the tower the carriage with a rigid wedge are visible. For this experiment the drop tower is improved and updated on own initiative and according to advise provided by researchers of previous experiments.

Chapter 3

Experiment Preparation

In order to prepare for the experiments some side objectives need to be addressed and sub-questions have to be answered. In the following sub-sections these objectives are discussed and questions answered.

3.1. Hand Calculations and Detailed Hypothesis

There are different researchers describing various formulas to calculate impact pressure of wedges and plates. A selection of these formula is given in this paragraph. By determining the impact pressures beforehand, sensors can be selected on the found values. Also, by calculating the expected forces on the wedge, the design for the deformable wedge can be made to withstand the forces. From earlier research of van der Zee and van der Eijk [45] [9] data was provided for analysis of pressures. The impact velocity and deadrise angle were different in the data from previous research compared to this report's research. Since experiment data is available from previous experiments, the mathematical theories are first compared with this data. When the pressures correspond, the variables such as deadrise and impact velocity can be changed to the planned increments as discussed in the previous chapter.

3.1.1. Wagner theory

To get a better understanding of the forces involved in the impacts, the formulas found in literature are used to estimate pressures on impact. Wagner describes a formula that estimates the maximum and average pressure over time on impact with water. Wagner does not account for trapped air at impact, hence the pressures do not apply for small deadrise angles. In figure 3.1 the maximum pressure is plotted against the deadrise angle.

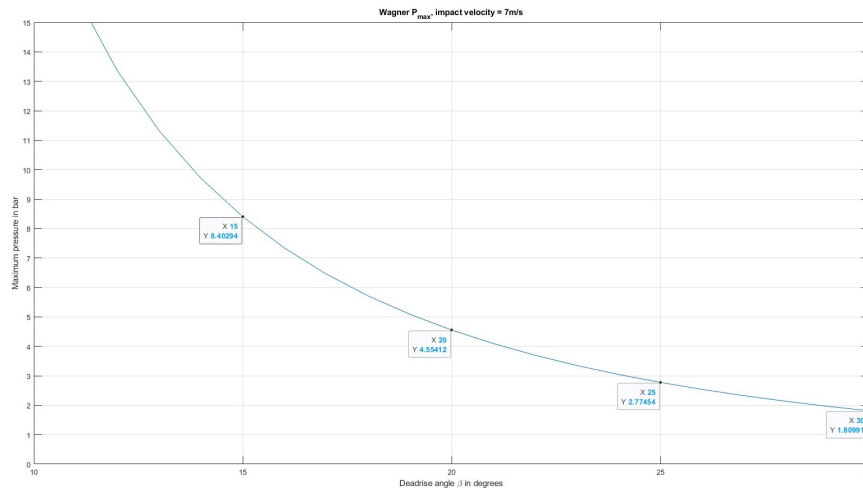


Figure 3.1: Wagner impact maximum pressure with 7m/s impact velocity and variable deadrise angle β

For an impact velocity of 7m/s the following values are found for average pressure:

Table 3.1: Expected maximum and average pressure for 15 and 30 degrees deadrise angle.

Deadrise angle in degrees	Pressure in bar	
	P_max	P_avg
15	8.4bar	2.9bar
30	1.8bar	1.3bar

3.1.2. Maximum pressure from experiment runs in previous tests

During previous experiments with 15 and 30 degree deadrise angle wedges, pressure measurements were recorded at the keel and chine of the wedge. The peak pressures from 15 and 30 degrees are shown next to pressures derived by Wagner in the table below:

Table 3.2: Measured maximum pressure on impact during experiments next to Wagner expected maximum pressure.

Deadrise angle in degrees	Pressure in bar	
	P max Wagner	P max experiment
15	8.4bar	4.76bar
30	1.8bar	1.36bar

3.1.3. Expected pressures for impact velocities and deadrise used in this experiment

Comparing the pressure found with Wagner and the measured pressure during previous experiments it becomes clear that, even though in the same order of magnitude, there is no perfect correlation between the two. This can stem from a couple of factors. First of all Wagner assumes constant velocity of the wedge during impact. The pressures collected during previous experiments are from a setup in which the wedge is decelerating from the moment of first contact with the free surface. Lower velocity leads to lower pressures and therefore the experiment pressures could be lower than expected with Wagner. However, knowing that with Wagner the pressures are higher than expected, the maximum pressures used in this experiment are calculated to get a conservative indication of magnitude to design the

wedge with.

Table 3.3: Wagner maximum impact pressure in bar for rigid wedge impact at various impact velocities and deadrise angles.

Deadrise angle in degrees	2m/s	4m/s	6m/s
10	1.6bar	6.3bar	14.3bar
20	0.4bar	1.5bar	3.3bar

3.1.4. Numerical analysis of wedge impact

As a second source of data, numerical analysis data is analyzed to provide an estimate on maximum pressures during impact. Martin van der Eijk kindly provided finite volume method data from a 15 and 30 degree deadrise angle wedge impact at $7m/s$. This data consists of a series of .csv files providing the pressure for each specific location on the wedge, each individual file represents a single time step. To analyze the complete duration of impact a MATLAB script is written to filter the required data points from the simulation. First, each file is cropped such that only the data points of one half of the wedge are still inside the file. Then, for each file the area underneath is estimated with a numerical rectangle method. The area underneath the graph represents the force per mm. To find a final force, the result is then multiplied with the width of the wedge.

The maximum peak load on the 15 degree deadrise wedge is $6502N$

The maximum peak load on the 30 degree deadrise wedge is $4794N$

With the force divided by the surface area of the wedge, it is calculated that the maximum pressure on the surface of the wedge is 2.33 and $1.72bar$ for 15 and 30 degree deadrise angle respectively.

The springs used in the experimental setup should have a spring stiffness that should be resilient to the impact forces occurring during the impact. Calculations on spring force are executed in section 3.5.

3.1.5. Expected response of wedge impact

Faltinsen (2000) [14] explained in detail what stages a wedge on impact encounters. By analyzing the response of other research on wedge impacts, an estimate can be made of the response on impact for this current research. Also, after post-processing, a comparison can be made to evaluate the validity of the experiment.

1. Structural inertia phase - The plate experiences a large force impulse during a small time relative to the highest natural period for the plate vibrations. This phase implies that structural elasticity is unimportant and the impact force is balanced by structural inertia forces.

2. The plate then starts to vibrate as a free vibration with an initial vibration velocity V and initial zero deflection. During this second phase, very large pressures may occur, they are sensitive to small changes in the physical conditions. The time duration of large pressures is very small. ($10^{-5}s$) The maximum strains occur much later, about $5 \times 10^{-3}s$. During Faltinsens' experiment the measured maximum strains showed a very small scatter for given impact velocity and plate, even when maximum pressure varied widely.

3.1.6. Release height required to achieve required impact velocity

In section 2.4.1 the impact velocities are determined at 2, 4 and 6m/s. To achieve these velocities the height required is calculated with the following formula:

$$x(t) = \int \int g - \frac{C_d * \rho * v(t)^2 * A}{2m} dt^2 \quad (3.1)$$

This formula is also considering air resistance with A = cross sectional area, C_d = drag coefficient g = gravitational acceleration of earth, m = mass of wedge ρ = air density, $v(t)$ = impact velocity, $x(t)$ = required height for set impact velocity. The area A varied so little for the different deadrise angles that the area of $236 * 218 = 51448mm^2$ was used for all calculations. For C_d the value for a flat plate (1.28) [36] was used for all calculations. The density of air at 20 degrees Celsius at normal pressure is $\rho = 1.2041kg/m^3$. The heights required for impact velocities 2, 4 and 6 m/s are presented in table 3.4. [17]

Table 3.4: Release height for determined impact velocity.

Required impact velocity	2m/s	4m/s	6m/s
Required release height	20.4cm	81.9cm	185.3cm

3.2. Sensor Selection and Calibration

Three different sensors are going to be used in the drop tower experiments. The discussed sensors are used to help analyze the impacts of the experiments and finally to answer the research question. An accelerometer, pressure sensor and linear displacement sensor are used in this experiment. Every sensor requires its own way of calibration to ensure reliable data collection. If a sensor is not calibrated correctly, or its deviations are not known, measurements can be misinterpreted.

The accelerometers are used to record change in velocity. One accelerometer is placed inside the carriage of the experiment, the second accelerometer is placed on one of the wedge plates. The difference in negative acceleration of the carriage between the rigid and deformable wedge will indicate the effects of the deformation of the wedge on impact.

The deformable wedge plates both have an accelerometer mounted as close to the chine as possible, the acceleration of the the plates is used to find high frequency vibrations in the plate during impact.

The pressure sensors are placed at the bottom of the wedges and record surface pressure during impact. The pressures recorded will indicate the forces on the wedge and together with deformation recordings will help answer the main research question of this thesis.

The linear displacement sensor is placed between the spine of the wedge and the end of the plate towards the chine. The rotation of the plate results in compression of the linear displacement sensor. The linear displacement in mm is translated to rotation in degrees in post-processing.

3.2.1. Accelerometer

The accelerometer available is the M353B18 piezoelectric sensor from PCB electronics. It has a maximum measuring range of $\pm 500g$.

Accelerometer Calibration

Previous drop tower experiments used an accelerometer with a range of 500g and produced acceleration measurements during impact of over 200g for a deadrise angle of 30 degrees. During tests with 0 and 15 degrees the accelerometer measured more than 500g. Previous experiments of van der Eijk show that accelerometers show extremely high peak accelerations on impact. Hand calculations suggest that these peaks should not be as high as measured. The sensors used in this paper's experiments thus needed to be calibrated.

Calibration of an accelerometer can be executed either statically or dynamically. For a static calibration the accelerometer is placed on a flat surface, then the measurement is checked. If the sensor is correct it should read 1g or $9,81m/s^2$. The sensor is then rotated upside down. The measurement should then read -1g. As only the accuracy on -1 and +1g are certified, this calibration type is mediocre since the measurement of 1g happens at the outer 1% of the measuring range of the sensor. Also, only 2 measurements are found to calibrate the sensor. It would be more valuable to have a range of accelerations to calibrate. Therefore a dynamic calibration could help improve the calibration.

Dynamic calibration requires a movement of the accelerometer of which the accumulated acceleration is known. The accelerometer is accelerated according to the predetermined movement. The measurements of the meter are compared with the expected values for a given time step. All the deviations are averaged to find average deviation of the meter.

In order to do so, simple movements that are relatively easy to simulate were analysed, namely:

- Piston attached to crank (in which a circular motion is directly translated to a linear motion)
- Free swinging pendulum

For the piston/crank calibration a set of parts needs to be machined which is a time consuming exercise. A simple pendulum setup can be found in a Charpy test which requires little time to acquire. For time constraint reasons the pendulum analysis is used for the accelerometer calibration experiment. In Matlab a script was written to calculate the expected angle in radians, and angular velocity in radians/s for each time step. The linear movement of the pendulum is described by the following equation of motion:

$$\ddot{\theta} + \frac{g}{L}\theta = 0 \quad (3.2)$$

The ordinary differential equation 3.2 does not describe a pendulum completely because it lacks friction and it utilizes small angle approximation. With small angle approximation it is assumed that $\sin(\theta) = \theta$ which linearizes the equation. Non-linear movement starts to affect the motion of the pendulum from an initial θ_0 of about 20 degrees. To describe the motion of the pendulum with higher accuracy, nonlinear acceleration and a damping coefficient have to be included in the equation of motion.

$$\ddot{\theta} + \frac{1}{M}(K\sin(\theta) - B\dot{\theta}|\dot{\theta}|) = 0 \quad (3.3)$$

With $B = 2C_B\sqrt{M * K}$, C_B = damping factor, L = length of pendulum from hinge to COG, g = gravitational acceleration, θ = angle of pendulum with respect to vertical, $K = m * g$, $M = m * L$, m = mass of pendulum.

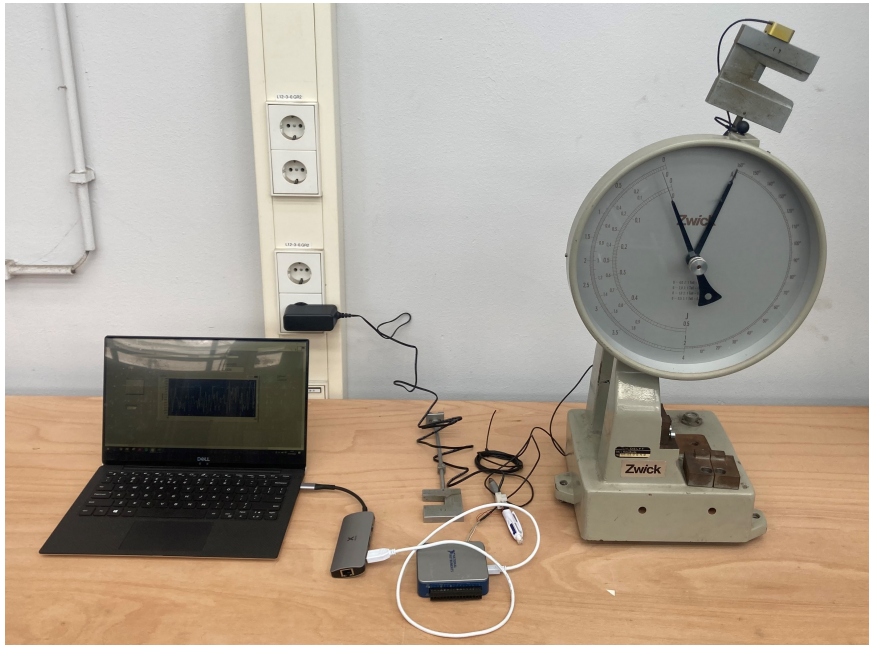


Figure 3.2: Pendulum acceleration calibration setup.

With the function "ode45" the outcome of equation 3.3 was approximated based on an explicit Runge-Kutta (4,5) formula.

One of the variables that influences acceleration is the length L , which describes the distance of the mass to the hinge point of the pendulum. The distance L_g describes the distance of the accelerometer to the hinge point of the pendulum. The length that was used for L in this simulation was the center of gravity of the complete pendulum, including the rod that connects to the mass. Since the accelerometer was placed below the center of gravity of the pendulum, at the furthest point from the axis of rotation, the angular velocity was found by multiplying the distance L_g from hinge to accelerometer.

Simulation and experiment setup

The pendulum that was simulated in Matlab is a Charpy test setup from the materials science lab at the TU Delft. The pendulum weighed $1042g$ and had a length of $270mm$. To find the center of gravity the pendulum was modelled in SolidWorks. The assumption was made that all parts of the pendulum were made from the same steel. After modeling the pendulum in SolidWorks, mass properties of the pendulum were checked. With the material "plain carbon steel" selected with mass density of $7800kg/m^3$ the total mass of the SolidWorks pendulum was $1041.2g$. This indicates that the model represented the pendulum used in the experiment. Figure 3.2 shows the experiment setup. At the end of the pendulum, the yellow anodized accelerometer is visible.

The sensor was placed underneath the Charpy pendulum with a known starting angle and dimensions. When the pendulum is released, two types of acceleration are occurring. The first one is the static acceleration, originating from earth's gravity. When the pendulum is at its lowest point, at 0 degrees, the static acceleration should read $1g$. The initial condition of the pendulum was 160 degrees, almost inverted. The initial static reading from the accelerate should read $\cos(160)g \approx -0.98g$. The second type of acceleration originates from the linear velocity and is called centripetal acceleration. When the pendulum is re-

leased it accelerates towards 0 degrees where it starts decelerating again. The highest linear velocity of the pendulum is at 0 degrees. Centripetal acceleration (A_c) is the acceleration pointing towards the center of the rotation and is calculated with the following formula:

$$A_c = \frac{V_t^2}{l} \quad (3.4)$$

In one complete cycle of the pendulum, two acceleration peaks were measured. Earth acceleration and centripetal acceleration were added together to find total acceleration in the Matlab model. Measurements from the experiment were compared against theoretical model of non-linear pendulum. The expected g force can be seen in figure 3.3.

The theoretical maximum acceleration for a free vibrating pendulum is around 4.8g at the CoG. If the accelerometer would have been placed more outwards, the accelerations would become higher due to higher linear velocity. The pendulum used in this experiment might be too small to calibrate the 500g accelerometer since the pendulum generates around 5g. 5g would be 1 percent of the measurable acceleration of the accelerometer which means that noise in the signal and non-linearity might influence the generated data.

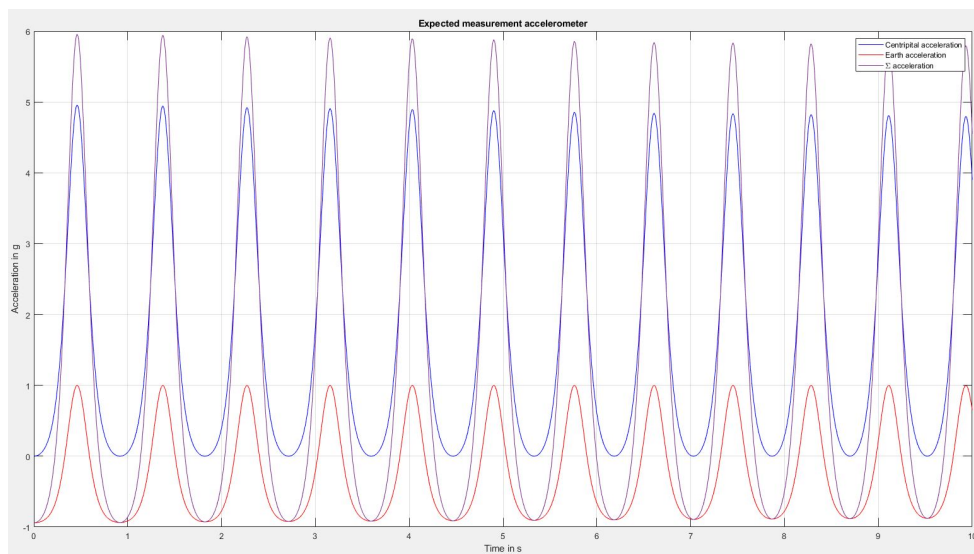


Figure 3.3: Matlab simulation of expected g force. Red line represents earth acceleration in g, blue line represents centripetal acceleration in g, purple line represents total acceleration in g.

In figure 3.3 the damping factor is implemented in the formula. This is visible in the red line (earth gravity), and the blue line (centripetal acceleration). The peaks of the earth gravity consistently go to 1 (bottom of pendulum swing) while the troughs are slowly going less "deep", this indicates that the pendulum is slowly losing energy and it is not coming back to its initial position after each cycle. The blue line shows the opposite, the troughs consistently return at 0 for each time the pendulum is at its highest point where $V_t = 0$ which corresponds to zero centripetal acceleration. The peaks of the blue line however, slowly decrease in height. This indicates that after each cycle the maximum velocity of the pendulum is less than the cycle before it. Which is the result of a lower initial position after each period.

Experiment

The placement of the accelerometer should be as close as possible under the pivot point of the pendulum to ensure maximum centripetal acceleration and earth gravitational measurement at 0 degrees of the pendulum. Wires were guided along the rod towards the pivot point and into data acquisition device. Voltage was recorded varying from 0 to 5V. $0g$ equals 2.5V. The pendulum was rotated to the initial position and locked in place with a latch. Measurement of static position of pendulum was checked and read almost $-1g$. The pendulum was released and data from accelerometer was recorded for 5 to 10 swing cycles. This process was repeated for at least 3 times for control. Expected g-force readings were plotted in Matlab and compared against data from accelerometer.

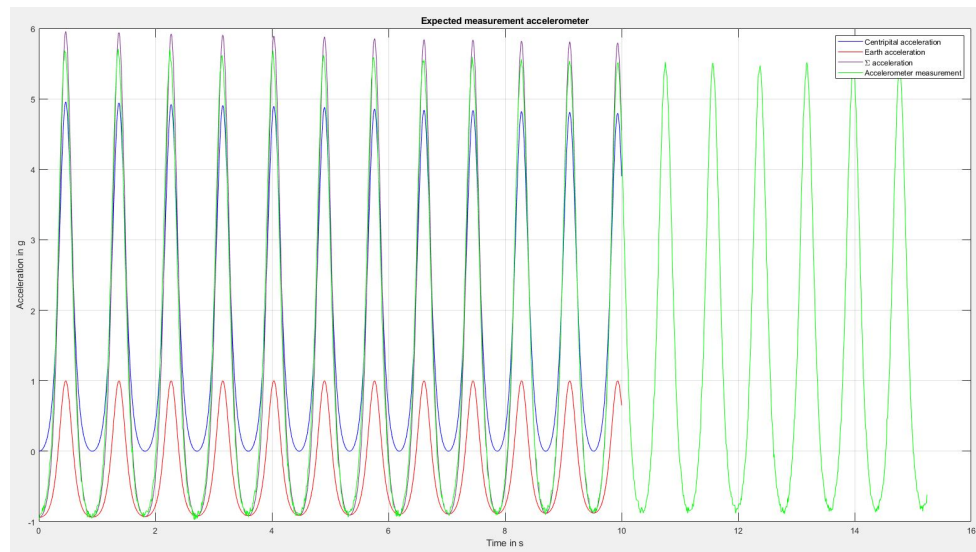


Figure 3.4: Matlab simulation of expected g force. The green line represents measured data from accelerometer in g.

Results and discussion

The results of the experiment were analyzed and fitted within the existing plot. The original data was cropped such that initial movement of the pendulum was t_0 and matched with the Matlab simulation. The data was plotted in the initial simulation shown in figure 3.3. The result is shown in figure 3.4. The measured data from the accelerometer (green line) generally shows good comparison with the simulation. The peaks are a fraction lower, this indicates that the maximum velocity of the pendulum is lower than calculated. A higher simulated peak acceleration could also result from faulty measurement of distance from accelerometer to pivot point of the pendulum but the deviation is too large since the measurement would have to be off by about $15mm$.

Curve Fitting of data

To find the damping ratio and possible other variables, a curve fitting script is written in Matlab. The curve fit is accomplished using the function "paramfun," which computes the trajectory across the times t using the parameters of the ODE fit. The difference between the newly calculated ODE trajectory and the circular arc is minimized using the function

lsqcurvefit to get the ideal parameters needed to simulate the recorded data of the experiment. As a result, it is discovered that there is still a variable that is incorrect because the two graphs did not perfectly fit. The imperfect fit indicates that there might be a first order damping factor that is not accounted for and requires further experiments. Figure 3.5 shows the fitted curve in red and the data points from the experiments in blue.

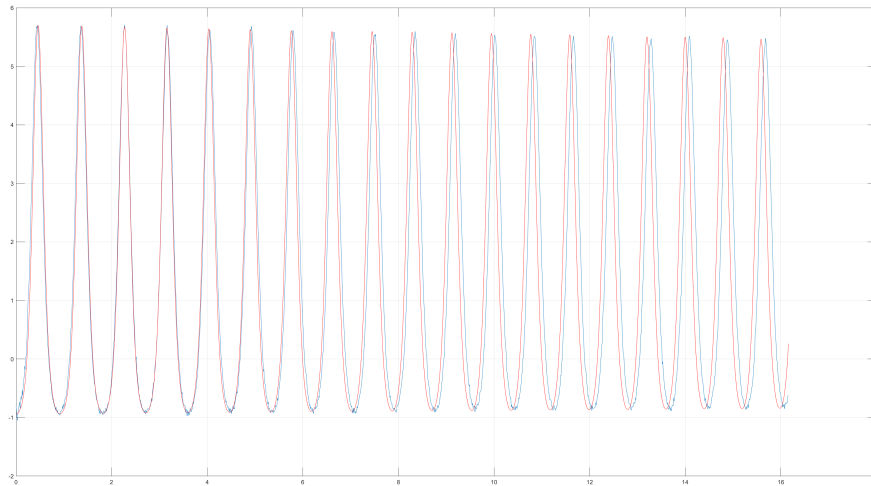


Figure 3.5: Matlab graph of curve fit, time is shown on x axis, acceleration shown on y axis.

From the curve fitting code it turns out that the the damping factor of 0.0005Ns/m was not entirely correct and had to be 0.0008Ns/m for a better fit. Also, the stiffness factor was changed slightly by the curve fit from 46.7143N/m to 46.9432N/m . This means that the g force constant of 9.81m/s^2 had to be changed slightly to 9.8581m/s^2 to create the best fit of the data. This means that the tested accelerometer is off by 0.5% which is within the specified non-linearity deviation of 1%.

Conclusion

The goal of this experiment was to find a method to dynamically calibrate an accelerometer. The tested method with a pendulum shows promising results regarding the simplicity of the setup. The pendulum method is limited in maximum g-force, hence the piston-shaft method is expected to be more suitable for accelerometers rated above 20g. Further research is needed to perfectly curve fit the simulation to the measured data, however, this first experiment shows promising signs of accurate calibration.

3.2.2. Pressure sensor

The expected maximum pressure were calculated with a formula provided by Wagner. Expected pressures do not exceed 10bar. Previous research by Van der Zee [45] on the same drop tower used for this experiment shows that pressure sensors used were adequate for all experiments. The same pressure sensors are used in the experiment for this report. The sensors used are 113B24 ICP pressure sensors from PCB Piezotronics. The maximum measurable pressure is 68.95bar

Pressure sensor calibration

The pressure sensors are calibrated by Peter Wellens at the lab of Deltares. A specially designed chamber is used in which the sensors are placed. The chamber is brought up to

specific pressures to verify correct measurement of the sensors.

3.2.3. Light gate

The light gates were used in a previous experiment to measure average speed over the distance between the two gates. The gates were placed $0.4m$ apart and an estimated $0.5m$ above the free surface. The setup from the previous experiment lacked a reliable method to measure impact velocity due to the fact that the wedge could still accelerate after the velocity measurement. To improve this system, a small plate with slots is placed on the carriage. All slots are 10mm wide and are spaced 10mm. By placing the sensor such that it measures velocity a few mm above the free surface the impact velocity can be estimated with more detail. By implementing this setup, only a single light gate is necessary to measure the velocity instead of two.

3.2.4. Linear displacement sensor

The linear displacement sensor is used to measure the displacement of the wedge plates. The sensor used is the Gefran PZ67-A. This sensor is water and shock resistant and can measure position with a sample frequency of ∞ . Therefore the sampling rate is limited to the recording device, which is set at 100.000Hz.

Linear displacement sensor calibration

The linear displacement sensor calibration is performed in a Universal Length Measuring Machine (ULM). This is a device that is already calibrated to measure specific lengths. This calibration is performed by the manufacturer of the sensor. With the sensor the calibration results are provided.

3.2.5. High Speed Camera

To get a detailed view on what is happening during impact of the wedge a high speed camera is used. The frame it should record is half water half air, big enough so that the wedge is fully in frame when still in air but also under the free surface.

3.2.6. Overview of all parts used in experiment

To create a better overview of the store-bought parts used in and around the experiment setup the following table was made.

Table 3.5: Overview of all parts used in experiment.

Part	Brand	Model
Pressure sensor	PCB piezotronics	113B24
Accelerometer	PCB piezotronics	M353B18
Linear position sensor	Gefran	PZ67-A
Light gate	TT Electronics	1497921
Shock absorbers	Traxxas	TRX7761R
Signal amplifier	PCB piezotronics	482A22
Measurement computer	National instruments	pxie-1078
8 Ch Bridge Input	National instruments	NI TB-4330
High speed camera	Photron	Fastcam SA-Z

3.3. Wedge Design

The design of the wedge needs to be such that it is strong enough to withstand the impacts and the plates of the wedge need to be stiff enough to have the least amount of bending while also being light to not have a relatively high moment of inertia. A high inertia will require more force to accelerate. To accomplish this, the wedge plates are made out of 4mm thick aluminium. The inertia of the plate, with an expected mass of 0.25kg is 0.001kgm^2 . In section 3.3.4 it is calculated if the plate thickness is enough for the expected forces. To make sure the wedge can freely move around its hinge point it is fitted with bearings on the axle.

The springs that will absorb the forces on impact will be housed in shock absorbers from model cars. These will have their oil removed to minimize damping effects. The shock absorbers are mounted to the edges of the plates at the chine and at the spine of the construction. At the spine there are multiple height options to position the wedge at different initial angles.

3.3.1. Design process

The design process of the wedge can be defined into four phases. The sketch phase, the initial design phase, the detailing phase, and the design for fabrication phase.

The design of the wedge started with a simple 2D sketch on paper. This sketch was then drawn on the computer for illustration as shown in figure . While the project evolved, the design of the wedge slowly evolved with it.

During the initial design phase the first 3D drawing was made to further elaborate the idea during discussions an early render of this design is shown in figure 3.6. At this point, no real attention was given to measurements except the outer dimensions. To build the 3D model in SolidWorks with relatable dimensions, a 1:10 scale model spring was bought to have a reference. The first wedge was designed with this spring as a reference.

During the detailing phase the springs necessary for the impacts were found. The dimensions of these springs required larger shock absorbers which were then found in 1:5 scale model car. The SolidWorks model was updated to the new spring and shock absorber sizes. When this was done the model was basically ready for fabrication.

In the final phase, design for fabrication, the model was updated such that all components could be made from readily available extruded aluminium or steel profiles. By designing the parts such that the least amount of work has to be done for fabrication, a lot of time was saved in the fabrication phase.

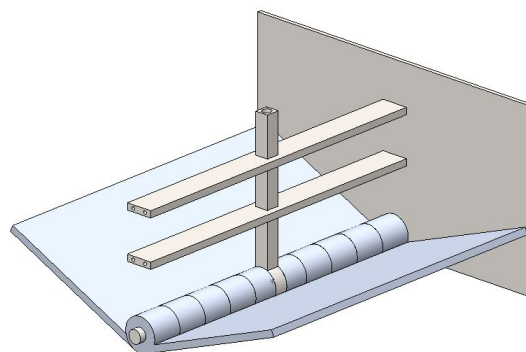


Figure 3.6: Early render of wedge design. Front plate removed for clear view of components.

3.3.2. Build process

Many different manufacturing techniques are used to produce all parts necessary to build the wedge. All processes were subtractive manufacturing techniques, meaning that raw materials are used to start with such as aluminium rod, plate or beams, then to be shaped into the parts needed by drilling, milling or lathing.

One of the most challenging parts is the hinge that holds the plate to the spines of the complete wedge. It was therefore CNC machined at the TU Delft IWS workshop with the help of its employees. Many challenging problems such as, alignment of holes and threaded outer diameters or the finding the right adhesive to glue two aluminium parts, arose during the fabrication of the parts. More details of the fabrication process can be found in appendix B. Most of the parts were designed specifically for this experiment. A list of some of those parts is provided below:

- Spring rings, to hold wider size springs in the shock absorbers
- Sensor housings for accelerometer and pressure sensors to keep them dry during the experiments
- Forks to hold upper part of shock absorbers in spine
- The spine of the wedge
- The carriage

Spring rings

Since custom springs are going to be used for the experiment, custom rings will have to be made to house the springs. These rings need to house multiple differently sized springs, hence they need a design with different cutouts for the spring diameters. The top ring was designed such that it fitted the outside diameter of the shock absorber reservoir with little play. The outer diameter of the ring is 50mm. The outer circumference of the ring has a raised edge so the spring is centered.

The bottom ring has similar outer dimensions. The inside dimensions are 6mm to fit the shock absorber rod. Also, a slot was milled so the ring could be placed easily.

Sensor housings

The sensor housings for the pressure sensors were challenging to make because of the small dimensions and low tolerances on the sensors. All holes needed to follow each other up in a specific order to make sure they would align as centered as possible. Figure B.1 shows one of the steps that was necessary to achieve the right tolerances on the pressure sensor housing.

The accelerometer housing was easier to manufacture. for the bottom part, an aluminium part was lathed with an M16 external thread. The top part received an internal thread to fit the bottom part. The initial design planned to make the top part from nylon or other plastic. However, when cutting the inside thread, the part elongated. After cutting, the nylon elastically returned to its previous inner diameter which resulted in a too tight fit on the bottom part. Figure B.2 shows the difference in outer diameter. The first diameter is the original diameter of the part. The second measurement is at the location where the cutting tool is located.

Spine

The spine consists of two 25x40x382mm aluminium bars. All holes drawn on the spine needed an exact placement. For convenience the spine was made in multiple axis CNC mill. Figure B.3 shows a picture of the milling process.

Carriage

The carriage was redesigned to fit the the new wedge design. To connect the spines to the carriage, special stainless steel plates were laser-cut. The basis of the carriage consists of a simple construction of two squares made out of Item[®] profiles connected with extruded 40x40x4mm aluminium corner pieces that hold the axles of the bearings.

Shock absorber

The shock absorbers were ordered from a RC model shop. Since the least amount of damping was required, the oil that enables the damping was removed from the cylinders. To ensure that air could pass the cylinder with ease the holes were reamed from 1.5mm to 3.0mm. Figure B.4 shows the difference in hole diameter.

Also, when the shock absorbers arrived, they were fitted with ball bearing joints with flanges. These flanges were not accounted for during design and thus needed to be removed. Figure B.5 shows the before and after of the joint.

Hinge

One of the first parts that was designed and later manufactured was the hinge system that connected the wedge plates to the main axle. Due to the complex shape it was decided to use a CNC machine to produce the first shape, visible in figure B.6. When removed from the CNC machine a block was still attached to the part which needed to be cut off. This cut needed to be made with high precision so the blade would not go through the final part. The process is shown in figure B.7. When the cut was made, the final part was placed inside a mill to mill off the remaining unnecessary material. To make sure the part was centred in the clamps of the mill, a simple rod tool was made and used, visible in B.8.

3.3.3. Wedge design explanation

The design of the wedge is such that the two sides can hinge independently. Both plates hinge around the same point. The connection between the plate and the hinge points is made with a CNC cut aluminium part. Each part houses a bearing to ensure smooth movement during high pressure impacts. The hinge points are spaced about 1.2mm apart to accommodate for manufacturing tolerances and to make sure they do not touch to prevent unwanted friction. In between the hinge points nylon rings are placed to minimize lateral movement along the axle that holds all the hinge points.

The two vertical bars visible in figure 3.7 are named "spines". The spines hold the main axle in place for the hinges, also they have slots on either side in which a fork shaped part is placed. The fork is there to accommodate the top part of the spring system. The slots in the spines enable the forks to be placed in multiple positions so the initial deadrise angle can vary.

The shock absorbers are attached to the fork at the top. At the bottom they are connected to the plates of the wedge. Within the shock absorbers multiple springs with vary-

ing spring stiffness can be placed. The varying springs are selected for the different impact velocities at which the wedge will be tested.

Due to different dimensions of the springs, dishes had to be designed to hold the custom springs in place. The dishes are placed at the top and bottom of the shock absorbers. The bottom dish has a slot machined in it for easy spring replacement during tests.

A render of the deformable wedge is shown in figure 3.7. At the top of the spines six plates are bolted in a cross shape. These six plates form a connecting bridge to the carriage of the system. The carriage is made out of eight pieces of Item[®]20 bar. The carriage is made to exact specifications to be placed perfectly inside the vertical track of the drop test setup. The carriage is guided inside the rails of the drop tower during the free fall with a set of bearings. Figure 3.8 shows a render of the wedge connected to the carriage.

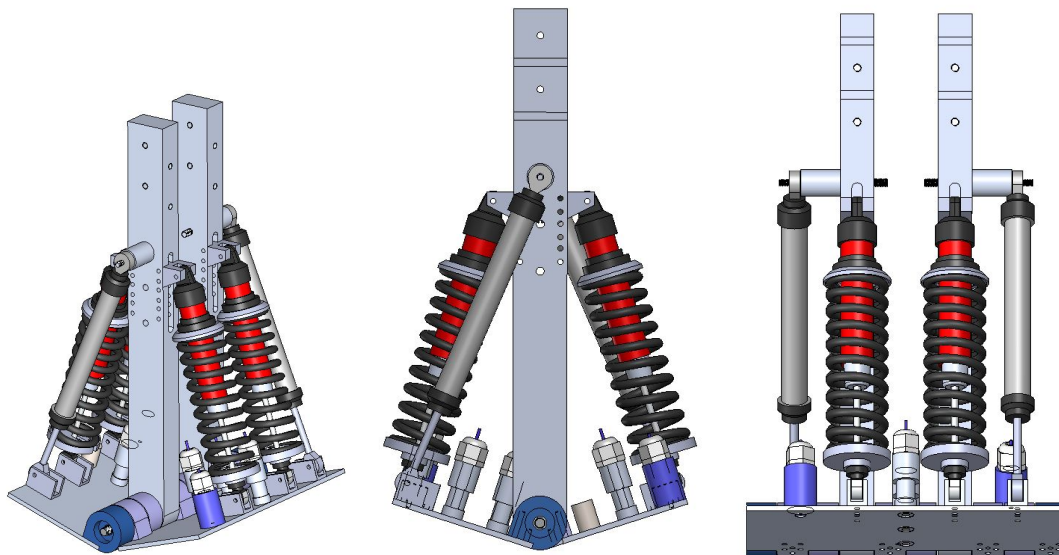


Figure 3.7: SolidWorks render of wedge design, left: Isometric view, Middle: Front view, Right: Side view.

3.3.4. Strength calculations

In this section the estimated forces during impact are used to calculate the dimensions of load bearing parts in the wedge. There are a few main components that will carry the load during impact. First of all, the plate will endure pressures of the fluid which will result in bending moments. For this experiment it is of interest to know the expected elastic deflection of the plate and to design a plate thickness that will not show plastic deformation due to the impacts. The second important part is the axle that holds the plates together and enables rotation of the plates. This axle as well is not allowed to show plastic deformation as a result of the repeated impacts. Thirdly, the plates are connected to the shock absorbers through a multitude of M4 bolts. These bolts should be able to withstand the shear force that occurs during impact.

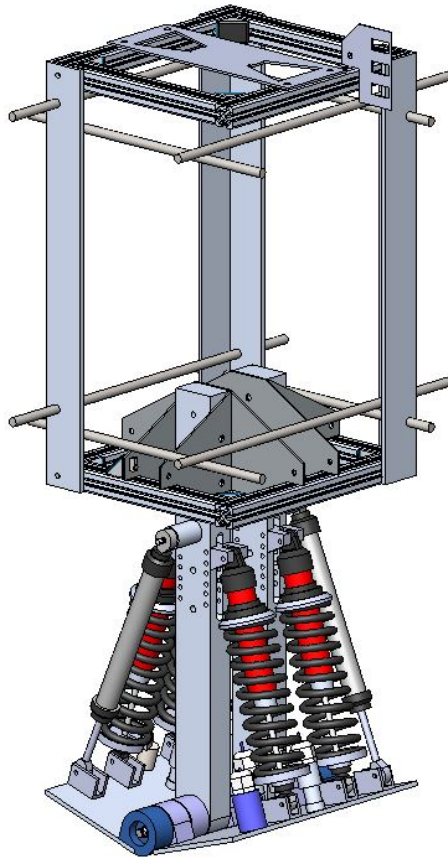


Figure 3.8: Complete wedge with carriage, front corner from carriage removed for better view of components.

Table 3.6: Properties of materials used in experiment setup (SF= Safety factor).

Property		
Yield strength stainless steel	215	<i>MPa</i>
Yield strength incl. stainless steel (SF=2)	107.5	<i>MPa</i>
Tensile strength stainless steel	620	<i>MPa</i>
Shear strength stainless steel	372	<i>MPa</i>
Yield strength Aluminium 6061	241	<i>MPa</i>
Yield strength incl. Aluminium 6061 (SF=2)	120.5	<i>MPa</i>

The properties in table 3.6 are used in the strength calculations.

Main axle

For the main axle a stainless steel rod of 236x8mm (length x diameter) is designed. This dimension originated from the type of bearings used in the hinging mechanism. These bearings were suitable for large loads and impacts and therefore suitable for the deformable wedge. The resulting bending moment and shear force on the main axle are calculated with estimated load during impact.

We use a conservative assumption for the analysis and assume that the complete load

found in the peak load of section 3.1.4 is distributed over the axles outside section, which is the section that will endure the highest bending moment. We assume the rod is clamped at the position where it connects to the spine. The length of the rod from the spine is 69.3mm . Table 3.7 shows the results of the stress calculations. The diameter of the axle is 8mm . The bearings and bearing housing parts are fitted with an interference fit that increase the outer diameter to 40mm . To be conservative the diameter used in calculations is 20mm . Effectively implementing a safety factor of 2 on the diameter.

Table 3.7: Results of shear and bending stress calculation for main axle.

Main Axle properties	Dimension	
Length axle	236	mm
Length specific segment	69.3	mm
Diameter	20	mm
Area	314.16	mm^2
Max vertical Load (obtained from EVA ¹)	6502	N
Percentage length on specific segment	29.4	%
Load on specific rod part	1909.3	N
Distributed Load	27.6	N/mm
Max shear	1909.3	N
Bending moment	66.2	Nm
Second moment of inertia	7.85E-09	m^4
Bending stress	84.2	MPa
Shear stress	6.1	MPa

Table 3.7 shows a maximum bending stress of 84.2MPa . With an allowable yield stress of 107.5MPa the expected load on the axle will not result in plastic deformation.

M4 bolts

The M4 bolts are primarily loaded in shear since the distance between the load and the support is about 1mm . Both bending stress and shear stress are calculated and presented in table 3.8. For the diameter of the bolts, not the outer diameter of 4mm is used but the inside diameter of the thread which is about 3.2mm .

Table 3.8: Results of shear and bending stress calculation for M4 bolts.

M4 bolts properties	Dimension	
Bending stress	165.1	MPa
Shear stress	132.0	MPa

The M4 bolts show values that do not fit within the safety factor margin of stress for stainless steel but are still well within the maximum allowable yield strength provided in table 3.6. Due to the conservative forces used in the calculations, it is expected the bolts will hold without any issues.

¹EVA is the abbreviation for Enhanced Volume of fluid with Aeration and is a software package used for wedge impacts with regular and aerated water

Plate - Keel to Chine bending

The plate is calculated in two bending shapes. First, bending between the keel and chine is calculated. The distance from keel to chine is 109mm. The distributed pressure is analyzed from a simulation from EVA.

Table 3.9: Bending stress for plate from keel to chine.

Plate properties	Dimension	
Width plate	236	<i>mm</i>
Distributed load keel - chine	27.552	<i>N/mm</i>
Length short end plate	109	<i>mm</i>
Simply support	1501.584	<i>N</i>
Equivalent load	3003.168	<i>N</i>
Max bending moment	40.9	<i>Nm</i>
h (thickness)	4	<i>mm</i>
Second moment of inertia	1.25867E-09	<i>m⁴</i>
Bending Stress	65.0	<i>MPa</i>

From table 3.9 it becomes evident that the plate will not deform plastically from keel to chine. With the distributed load (w), distance from keel to chine (L), Young's modulus (E) and second moment of inertia (I), the deflection on impact is determined with the following equation [18]:

$$\delta_{max} = \frac{5wL^4}{384EI} \quad (3.5)$$

The maximum deflection is expected to happen at 54.5mm from the keel and is determined to be 0.59mm. Given the plate dimensions this is a deflection that is negligible.

Plate - Corner section

The second analysis is performed on the weakest part of the wedge which is the outer corner that holds the accelerometer case. This part is the weakest since it has least support during impact. A sketch of the specified plate section is provided in figure 3.9.

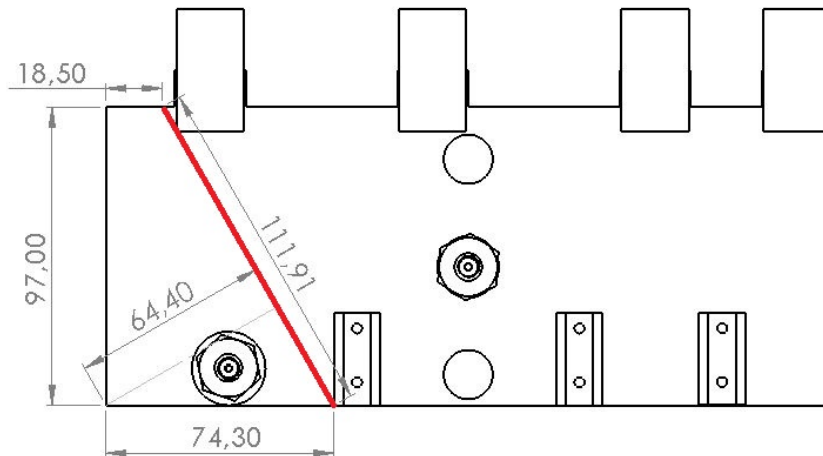


Figure 3.9: Sketch of specified corner that is analyzed for bending stress and deflection. The red line indicates the specific bending line.

A pressure of 0.7MPa is used to determine the total equivalent load on the plate.

The plate is simplified to a beam with a linear increasing distributed load as visible in figure 3.10. The distributed load has the same equivalent load as the total force on the plate exerted by the pressure.

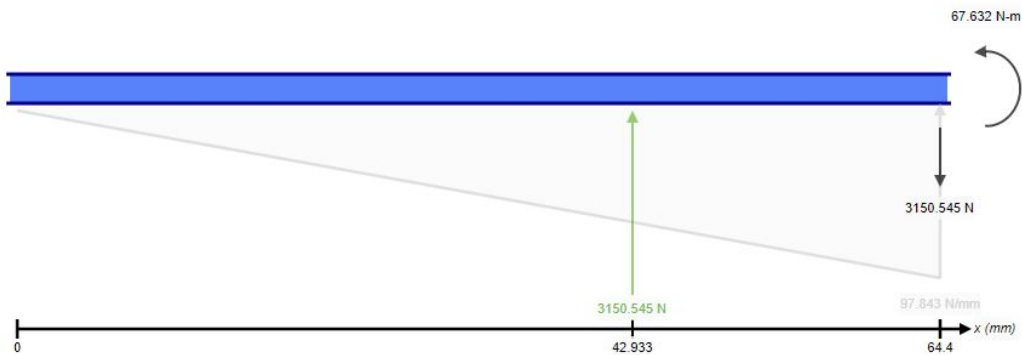


Figure 3.10: Simplified approach on distributed load on plate.

Table 3.10 shows that the bending stress on the plate exceeds the yield strength including safety factor. This means that there is a chance of bending for this section of the plate. Though, the final yield strength is not exceeded which was the reason to not change the plate dimensions and accept the risk of slight plastic deformation.

With the maximum distributed loading (w_1), maximum distance from bend (L), Young's modulus (E) and second moment of inertia (I), the deflection on impact at the largest distance from the bend line is determined with the following equation [18]:

$$\delta_{max} = \frac{w_1 L^4}{30EI} \quad (3.6)$$

Table 3.10: Bending stress for plate section.

Dimensions plate section		
Height	97	<i>mm</i>
Width 1	18.5	<i>mm</i>
Width 2	74.3	<i>mm</i>
Diagonal	111.9	<i>mm</i>
Area	4500.8	<i>mm²</i>
Thickness plate	4	<i>mm</i>
Maximum pressure	0.7	<i>Mpa</i>
Equivalent point load	3150.6	<i>N</i>
Maximum distance from bend	64.4	<i>mm</i>
Estimated distance point load from bend	21.5	<i>mm</i>
Highest load in distributed load	97.8	<i>N/mm</i>
Maximum bending moment	67.6	<i>Nm</i>
Second moment of inertia	5.97E-10	<i>m⁴</i>
Young's modulus aluminium 6061	6.80E+10	<i>Pa</i>
Bending Stress	226.6	<i>Mpa</i>
Max deflection	1.38	<i>mm</i>

3.3.5. Dimensions

The final wedge design has a plate area of $109 \times 236 \text{mm}^2$ on both sides of the wedge. The combined area of the plates is $218 \times 236 \text{mm}^2$. The total height from the top of the carriage to the keel of the wedge is 693mm. Further details of the wedge are shown in figure ?? The dimensions of the carriage are the same width and breadth as the wedge to fit within the rails provided from earlier experiments. The distance between the axles of the bearings are also determined by the dimensions of the tower rails. The exact dimensions of the tower and its tracks are provided in 3.7.

3.4. Pressure sensor placement

Zhao, Faltinsen and Aarsnes (1996) [40] describe the location of highest pressures for individual wedge designs. Figure 9 from the book (figure 3.15 in this report) shows that for some deadrise angles the peak pressure is located at the keel of the wedge while for others the maximum pressure is located at the chine. The maximum pressure on impact is one of the main data points to collect, therefore the sensors are placed as far towards the keel and chine as possible. Since only a limited number of sensors is available, the following sensor placement is used; one side of the wedge will receive three sensors of which two will be placed at the extremes of the wedge while the third is placed in between those two. A fourth and final sensor is placed in complete symmetry of the middle sensor on the other side of the wedge. By doing so, the three sensors data can be fitted to earlier found pressure curves. The fourth sensor is used to verify the symmetry of impact. Figure 3.15 visualizes the location of the pressure sensors compared to the peak pressure locations determined by Zhao Faltinsen and Aarsnes (1996) [40]. In the left image of figure 3.15, the length of the wedge is made dimensionless and runs from -1 to 1. The dimensions of the plate are calculated into the dimensionless coordinates and are -0.47, 0.17 and 0.82 for P3, P2 and P1 respectively with pressure sensor shortened to "P".

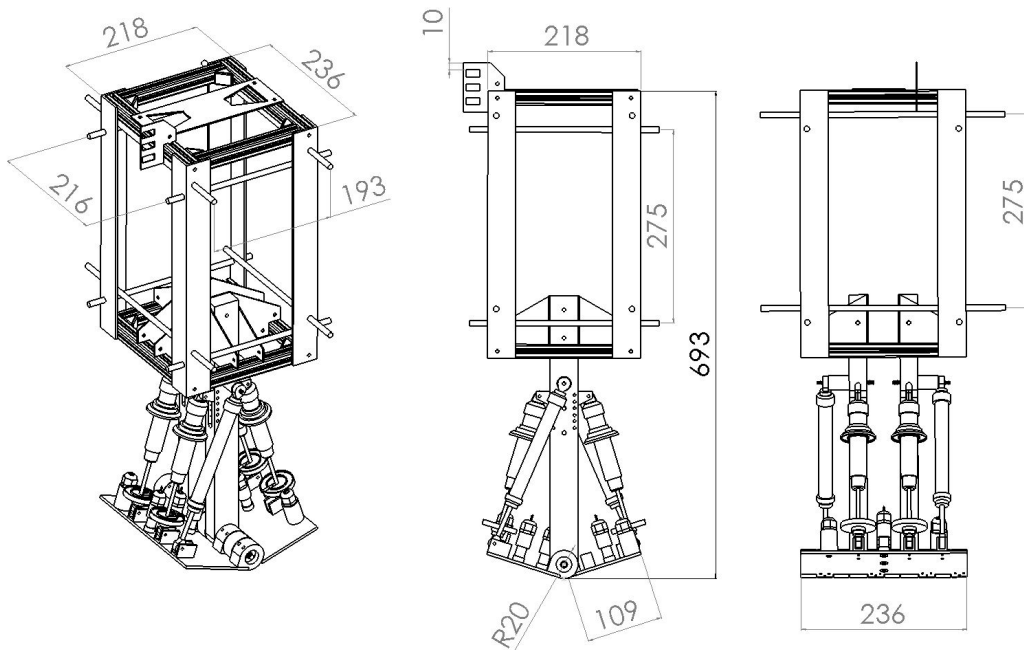


Figure 3.11: Full wedge dimensions in mm.

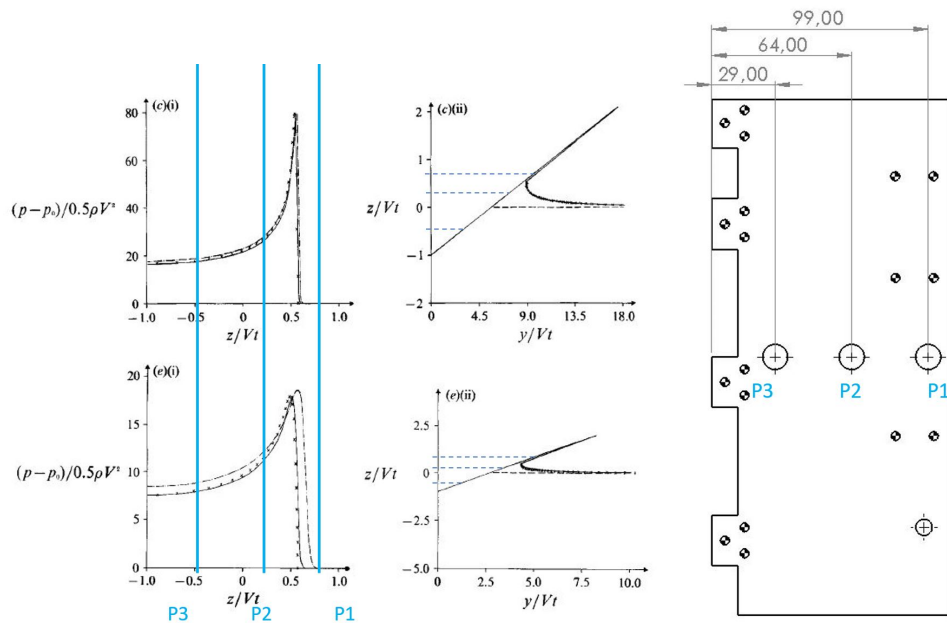


Figure 3.15: Left: Pressure distribution on symmetric wedges during water entry with constant vertical velocity. (c)=10 degrees deadrise angle (e)=20 degrees deadrise angle. (figure from: Zhao and Falinsen (1993) [53]) Right: Drawing of wedge plate with position of pressure sensors from keel in mm.

3.5. Springs

With the determined average force on impact from the hand calculations and FVM analysis we can estimate the forces that the spring will have to carry. The spring in the wedge should have such a stiffness so that it can absorb the force of the impact to such an extent that deflection can be measured while not completely collapsing under the impact and also not

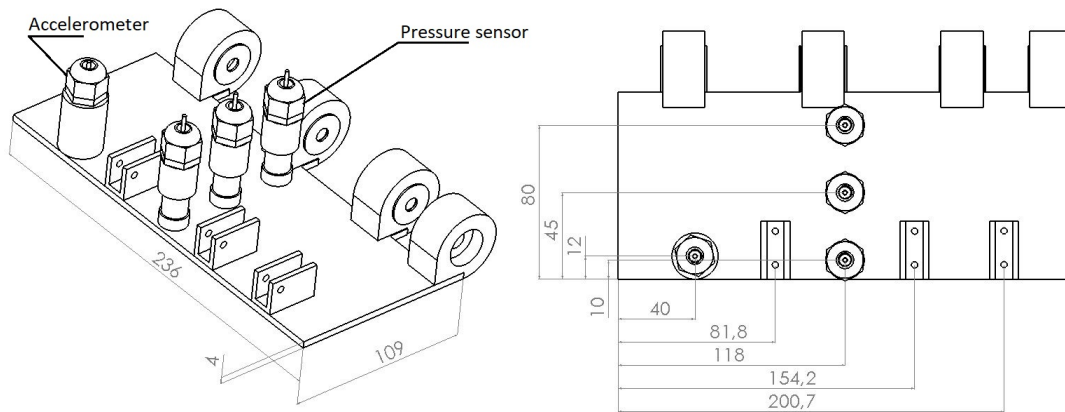


Figure 3.12: Wedge plate 1 dimensions in mm. Accelerometer housing on bottom left of plate, three pressure sensor housings in the middle of the plate.

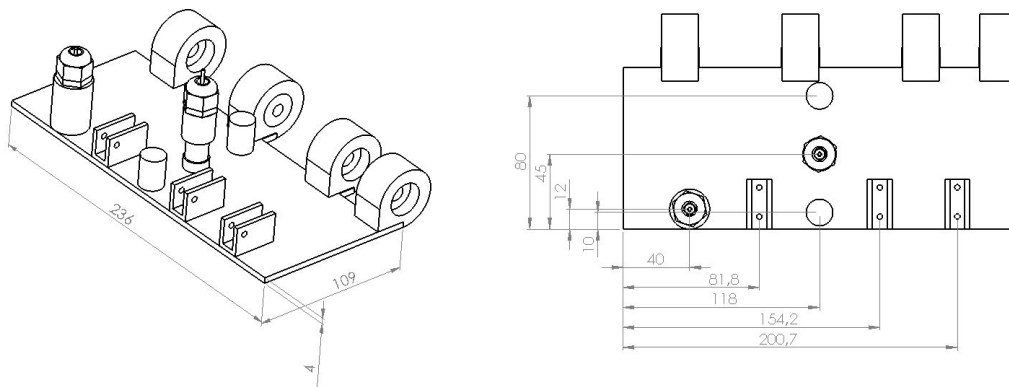


Figure 3.13: Wedge plate 2 dimensions in mm. Accelerometer on bottom left of plate, single pressure sensor housing in middle of plate. The two other cylinders are there to create equal inertia on both plates.

being to stiff so it does not allow for any movement of the wedge.

For this calculation the formula for average pressure on impact is used. The lowest average pressure is occurring at highest deadrise angle (20 degrees) and lowest impact velocity (2m/s). The highest average pressure on impact is occurring at lowest deadrise angle and highest impact velocity. Average pressures are 0.04MPa and 0.32MPa respectively. The force is

$$F_{average} = area * P_{average} \quad (3.7)$$

with the area of the plate is $109mm * 236mm = 25,724mm^2$ comparing the highest expected force to the lowest

$$F_{average-high} = 25,724mm^2 * 0.32MPa = 8231N, \quad (3.8)$$

and

$$F_{average-low} = 25,724mm^2 * 0.04MPa = 1029N, \quad (3.9)$$

the spread of the force is so large that multiple spring stiffnesses are necessary to allow for deformation across all experiments.

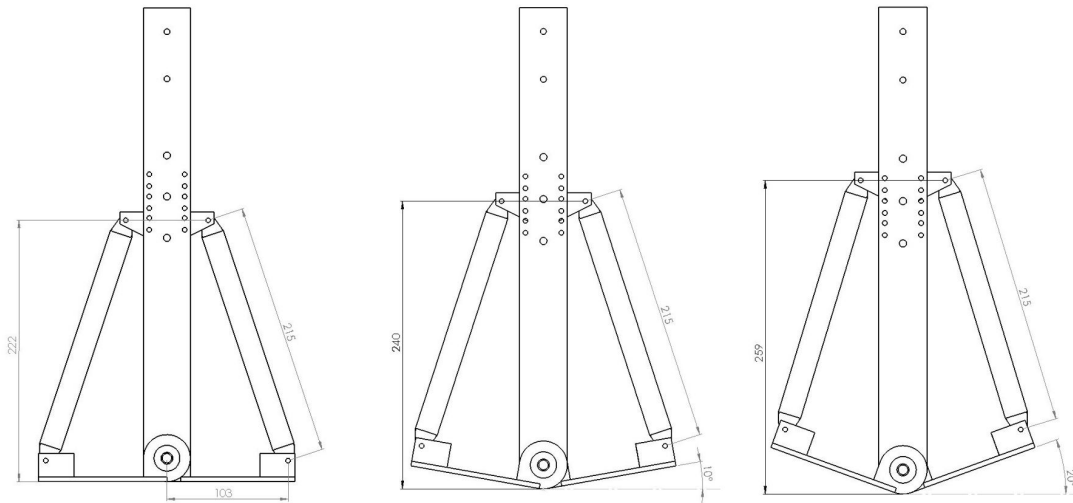


Figure 3.14: The three angles of the adjustable deformable wedge, please note that in this figure the solid rods are installed instead of the springs. All dimensions in mm.

In figure 3.16 the wedge and its forces are simplified to a static force balance to get an estimate of the forces that need to be carried by the springs. The simplification leads to equation 3.10

$$F_{spring} = \frac{1}{2} * F_{distributed} * b \quad (3.10)$$

In the following calculation we use the 10 degree deadrise angle to calculate the required spring stiffness to withstand the average force on the wedge.

The average force from the impact is calculated in equation 3.8 and is 8231N. The spring force perpendicular to the plate should then be 4115N. Due to the angle γ of the spring with respect to the plate of 8.1deg the true force of the spring should be

$$\frac{4115N}{\cos(8.1deg)} = 4156N \quad (3.11)$$

This force is then split over the two springs causing both springs to carry an equal part of $4156/2 = 2078N$

Distributed over 50mm a spring stiffness of

$$\frac{2078N}{50mm} = 41.6N/mm \quad (3.12)$$

is required if this force would be constantly applied on the spring with the spring not displacing more than 50mm.

Based on the calculations above, three springs with varying spring stiffness were ordered.

- 3.82N/mm
- 10.53N/mm
- 29.50N/mm

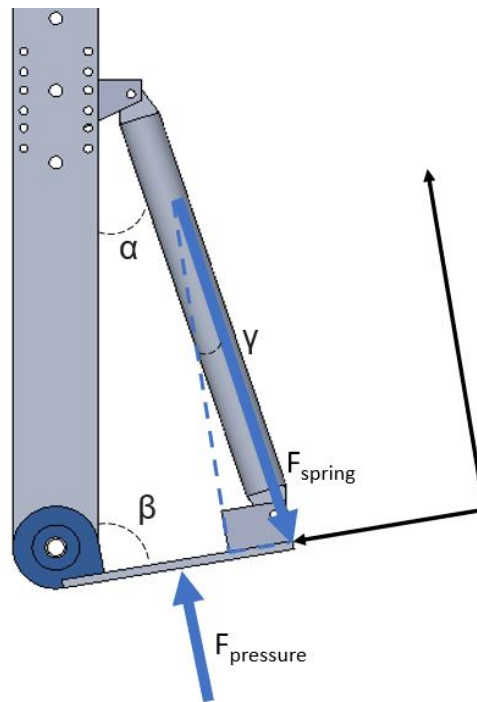


Figure 3.16: Simplified view of wedge to show forces during impact at 10 degree deadrise angle. $\alpha = 18.1\text{degrees}$, $\beta = 80\text{degrees}$, $\gamma = 8.1\text{degrees}$.

The spring stiffness ordered compared to the spring stiffness required are not a perfect match on purpose. For this there are three reasons. Firstly, the inertia of the plate including all its components will act as a force working in almost the same direction as the spring. Therefore the spring will have to provide less force to overcome the force of the pressure on the plate. Secondly the springs will have to be pre-loaded for them to be providing a linear force perpendicular to the spring. Pre-loading the spring means that prior to the deflection of the plate, a force is already present in the spring, pushing the plate down. Finally, the force on the plate induced by the impact is expected not to be present for long enough to compress the system the full 50mm.

Reviewing earlier tests the impact duration is estimated to be around 20ms. With the function

$$a = \frac{2 * (\Delta d - v_i * \Delta t)}{\Delta t^2} \quad (3.13)$$

with Δd = distance travelled, v_i = initial velocity and Δt = acceleration time the acceleration is estimated to be 250g at the chine of the wedge. With high accelerations such as these, the inertia force of the wedge is helping the springs.

Also, the working direction of the spring with respect to the rotating plate changes during impact, therefore changing the effective force applied to the plate. The effects of this should be accounted for during data analysis.

3.5.1. Spring stiffness test

The stiffness of the springs was tested in a setup consisting of a load cell, a measuring computer and a large drill press. With the load cell centered and secured underneath the head of the press, one by one, the springs were placed in between the two. For each test run, a 120

second routine was run. Every twenty seconds the drill was set to a lower position, compressing the spring incrementally. By recording the step size and recording the resulting forces, an average force per mm is calculated for all springs.

Table 3.11: Spring stiffness for each spring determined, values in N/mm.

	3.82N/mm	10.58N/mm	29.50N/mm
Spring 1	3.60N/mm	8.66N/mm	28.91N/mm
Spring 2	3.73N/mm	8.89N/mm	28.94N/mm
Spring 3	3.68N/mm	8.70N/mm	28.65N/mm
Spring 4	3.76N/mm	8.73N/mm	29.10N/mm
Average	3.69N/mm	8.74N/mm	28.90N/mm

Table 3.11 shows the measured spring stiffness in N/mm for each individual spring and the average over four. The springs do not match the specified stiffness. All springs are within 2 percent of the average of the four which can be considered relatively equal. It should be noted though that there is a slight difference which could cause an uneven distribution of forces on the plate during impact.

3.6. R-ratio of wedge plate/spring system

The R ratio is the ratio between loading period and first wet natural period. It tells the difference between quasi-static and dynamic behaviour. If the response of the wedge can be determined beforehand, the results of the experiment can be evaluated on their validity. In the following section an attempt is made to find the R ratio for this specific experiment. Stenius et al. (2007) [44] provide a formula that determines R as

$$R = 4 \left(\frac{\mu_{NP}}{\pi} \right)^2 \frac{\tan(\beta)}{V} \sqrt{\frac{D}{\pi \rho_w b^3}}, \quad (3.14)$$

where β is the panel deadrise, V is incident impact velocity, D is sectional bending stiffness, ρ is the density of water and b is the width of the panel extending from keel to chine. μ_{NP} is a boundary condition factor (for clamped boundaries $\mu_{NP} = 4.73$ and for simply supported boundaries $\mu_{NP} = \pi$).

To determine the R ratios for this experiment the following values are used:

$$D = \frac{E * H^3}{12 * (1 - \nu^2)}, \quad (3.15)$$

with Young's modulus aluminium $E = 68.9GPa$, thickness of the plate $H = 4mm$, and Poisson's ratio $\nu = 0.3$. $D = 170.4$. for b half the width of the carriage is used $b = 0.109m$

According to Stenius et al. (2007) hydroelastic effects can be expected for $2 < R < 5$. In the research of Stenius et al. they design the R formula such that they incorporate the natural period of the plate. In the experiment proposed for this thesis, the natural period of the mass of the plate and spring should be considered. Hence, the formula is rewritten to provide an estimate not for hydroelastic effects on the plate but for dynamic response of the plate.

To estimate the R-ratio of the specific wedge design at the proposed deadrise angles, the loading period and the first wet natural period are determined.

The loading period T_{LP} is found with

$$T_{LP} = \frac{4 * b * \sin(\beta)}{\pi * V_0} \quad (3.16)$$

By simplifying to a 2D model, and rotating the system to a hanging pendulum setup, the natural frequency of a plate with a spring connected can be simplified to a rod with length L . The equation of motion of the rod pendulum with a spring attached horizontally to the bottom part of the pendulum is then:

$$\ddot{\theta} + \frac{3g}{2L} * \theta - \frac{1}{2} * k * L^2 \theta = 0 \quad (3.17)$$

The EOM can then be used to find the natural frequency:

$$\omega_n = \sqrt{\frac{3g}{2L} - \frac{1}{2} * kL}, \quad (3.18)$$

with g = earth's gravity, L = length of the rod, k = spring stiffness

The natural period is equal to

$$T_{NP} = \frac{2\pi}{\omega_n} \quad (3.19)$$

Thus the natural period becomes:

$$T_{NP} = \frac{\sqrt{2}}{\sqrt{\frac{|3g - kL^2|}{L}}} \quad (3.20)$$

The R ratio is described as

$$R = \frac{T_{LP}}{T_{NP}} \quad (3.21)$$

Since both T_{NP} and T_{LP} are known we can now find R . All R-ratios are determined and presented in table 3.12 and 3.13

Table 3.12: R ratios for 10 degree deadrise angle.

	3.82N/mm	10.53N/mm	29.5N/mm
2m/s	0.11	0.25	0.46
4m/s	0.05	0.13	0.23
6m/s	0.03	0.08	0.15

Table 3.13: R ratios for 20 degree deadrise angle.

	3.82N/mm	10.53N/mm	29.5N/mm
2m/s	0.20	0.50	0.91
4m/s	0.10	0.25	0.46
6m/s	0.07	0.17	0.30

Following the results from the tables above, no dynamic response is expected during impacts. It must be noted that this formula only works for a half period of response for the wedge since the design of the wedge only allows for compression of the system. Vibrations can only occur if the fluid is able to build up a big enough equilibrium force in which the wedge will start to vibrate without the shock absorbers extending fully.

3.7. Drop tower

The drop tower consists of four Item[®] beams placed in a square to exact dimensions. To minimize frictional losses with the carriage the four individual rails are assembled such that they are as vertical as possible in x and y direction (z-axis being up). Also the distance between the insides of the tracks need to have as little fluctuations across the full length of the tracks. The front inside width of the tracks is 218mm, the inside width of the tracks is 241mm. The axles on the carriage are designed such that including the bearings there is 0.5mm play on both sides of the track. Figure 3.17 shows a render of the tower with the carriage placed inside.

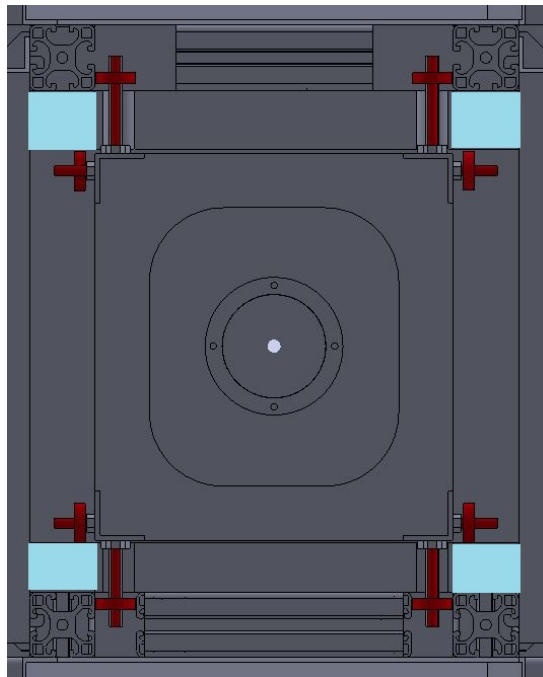


Figure 3.17: Top view of tower and carriage. The axles and bearings are highlighted in red. In the corners the Item[®] beams are visible and on the Item[®] profiles, in light blue, four beams of plastic are placed to provide smooth transition between tower and water tank.

The top of the tower is supported against the ceiling with bolts. The height of the tower from the ceiling to the water tank is 332cm. At the bottom the tower is connected to the tank with a system of item profiles. Since the item profiles have to connect to the outside of the tank, plastic strips have to be mounted to the item profiles. At the top of the tower a 12V electromagnet is placed that is connected to the national instruments recording computer. The magnet is disconnected from the power at the start of the recording of all sensors, releasing the wedge into its free fall. The maximum release height from the free surface is about 2.80m, this would result in a theoretical maximum impact velocity of around 7.36m/s, including air resistance. [17]

3.8. Water tank

The water tank is situated at the bottom of the the tower. The bearings of the carriage running from the track to the tank. The inner dimensions of the tank are 1150x241x903mm (width x depth x height). From the top to about halfway down into the tank slots are machined to accommodate free movement of the axles that hold the bearings. At the end of

the slots, pieces of about 10mm thick neoprene are placed to act as dampening stoppers.

3.9. Limitations of setup

This section discusses the limitations of the experiment setup. By understanding the limitations, a better analysis can be made of the acquired data.

3.9.1. Wedge

The wedge is the main component of the experiment, hence it is important to know its exact dimensions but also its deficiencies and other important properties

Mass

The mass of the wedge fluctuates per setup due to heavier springs for higher stiffness and the addition of the linear position sensors for the deformable experiment. Table 3.14 shows all masses of the different setups of the wedge. A heavier wedge will result in higher pressures because it will have a higher impact velocity which leads to a higher pressure since pressure scales with impact velocity V^2 . The weight of the wedge can not be measured for each individual experiment, slight fluctuations of the weight of the wedge are expected due to standing water in the item profiles or lower deadrise angle of the wedge for example.

Table 3.14: Wet and dry weights of wedge.

Setup	Dry weight in kg	Wet weight in kg
Rigid	9.45	9.53
Deformable with spring 3.82N/mm	9.33	9.41
Deformable with spring 10.58N/mm	9.68	9.76
Deformable with spring 29.5N/mm	10.29	10.37

Angle

The design of the wedge is such that the different settings on the spine of the system correlate to 10 and 20 degrees deadrise exactly. there are two main factors that can influence this deadrise and therefore the measurements of the pressures or accelerations. First, during production of the holes and parts that hold the springs in place there is going to be some imperfection in the measurements due to deviations in digital measurements and by human error. Secondly, the exact center to center distance of of the holes in the the store bought shock breakers can deviate slightly, resulting in a variable angle. A higher deadrise angle will influence both pressure and accelerations on impact. The actual deadrise is measured with the tangent of the rise over the run. Table 3.15 shows the measured rise, run and calculated angles.

Table 3.15: Average deadrise in degrees calculated by rise over the run.

setup of wedge	Run	Rise in mm		Deadrise in degrees		Average deadrise in degrees
		high	low	high	low	
Plate 1 - 10 degrees	114	20.64	20.41	10.5	10.4	10.4
Plate 2 - 10 degrees	114	20.33	20.91	10.3	10.6	10.5
Plate 1 - 20 degrees	116	40.9	39.9	21.1	20.5	20.8
Plate 2 - 20 degrees	116	40.21	39.97	20.7	20.6	20.6

Stiffness of plates

The plates of the wedge are 4mm thick aluminium (6061) alloy. With a mass of $2.7\text{g}/\text{cm}^3$. At the chine of the aluminium wedge plates, the different mounts for the springs and linear position sensor are mounted. The measurement of the plates relies on the assumption the the plate does not deform during impact, but it inescapably will deform slightly. The elastic deformation of the plates is considered negligible. To find possible elastic deformation on impact a rigid run is performed with the linear displacement sensors recording. A perfect wedge with no play and infinite stiffness should show no deformation in the wedge plates.

Drag (10 and 20 degrees)

During the free fall of the wedge it will encounter air resistance. This air resistance will increase for increasing velocities. The formula that describes air resistance is

$$F = \frac{1}{2} \rho C_D A V^2 \quad (3.22)$$

with; ρ = density of air in kg/m^3 , A = frontal area of structure in m^2 , V = velocity in m/s and finally C_D = a non dimensional drag coefficient. The shape of an object determines the C_D . With the increasing deadrise angle the C_D decreases and therefore the resulting air resistance decreasing with it. Hence, higher impact velocity is expected with increasing deadrise angle. Also, the velocity is squared in equation 3.22. Hence, the difference for increasing deadrise is likely to become more significant for higher impact velocity tests.

Springs

The springs used in the setup are housed inside the shock absorbers. To hold the springs in place while the plates are not loaded by pressure, the springs are slightly pre-loaded. This also helps overcome the non-linear stiffness in the springs. The setup available to measure the pre-load in the springs is not equipped with a live measurement of the load. It is therefore hard to set all the springs to the right pre-load. Varying pre-load will result in uneven reaction forces during deformation of the wedge.

The smallest springs that were used inside the setup were housed with the original plastic spring mounts. These plastic mounts have the tendency to deform slightly under loading which will result in a non-linear dynamic loading pattern.

3D effects

Computer simulations for wedge impacts are mostly 2D simulations. For best comparison against computer simulations a 2D effect should be tried to create on impact. This means that on impact, the majority of the water moves only in a single plane (in this case Z-Y plane, Up, down and sideways.) To generate a 2D effect, the wedge and tank are designed such that the largest amount of displaced water moves towards the farthest end of the tank. However, not all water can be forced in this ideal direction. Some of the water will be dispersed towards the short end of the tank and will flow past the short side of the plates. Hence, not a perfect 2D flow can be represented. The effect of this loss is hard to estimate.

3.9.2. Tower

The tower that guides the carriage and wedge towards the free surface can unfortunately not be perfect, the following subsections explain the most important limitations.

Friction

The tracks that form the boundaries of the track the carriage can move in are placed as vertical as possible with the least amount of variation in distance between them. This distance however, can not be guaranteed to have some variability, therefore some parts of the track might induce slightly higher friction due to contact with the guide wheels of the carriage. The effect of this extra friction is not taken into account in the preparations of the tests.

Angle

The total angle of the tower with respect to the free surface should be 90 degrees with the x- as well as the y-axis for a perfect free fall of the wedge. The tower is assembled with the help of lasers to indicate the desired vertical angle. The laser level assessment will have to be performed by eye and can therefore never be perfect.

3.9.3. Tank

Water depth

The water depth inside the tank determines the distance of the free fall. A longer free fall will result in a higher impact velocity. Every impact induces a splash of water that causes some spillage. The water level is checked after each impact and the tank refilled if necessary. However, not every impact will have a similar free fall distance. Reading the the water height is done with a ruler placed inside the tank, the reading error is 0.5mm.

Water temperature

The density of water is one of the factors that affects peak pressure. A change in temperature changes its viscosity and density which in return can alter the outcome of the pressure sensors. The water temperature of the tank can be altered by refilling the tank with tap water which is likely to have a lower temperature than the water already present in the tank. To monitor the temperature, it is best to measure the temperature after each refill.

Water movement

After each impact the free surface of the water is brought into motion. As long as the free surface of the water is not still the next drop should not be performed since a fluctuating surface can result in higher or lower peak pressures on impact. A limitation of the experiment is that subsurface the water can still be moving around even though the free surface is seemingly still. Movement of water particles can cause variance in pressure measurements. Subsurface velocity is not monitored and is therefore a limitation to the research.

Vibrations of structure

The water inside the tank will transport pressure waves towards the boundaries of the tank. Here some of the energy is transferred in to vibration of the tank walls. The walls of the

tank have a frequency of about 20Hz. Any 20Hz frequency measured can therefore not be distinguished from resonating parts of the tank.

3.9.4. Measurements

Potentiometer

The linear potentiometer used to measure deformation of the wedge is the Gefran PZ67-A 75mm. This sensor is connected to the spine of the wedge and to the chine of the wedge plate. The construction is made such that there is as little play as possible in the system. Even though no play was the goal, there is always a possibility of play that evolves over time during the experiments. Play will result in an immeasurable displacement of the plate with the potentiometer.

The working principle of the potentiometer is a sliding contact mechanism of which the resistance increases linearly over the distance of the contact. The voltage over the resistance is measured. The larger the extension of the potentiometer the lower the voltage. Full extension of the potentiometer results in 0V. Full compression of the potentiometer results in 5V or the other way around depending on the way it is connected to the system.

Due to the physical connection of this sensor some resistance is unavoidable. The displacement force of the sensor is $\leq 20N$. The displacement force acts as a damper during the deformation tests, dampening any vibrations on impact.

The measuring range of the potentiometer is 75mm, with an infinite resolution. Non-linearity will occur below 1% of its measuring range.

Accelerometer

Acceleration is measured with the PCB Piezotronics M353B18 accelerometer. The working principle of this sensor is the compression of a quartz crystal that unloads an electric charge as a result. The discharge time constant is 0.5 to 2 seconds. The sensitivity is $1.02mV/(m/s^2)$ with a resolution of $0.05m/s^2rms$. Any acceleration fluctuation below $0.05m/s^2rms$ will therefore not be measured. The measuring range of the accelerometer is $\pm 4905m/s^2pk$ with non-linearity below 1% of its measuring range. All accelerations below $49.05m/s^2$ are less reliable.

Pressure

The sensor used to measure pressure is the PCB Piezotronics 113B24 ICP pressure sensor. The working principle is similar to the one of the accelerometer. The discharge time constant is 100 seconds. This means that at constant pressure, 63% of the signal is lost after 100 seconds due to the discharge of the crystal. It is therefore that this pressure sensor is not suitable for the measurement of (quasi-)static pressure. The sensitivity is $0.725mV/kPa$ with a resolution of $0.035kPa$. Any pressure fluctuation below $0.035kPa$ will therefore not be measured. Maximum measurable pressure is $6895kPa$ with non-linearity below 1% of its measuring range. Any pressure measurements below $68.95kPa$ are less reliable.

Velocity

A light gate sensor is used to measure the velocity of the wedge before impact. The working principle is a combination of a Light Emitting Diode (LED) and a Light Receiving Diode, better known as a photodiode. The photodiode generates a voltage when a specific infrared wavelength is received. The emitting diode emits the required infrared light. If the

light beam is blocked the receiving diode does not generate a voltage. The voltage of the receiving diode is recorded. The duration of the intermission is measured to analyze the velocity.

The voltage output of the photodiode is 0.16V. The less infrared light hits the diode the lower the signal. The emitting and receiving end of the light gate should be wiped clean of any water or other sources that can influence the voltage output of the photodiode.

Measurement analysis

Each individual drop is repeated 5 times. All five repetitions are analyzed such that the average and standard deviation of each point in time is calculated to be plotted in the graphs. The difficulty is to find the point in time to sync all data recordings. Since not one impact is exactly the same to the previous or the next, there is a high chance that recordings cannot be matched perfectly, which will cause slightly skewed average and standard deviations.

3.10. Test plan

A test plan is created to keep an overview of all the runs necessary to create a data set with the highest versatility. The plan is in figure 3.18, the three different springs are indicated with the numbers 0, 1 and 2, running from lowest stiffness to highest stiffness. Impact velocity is in m/s, deadrise angle is in degrees. Finally the column "Run #" is the run number allocated by the computer program during the experiments. Test 1 until 14 are deformable runs. Test 15 until 22 are rigid runs. Test 22 and 23 are runs without potentiometer to compare with runs with potentiometer. During test 10, run 148 did unfortunately not save correctly, which was noticed after the runs for that day were completed. This led to a lower accuracy for average pressures, acceleration and deformation.

Test #	Spring	Impact Velocity	Deadline	Code	Run #	Test #	Spring	Impact Velocity	Deadline	Code	Run #	Test #	Spring	Impact Velocity	Deadline	Code	Run #	Test #	Spring	Impact Velocity	Deadline	Code	Run #	Test #	Spring	Impact Velocity	Deadline	Code	Run #		
1	0	2	20	110220	93	1	1	4	20	711420	115	1	2	6	20	1312620	153	1	x	2	20	151x20	77	1	x	2	20	151x20	77		
2	0	2	20	120220	95	2	1	4	20	721420	116	2	2	6	20	1322620	154	2	x	2	20	152x20	78	2	x	2	20	152x20	78		
3	0	2	20	130220	96	7	3	4	20	731420	118	13	3	2	20	1332620	155	15	3	x	2	20	153x20	79	15	3	x	2	20	153x20	79
4	0	2	20	140220	97	4	1	4	20	741420	137	4	2	6	20	1342620	156	4	x	2	20	154x20	80	4	x	2	20	154x20	80		
5	0	2	20	150220	99	5	1	4	20	751420	138	5	2	6	20	1352620	157	5	x	2	20	155x20	81	5	x	2	20	155x20	81		
1	0	2	10	210210	100	1	1	4	10	811410	120	1	2	6	10	1412610	148	1	x	2	10	161x210	72	1	x	2	10	161x210	72		
2	0	2	10	220210	101	2	1	4	10	821410	121	2	2	6	10	1422610	149	2	x	2	10	162x210	73	2	x	2	10	162x210	73		
3	0	2	10	230210	102	8	3	4	10	831410	122	14	3	2	10	1432610	150	16	3	x	2	10	163x210	74	16	3	x	2	10	163x210	74
4	0	2	10	240210	103	4	1	4	10	841410	123	4	2	6	10	1442610	151	4	x	2	10	164x210	75	4	x	2	10	164x210	75		
5	0	2	10	250210	104	5	1	4	10	851410	124	5	2	6	10	1452610	152	5	x	2	10	165x210	76	5	x	2	10	165x210	76		
1	0	4	20	310420	110	1	2	4	20	912420	139	1	1	6	20	2211620	183	1	x	4	20	171x420	57	1	x	4	20	171x420	57		
2	0	4	20	320420	111	2	2	4	20	922420	140	2	2	6	20	2221620	184	2	x	4	20	172x420	58	2	x	4	20	172x420	58		
3	0	4	20	330420	112	9	3	2	20	932420	141	22	3	1	20	2231620	185	17	3	x	4	20	173x420	59	17	3	x	4	20	173x420	59
4	0	4	20	340420	113	4	2	4	20	942420	142	4	1	6	20	2241620	186	4	x	4	20	174x420	60	4	x	4	20	174x420	60		
5	0	4	20	350420	114	5	2	4	20	952420	143	5	1	6	20	2251620	187	5	x	4	20	175x420	61	5	x	4	20	175x420	61		
1	0	4	10	410410	105	1	2	4	10	1012410	144	1	1	6	10	2311610	191	1	x	4	10	181x410	63	1	x	4	10	181x410	63		
2	0	4	10	420410	106	2	2	4	10	1022410	145	2	1	6	10	2321610	192	2	x	4	10	182x410	64	2	x	4	10	182x410	64		
4	0	4	10	430410	107	10	3	2	10	1032410	146	23	3	1	10	2331610	193	18	3	x	4	10	183x410	67	18	3	x	4	10	183x410	67
4	0	4	10	440410	108	4	2	4	10	1042410	147	4	1	6	10	2341610	194	4	x	4	10	184x410	68	4	x	4	10	184x410	68		
5	0	4	10	450410	109	5	2	4	10	1052410	148	5	1	6	10	2351610	195	5	x	4	10	185x410	69	5	x	4	10	185x410	69		
1	0	6	20	510620	158	1	1	6	20	1111620	130	1	x	6	20	201x620	176	1	x	6	20	201x620	176								
2	0	6	20	520620	159	2	1	6	20	1121620	131	2	x	6	20	202x620	177	2	x	6	20	202x620	177								
5	3	0	20	530620	160	11	3	6	20	1131620	132	20	3	6	20	203x620	178	20	3	x	6	20	203x620	178							
4	0	6	20	540620	161	4	1	6	20	1141620	133	4	x	6	20	204x620	179	4	x	6	20	204x620	179								
5	0	6	20	550620	162	5	1	6	20	1151620	134	5	x	6	20	205x620	180	5	x	6	20	205x620	180								
1	0	6	10	610610	163	1	1	6	10	1211610	125	1	x	6	10	211x610	171	1	x	6	10	211x610	171								
2	0	6	10	620610	164	2	1	6	10	1221610	126	2	x	6	10	212x610	172	2	x	6	10	212x610	172								
6	3	0	10	630610	165	12	3	6	10	1231610	127	21	3	x	10	213x610	173	21	3	x	6	10	213x610	173							
4	0	6	10	640610	166	4	1	6	10	1241610	128	4	x	6	10	214x610	174	4	x	6	10	214x610	174								
5	0	6	10	650610	167	5	1	6	10	1251610	129	5	x	6	10	215x610	175	5	x	6	10	215x610	175								

Figure 3.18: Overview of test plan that is used during the experiments.

Chapter 4

Experiments

The experiments performed provide this research with eight sources of information, originating from the eight sensors placed either inside the wedge or on the experiment setup. All sensors record for a duration of 5 seconds. Table 4.1 shows the used channels and sensors for the rigid and deformable tests.

Table 4.1: All sensors used in each experiment.

Channel	Rigid experiment	Deformable experiment
1	Pressure sensor 1	Pressure sensor 1
2	Pressure sensor 2	Pressure sensor 2
3	Pressure sensor 3	Pressure sensor 3
4	Pressure sensor 4	Linear potentiometer 1
5	Accelerometer 1 (Plate)	Accelerometer 1 (Plate)
6	Accelerometer 2 (Carriage)	Accelerometer 2 (Carriage)
7	- empty -	Linear potentiometer 2
8	Lightgate	Lightgate

The experiment has 4 pressure sensors on the surface of the wedge. Three are placed on one side (plate one, presented in figure 3.12) while the last is placed on the other side of the wedge (plate two, presented in figure 3.13). The single pressure sensor is used to check for symmetry of impact. This symmetry test is also done with the accelerometers and linear displacement sensors placed on either side of the wedge.

All drop data per combination is added to find the average over the runs, also, the standard deviation is calculated. The average of five runs is shown as a solid line in all plots in the coming sections. The standard deviation for each individual measurement is calculated and both subtracted and added to the mean and shown in a faded color.

To enhance readability, most graphs are placed in appendix C. All figures in appendix C are indicated with a "C".

4.1. Uncertainty analysis

There is some measurement error included in every measurement. An analysis of the results' uncertainty has been conducted to identify their significance. Errors are assumed to be unbiased, normally distributed, and independent occurrences. By repeating measurements at least five times and taking the average, the measurement error has been reduced for all impact velocity, pressure, acceleration and deformation data.

4.1.1. Accelerometer

A linearity error of $\leq 1\%$ is stated in the product sheet. This means that every measured value has a measurement uncertainty of 1%. The result from the accelerometer calibration analysis returns a calibration factor of 0.48%. This calibration factor fits within the boundaries of the provided linearity error on the product data sheet.

4.1.2. Pressure sensors

The pressure sensors were calibrated by the manufacturer. The results are provided in table 4.2.

Table 4.2: Uncertainty and linearity of all pressure sensors used in the experiment.

Pressure sensor #	Serial #	Linearity	Uncertainty
1	LW43493	0.07%	$\pm 1.3\%$
2	LW47339	0.05%	$\pm 1.0\%$
3	LW43494	0.06%	$\pm 1.3\%$
4	LW45663	0.10%	$\pm 1.0\%$

4.1.3. Potentiometer

The potentiometers were delivered with a linearity error chart. Both potentiometers showed $\geq 0.05\%$ linear error over the full length of the measurement. This means that every value has a measurement uncertainty of 0.05%

4.2. Hammer test analysis

When analyzing all recorded data it is of interest to have the ability to distinguish the various vibrations recorded in the measurements during impact. To analyze the various eigenfrequencies of the wedge a hammer test is performed with the wedge submerged as well as emerged from the water. The wedge is suspended in air and a recording is started. During a recording of 20 seconds, the plates of the wedge are struck with a hammer to induce vibrations. This process is repeated with a submerged wedge.

4.2.1. Emerged hammer test

Figure 4.1 shows an isolated impact from the hammer. From this graph the independent frequencies are almost impossible to distinguish.

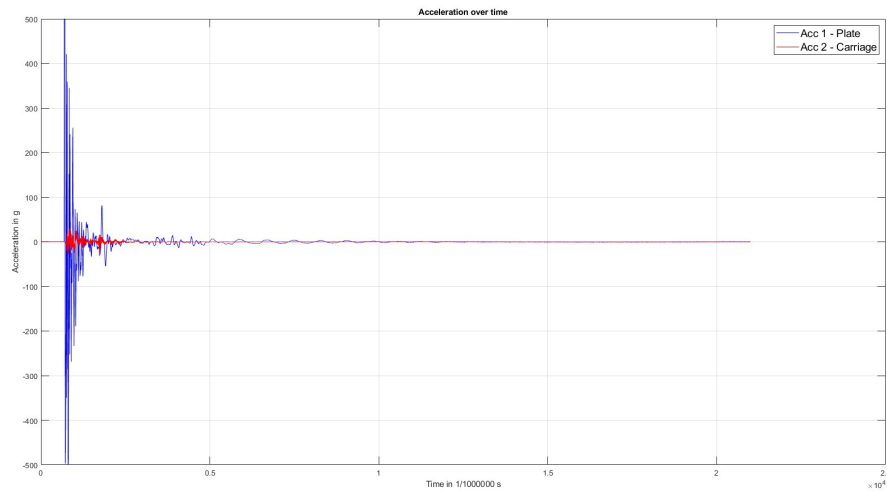
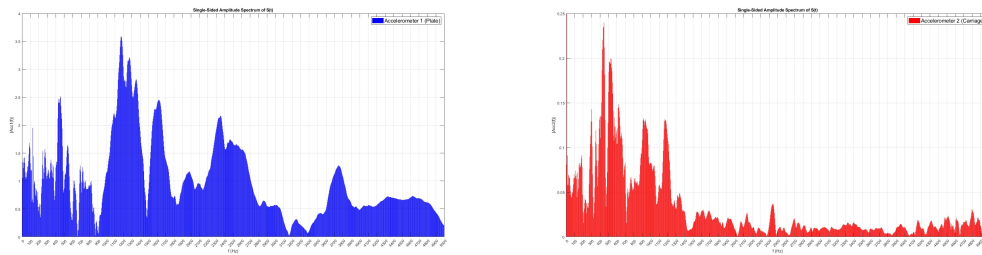


Figure 4.1: Graph of isolated single impact of emerged hammer test.

To get a better view of all the present vibrating frequencies, a fast Fourier transform is performed on the isolated impact. A fast Fourier transform (FFT) separates all individual frequencies (x-axis) and their amplitudes (y-axis). Figure 4.2 shows the FFT for the isolated impact in figure 4.1.



(a) FFT Plate

(b) FFT Carriage

Figure 4.2: Fast Fourier transform analysis of emerged hammer test

The Fourier analysis shows peaks in frequency around 450, 1200, 1300, 1600, 2350 and 3750Hz on the plate. The carriage has the largest frequency peaks around 450, 550, 900, and 1200Hz.

4.2.2. Submerged hammer test

For the submerged hammer test the wedge was suspended with the plates in water and the plates were struck with a hammer. This test is not really representative for an impact situation due to the water being completely around the plate. During impact the water is only in contact the bottom part of the wedge while the top part initially stays dry.

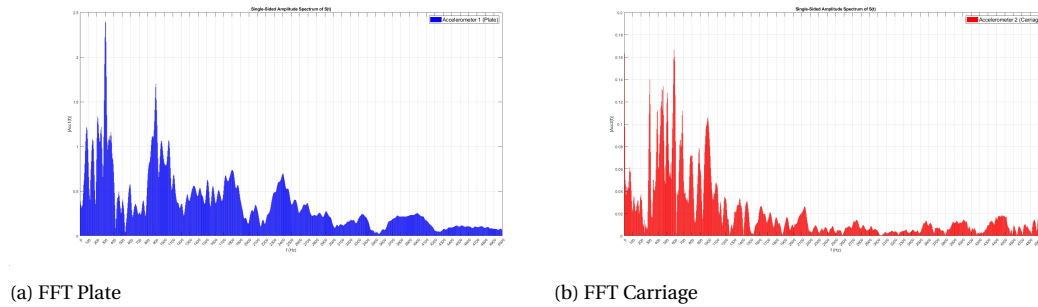


Figure 4.3: Fast Fourier transform analysis of emerged hammer test.

The Fourier transfer shows distinctive peaks around 300, 900, 1800 and 2400Hz on the plate. These frequencies are also expected to be lower than the dry test because of added mass. The carriage shows peaks in vibration around at 300, 450, 600, 800, 900 and 1000Hz. With these peaks from the submerged and emerged hammer test, better analysis can be done of the recordings made during the experiments.

4.3. Impact velocities

For this research the three impact velocities that were selected were 2, 4 and 6m/s. To reach these velocities different initial release heights are calculated with equation 3.1. The release heights were 20.4cm, 81.9cm and 185.3cm respectively. In these heights, air resistance is already taken into account. However, the final velocity is measured with a light gate for each run and analyzed. The final velocity is measured four times with the improved velocity measurement system.

4.3.1. 2m/s

To reach an impact velocity of 2m/s the wedge is released from a height of 204mm. Overall the 2m/s free fall showed the best consistency in velocity. This can have multiple reasons. The first reason is the height and therefore amount of rails from the tower required to reach the velocity. The carriage has less track to impact and therefore can reach its final velocity with higher consistency. Also, only half of the carriage had to transfer from tower to the tanks since the bottom half of the carriage started its test already in the tank. Finally, since the 2 m/s velocity is the lowest, the registration contains the largest number of data points in between each slot to calculate the average velocity. A higher number of measurements equals more accuracy of the velocity calculation.

The average final velocity was 1.929m/s and 1.931m/s for 10 and 20 degree deadrise angle respectively.

Using linear extrapolation and the average remaining free fall distance of 10mm the estimated impact velocity is 2m/s.

4.3.2. 4m/s

The 4m/s tests showed a higher standard deviation in the tests compared to the 2m/s tests. The explanation for this is already provided in the previous section. The average final velocity was 3.935m/s and 3.940m/s for 10 and 20 degree deadrise angle respectively. The slight difference in velocity for the different deadrise angles is expected to originate from measurement errors.

4.3.3. 6m/s

The 6m/s tests showed a higher standard deviation in the tests compared to the 2m/s tests. The explanation for this is already provided in the previous section. The average final velocity was 5.981m/s and 5.863m/s for 10 and 20 degree deadrise angle respectively. This difference is unexpected. The opposite difference in velocity would have made more sense, because it could then be attributed to air resistance. This effect is not visible at the lower two velocities due to the fact that the air resistance factor is lower than all other frictions the carriage experiences during free fall. The only explanation that can be given is measurement error.

4.3.4. Overview of all rigid impact velocities

Table 4.3 shows all average final velocities of the wedge setups used in the rigid experiments. It shows that for the 2 and 4m/s impacts the final velocity did not vary substantially, where the 6m/s shows a clear difference between 10 and 20 degrees deadrise. The wet mass of the rigid wedge is 9.53kg.

Table 4.3: All measured average velocities in rigid experiment. Indicated per velocity and deadrise combination.

Expected velocity and deadrise	Average final velocity of all five impacts
<i>2m/s</i> , 10deg	<i>1.93m/s</i>
<i>2m/s</i> , 20deg	<i>1.93m/s</i>
<i>4m/s</i> , 10deg	<i>3.93m/s</i>
<i>4m/s</i> , 20deg	<i>3.94m/s</i>
<i>6m/s</i> , 10deg	<i>5.98m/s</i>
<i>6m/s</i> , 20deg	<i>5.86m/s</i>

4.3.5. Overview of all deformable impact velocities

Reviewing all the impact velocities from the deformable experiment it becomes clear that the impact velocity tends to be higher for the 20 degree deadrise angle compared to its 10 degree counterpart with the same release height for 6m/s. This can be explained by the effect of air resistance having an increasing impact on the velocity of the wedge. Table 4.4 shows all impact velocities and the corresponding wet mass of the wedge.

Table 4.4: All measured average maximum velocities, indicated per expected velocity and deadrise combination. In the third column the total wet mass of the wedge is provided

Expected velocity and deadrise	Final velocity in m/s	Total (wet) mass of wedge in kg
2m/s, 10deg, 4N/mm	1.94	
2m/s, 20deg, 4N/mm	1.94	
4m/s, 10deg, 4N/mm	3.93	9.41
4m/s, 20deg, 4N/mm	3.92	
6m/s, 10deg, 4N/mm	5.96	
6m/s, 20deg, 4N/mm	5.75	
4m/s, 10deg, 10N/mm	3.88	9.76
4m/s, 20deg, 10N/mm	3.92	
4m/s, 10deg, 30N/mm	3.91	10.37
4m/s, 20deg, 30N/mm	3.85	
6m/s, 10deg, 10N/mm	5.95	9.76
6m/s, 20deg, 10N/mm	5.97	
6m/s, 10deg, 30N/mm	5.91	10.37
6m/s, 20deg, 30N/mm	5.99	

4.4. Impact rigid wedge

The rigid tests are performed to create a base line to later use to compare the deformable tests to. During the tests it turned out that the 0 degree deadrise angle impacts produced accelerations above 500g which is a risk for permanent damage to the acceleration sensors. To prevent damage due to too high accelerations the planned 0 degree deadrise angles were cancelled. First, all graphs are presented for each separate run, then all graphs are discussed. The 6m/s experiment was performed without pressure sensor four due to time constraints. Symmetry of the impact can therefore not be guaranteed based on the pressures.

4.4.1. Pressure analysis

The pressure of the rigid tests is analyzed by comparing the pressures of pressure sensor two and four for symmetry. Then the impact pressures in general are discussed

Symmetry

Table 4.5 shows all rigid average maximum pressures. Generally there is agreement between the averages of pressure sensor 2 and 4. The largest difference in pressure is recorded in the 4m/s, 10 degree impact. Overall it can be observed that the pressure difference varies around 10% between the pressure sensors. This difference most likely comes from a slight angle under which the carriage is impacting the free surface. This angle results in a lower deadrise on one end of the wedge and higher deadrise on the opposite side. A play of 3mm at the carriage results in a 10% higher or lower pressure. From the 10% difference in pressure it can be concluded that the impact angle of the complete wedge with respect to the free surface is important for a symmetric impact and pressures on the system.

General

Generally a few key points can be observed from the six pressure graphs presented in figure C.4. They are stated below:

For all impacts a clear peak pressure for all pressure sensors is recorded on impact with the free surface. As expected, pressure sensor 3, being the closest to the keel of the wedge records the first increase in pressure, followed by pressure sensor 2 and 4 on the other side, Finally pressure sensor 1 records a pressure, being closest to the chine of the wedge. Generally, the standard deviation is not far from the average. Only the 2m/s at 10 degree deadrise impacts showed higher standard deviation compared to the rest of the tests.

For all impacts, except 2m/s at 10 degrees, pressure sensor 3 records the highest average peak pressure. The idea of multiple impact pressures and deadrise angles was to find impacts with varying pressure distributions over the wedge, causing the highest peak pressure to occur on pressure sensor 3 for some impacts and on pressure sensor 1 for other impacts. Unfortunately, this did not happen as pronounced as planned. This might have to do with the fact that the wedge is not completely angular at the keel due to its novel hinging system.

In some pressure recordings, a pressure fluctuation is visible before the peak pressure. This fluctuation can be justified with two factors. The first one being a high velocity airflow past the pressure sensors' diaphragm. This fast flowing air is caused by the first flow of water being accelerated outward from the wedge, pushing air in front of it. Because of the Bernoulli principle of conservation of mass and momentum the pressure drops with increasing air flow.

The pressure fluctuation after the pressure peaks can originate from multiple factors. When performing a fast Fourier transform (FFT) analysis on one of the pressure recordings, it showed that mainly low frequent vibrations are present. Frequencies that were most prominent were 50Hz and 100Hz, then small peaks are visible for 750Hz and 1000Hz. The low frequencies can be related to vibrations of the tank. The high frequency measurements can be linked to the resonating parts in the wedge such as the plate.

All maximum pressures

Table 4.5: All measured average velocities and maximum values from average pressure of five runs in rigid experiment. Indicated per velocity and deadrise combination.

Expected velocity and deadrise	Final velocity in m/s	Maximum pressure in Pascal			
		P1	P2	P3	P4
2m/s, 10deg	1.93	7.14E+04	9.27E+04	8.12E+04	8.12E+04
2m/s, 20deg	1.93	2.12E+04	2.99E+04	3.13E+04	2.99E+04
4m/s, 10deg	3.93	3.01E+05	2.97E+05	3.25E+05	2.71E+05
4m/s, 20deg	3.94	7.40E+04	9.01E+04	1.18E+05	1.00E+05
6m/s, 10deg	5.98	3.95E+05	5.39E+05	6.83E+05	x
6m/s, 20deg	5.86	1.72E+05	2.15E+05	2.64E+05	x

4.4.2. Acceleration analysis

Next to the graphs shown in figure C.3 an FFT is performed for all impacts. For most impacts, the plate mounted accelerometer recorded frequency peaks around 100 and 150Hz. For the 10 degree deadrise angle impacts peaks in frequency were visible around 300 to

400Hz where the 20 degree impacts showed either lower or higher frequency peaks, 250Hz or 450Hz.

The carriage showed peak frequencies around 50 and 100Hz for all impacts.

The following conclusions can be drawn from this set of graphs.

The increasing acceleration for increasing impact velocity and decreasing deadrise angle follows all expectations and can be explained. First, decreasing deadrise results in a less optimal hydrodynamic shape to penetrate the water surface. Water will have to be displaced at a higher rate on impact for a lower deadrise angle, hence the water needs to be accelerated faster, resulting in higher forces. A similar explanation follows for increasing impact velocity. The wedge penetrates the water at higher velocity and therefore the mass of the water has to be displaced at a higher rate, resulting in higher forces.

Higher accelerations on the plate were visible for all impacts, regardless of deadrise or impact velocity. Also, vibrations continued longer on the plate compared to the carriage on all impacts.

4.4.3. Comparison with previous drop test experiment

In earlier experiments a wedge with 15 degrees deadrise angle is dropped to reach a final velocity of about 6.2m/s. To find out if the recent experiments yield results that seem likely they are compared to the previous experiment. The previous experiment made use of a completely different concept. The wedge was made out of mostly wooden components and had to be buoyant. The keel of the wedge was sharper compared to the wedge used in the current experiment and the sensors were placed in different locations.

Pressure comparison

The maximum pressure recorded on the pressure sensors during this impact was between 300kPa and 400kPa. In this experiment the wedge was set at 10 and 20 degrees deadrise angle. If the impacts in this experiment are valid, the 10 degree deadrise at 6m/s should show pressures slightly higher than the found results from earlier experiments and the opposite should be true for the 20 degree deadrise.

The average pressure on impact of the 10 degree deadrise impacts are between 400kPa and 700kPa. The average pressure on impact of the 20 degree deadrise impacts are between 175kPa and 250kPa. This means that the found pressures for the 6m/s impacts are following the expected trend, which can be seen as a validation of the current measurements.

Acceleration comparison

Similar to the pressure comparison, a run of the previous experiment for 15 degrees is analyzed with an FFT and compared to the experiments performed for this report. The previous experiment had a single accelerometer placed on the wedge. To analyze the vibrations of the tank, a second accelerometer was placed on the tank. The FFT graph for the wedge shows considerably more accelerations during free fall. The following conclusions are made: on impact the wedge showed peaks in vibration around 50 to 150Hz and around 2500Hz. As a result of the impact the tank showed vibrations of 100Hz. The maximum recorded acceleration on impact was 125g

The maximum recorded acceleration with the recent test were slightly over 300g for the 10 degree impact and about 100g for the 20 degree impact. This means that the impacts overall fit the expected accelerations on impact.

4.5. Impact deformable wedge

4.5.1. Preload springs

Table 4.6 shows the preload in the springs for every spring setup used during the experiments. It is clear that the preload for the 10.58N spring is not evenly distributed. This is because the setup that was used did not provide live readout of the tension which made it really hard and time consuming to analyze the preload. With the expected pressures the pre load is negligible which might help overcome this issue.

Spring 1 and 2 were connected to plate 2 and spring 3 and 4 were connected to plate 1 in all experiments.

Table 4.6: Preload in springs in N.

spring	Spring stiffness in N/mm		
	3.82	10.58	29.5
1	4.7N	42.7N	20.8N
2	4.7N	0.7N	20.6N
3	3.0N	15.8N	22.3N
4	1.1N	2.7N	16.2N

4.5.2. Pressure analysis

The average maximum pressures of all deformable impacts are shown in table 4.7.

Table 4.7: All measured average velocities and maximum values from average pressure of five runs in rigid and deformable experiment. Indicated per velocity and deadrise combination.

Expected velocity and deadrise	Final velocity in m/s	Maximum pressure in Pascal		
		P1	P2	P3
2m/s, 10deg, 3.82N/mm	1.94	3.46E+04	7.52E+04	8.30E+04
2m/s, 20deg, 3.82N/mm	1.94	1.16E+04	2.95E+04	2.97E+04
4m/s, 10deg, 3.82N/mm	3.93	7.05E+04	2.57E+05	2.81E+05
4m/s, 20deg, 3.82N/mm	3.92	3.05E+04	1.04E+05	1.06E+05
6m/s, 10deg, 3.82N/mm	5.96	1.44E+05	4.93E+05	6.07E+05
6m/s, 20deg, 3.82N/mm	5.75	6.29E+04	1.81E+05	2.31E+05
4m/s, 10deg, 10.58N/mm	3.88	1.24E+05	2.58E+05	2.80E+05
4m/s, 20deg, 10.58N/mm	3.92	4.04E+04	1.05E+05	1.07E+05
4m/s, 10deg, 29.5N/mm	3.91	1.59E+05	2.92E+05	2.69E+05
4m/s, 20deg, 29.5N/mm	3.85	5.46E+04	1.07E+05	1.14E+05
6m/s, 10deg, 10.58N/mm	5.95	2.46E+05	5.34E+05	6.83E+05
6m/s, 20deg, 10.58N/mm	5.97	7.86E+04	1.97E+05	2.40E+05
6m/s, 10deg, 29.5N/mm	5.91	3.33E+05	5.18E+05	6.39E+05
6m/s, 20deg, 29.5N/mm	5.99	9.78E+04	1.99E+05	2.30E+05

The following observations are made from the pressure graphs of the deformable tests; Not all impacts recorded a highest peak pressure on pressure sensor 3. This is remarkable since on the rigid impacts all impacts showed the highest pressure on this sensor. This difference in peak pressure can only be a result of the deformation on impact. Most pressures show a decrease in pressure before the peak. This is expected to be a result of the airflow past the sensor right before impact. For this experiment it can also be a low pressure zone

created by the deformation of the plate during impact. Finally it is clear to see that the duration of the peak pressure decreases with the increasing impact velocity and decreasing deadrise angle.

4.5.3. Acceleration analysis

Carriage

All acceleration graphs of the impact during the deformable experiments were reviewed. Some remarkable sightings are discussed below.

After initial acceleration, almost every graph shows a second peak acceleration within 6 to 8ms. This acceleration consists of high frequency vibrations. Also the carriage mounted accelerometer shows two short peaks in the same time the plate shows the first acceleration.

Plate

On impact, the plate shows more oscillations in acceleration compared to the rigid impacts. Increasing spring stiffness results in decreasing vibration period, while the frequency of the vibrations does not increase. Possible explanation for this is that the mass and spring stiffness combination has a distinct eigenfrequency that is less induced by the same impact. When spring stiffness is increased while impact velocity and deadrise remain unchanged, the first acceleration peak after impact does not change substantially.

4.5.4. Deformation analysis

From the analysis of the data from the potentiometer it turns out that most deformation happens post initial impact. To show the deformation during impact the pressure and deformation are plotted in the same figure.

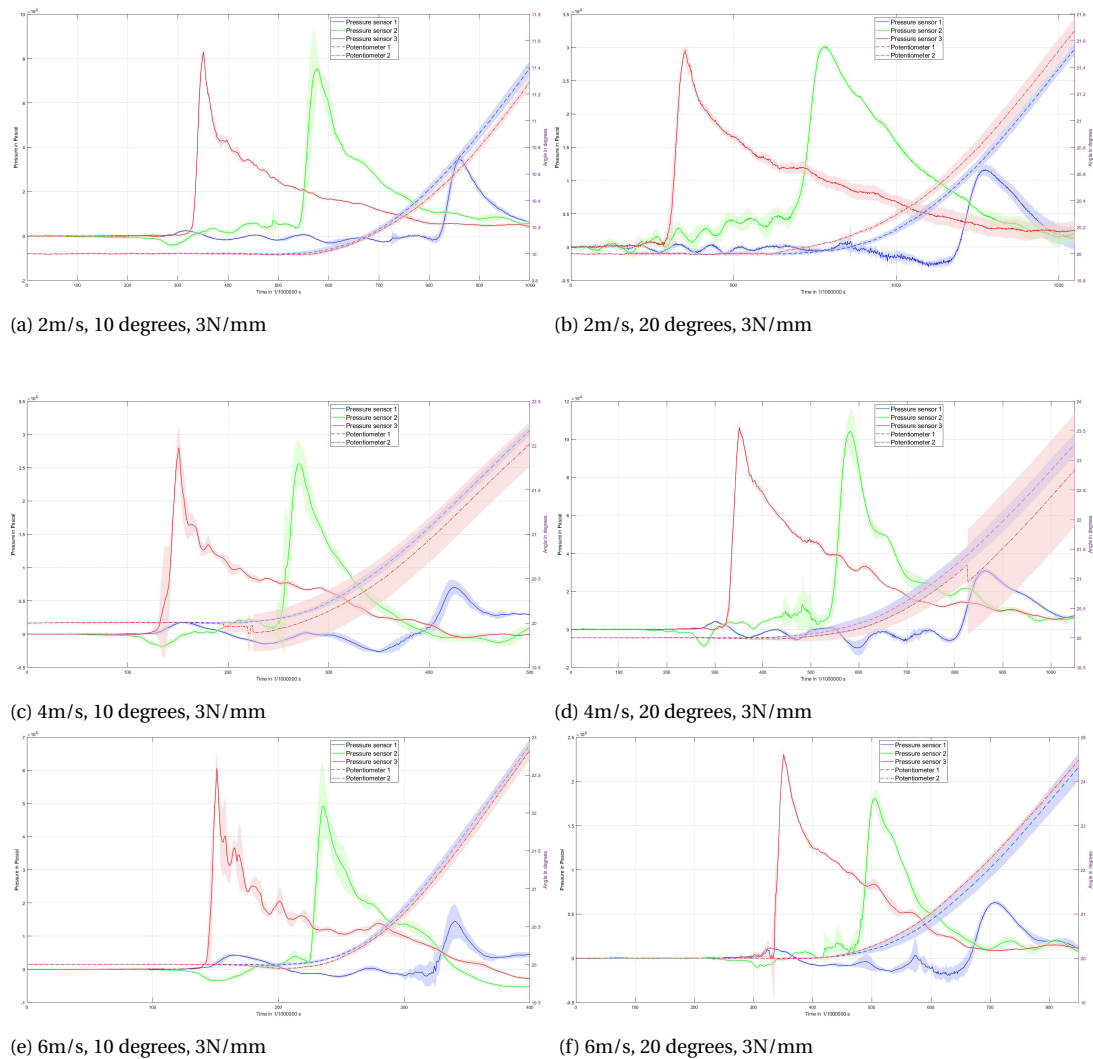


Figure 4.4: Overview of all pressure and deformation graphs, focused on the initial impact period.

4.6. Post-impact rigid wedge

During the post-impact analysis it turned out that a property of the sensors influenced the results in the readings. Since post-impact behaviour of the wedge shows quasi-static responses, the quartz sensors show a decay in their signals. This can be accounted for but for a first analysis this is not required.

4.6.1. Pressure analysis

From the post-impact pressure analysis the following conclusions can be drawn: All post-impact pressures oscillate around 5000Pa with a frequency of about 20 to 28Hz and an amplitude of 2500Pa, from earlier experiments, these oscillations trace back to vibrations of the tank wall. Next to this relatively low frequency, other frequencies around 120Hz were also present. The origin of the 120Hz frequencies are expected to be the result of the vibrating tank which has an eigenfrequency in the vicinity of this frequency.

4.6.2. Acceleration analysis

For acceleration the same 20-28Hz oscillations visible in accelerometer 1 and accelerometer 2, together with 400Hz vibrations. It could be that the oscillation of pressure is linked to the oscillations of the plate which translate through the spines of the wedge into the accelerometer on to the accelerometer on the carriage. Finally, also 400Hz vibrations are visible in both accelerometers.

4.7. Post-impact deformable wedge

4.7.1. Pressure analysis

For some impacts, similar 20-28Hz oscillations in pressure were visible, for example the 6m/s, 10deg, 30N/mm combination. For all different wedge setups, different oscillations with varying amplitudes and frequencies were visible. For all impacts, all post-impact pressures oscillate around 5000Pa. The wedge setup with the most interesting deformation response was the 29.5N/mm spring for both deadrise angles (10 and 20 degrees) with impact velocity of 4m/s and 6m/s. The response of this specific setup shows an oscillating wedge plate during the full range of the impact and post-impact. Figure 4.5 shows the graph with the oscillation of the plate. During further analysis of this phenomenon, the oscillations of the plate are referred to as fluttering. In section 3.6, an estimate was made regarding the R-ratio. No dynamic response was expected but now the results imply otherwise.

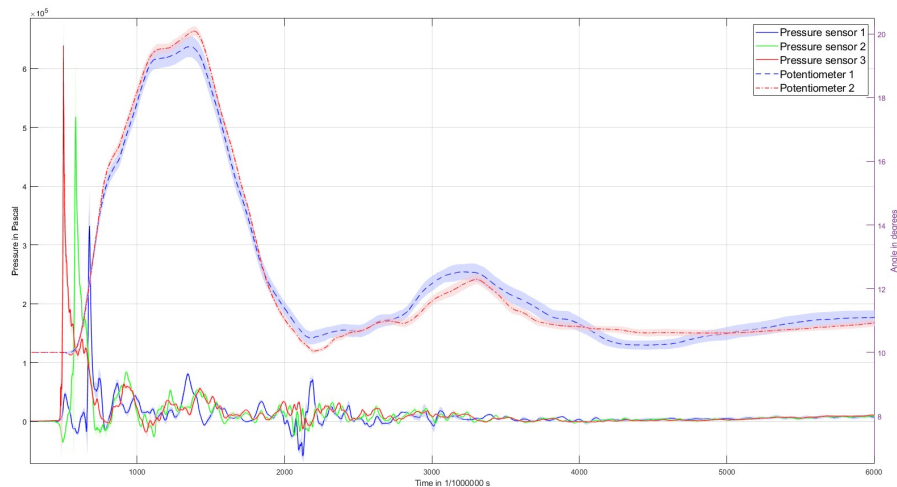


Figure 4.5: Pressure and deformation of wedge impact with following setup: 6m/s, 10 degree deadrise angle and 29.5N/mm spring.

4.7.2. Acceleration analysis

On the plate-mounted accelerometer, peaks in frequency are recorded around 60, 180 and 300Hz. On the the carriage mounted accelerometer, lower peaks in the frequency analysis are visible. Around 10, 20 and 35Hz.

4.7.3. Deformation analysis

All graphs from this analysis can be found in figure C.5, C.6 and C.7.

Table 4.8: Maximum deformation in degrees on impact. Third value in experiment column is spring stiffness in N/mm.

Experiment	Maximum pressure in Pascal			Max def. in degrees		Post-impact def. in degrees	
	P1	P2	P3	Plate 1	Plate 2	Plate 1	Plate 2
2m/s, 10deg, 3.82	3.46E+04	7.52E+04	8.30E+04	7.4	8.2	2.3	1.2
2m/s, 20deg, 3.82	1.16E+04	2.95E+04	2.97E+04	5.5	6.2	3	2.3
4m/s, 10deg, 3.82	7.05E+04	2.57E+05	2.81E+05	19.2	20.4	3.8	2.8
4m/s, 20deg, 3.82	3.05E+04	1.04E+05	1.06E+05	15.2	15.6	5	2.6
6m/s, 10deg, 3.82	1.44E+05	4.93E+05	6.07E+05	32.1	31.8	5.3	3.8
6m/s, 20deg, 3.83	6.29E+04	1.81E+05	2.31E+05	26.1	26.7	6.6	5.1
4m/s, 10deg, 10.58	1.24E+05	2.58E+05	2.80E+05	12.0	12.8	1.6	1.7
4m/s, 20deg, 10.58	4.04E+04	1.05E+05	1.07E+05	9.4	9.8	1.6	1.6
4m/s, 10deg, 29.50	1.59E+05	2.92E+05	2.69E+05	5.2	5.6	0.6	0.5
4m/s, 20deg, 29.50	5.46E+04	1.07E+05	1.14E+05	3.8	3.8	0.8	0.9
6m/s, 10deg, 10.58	2.46E+05	5.34E+05	6.83E+05	19.4	19.8	2.2	1.6
6m/s, 20deg, 10.58	7.86E+04	1.97E+05	2.40E+05	15.6	16.1	0.25	0.3
6m/s, 10deg, 29.50	3.33E+05	5.18E+05	6.39E+05	9.6	10.1	1.1	1
6m/s, 20deg, 29.50	9.78E+04	1.99E+05	2.30E+05	7.3	7.6	1	0.8

If we plot the maximum deformation on a y-axis against an increasing impact velocity and deadrise on the y-axis, we see an almost linear line in decrease for a linear decreasing impact velocity. As the force scales with velocity squared, a quadratic decrease in max. deformation was expected for a single spring stiffness.

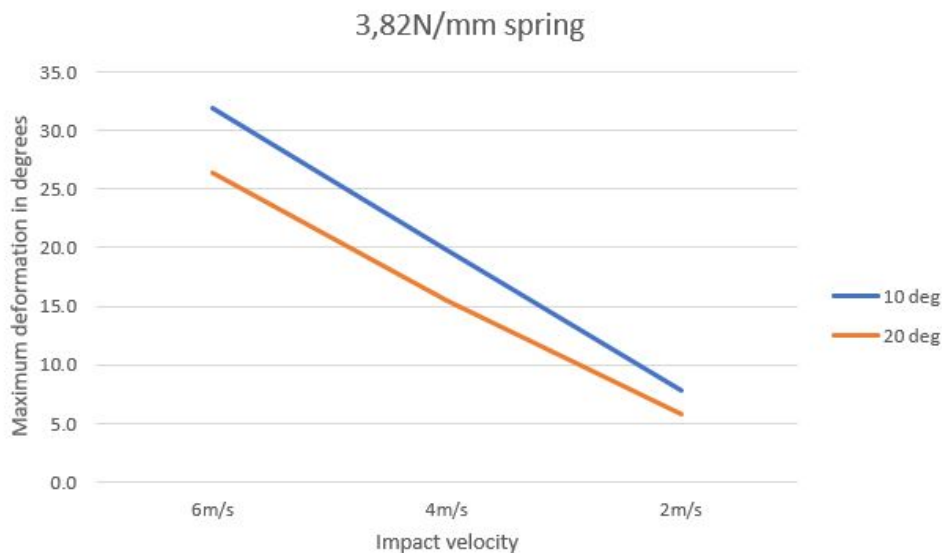


Figure 4.6: Progression of deformation with varying deadrise and impact velocity.

In figure 4.7 and 4.8 the same linear decrease is visible, now with the impact velocity as a constant in both individual graphs. The spring stiffness increases quadratically in these graphs. It was expected that the maximum deformation would also decrease quadratically then. But for the cases with 4m/s, the maximum deformation decreases linearly. For 6m/s

the decrease in max deformation is somewhat non-linear, but the non-linearity is not pronounced.

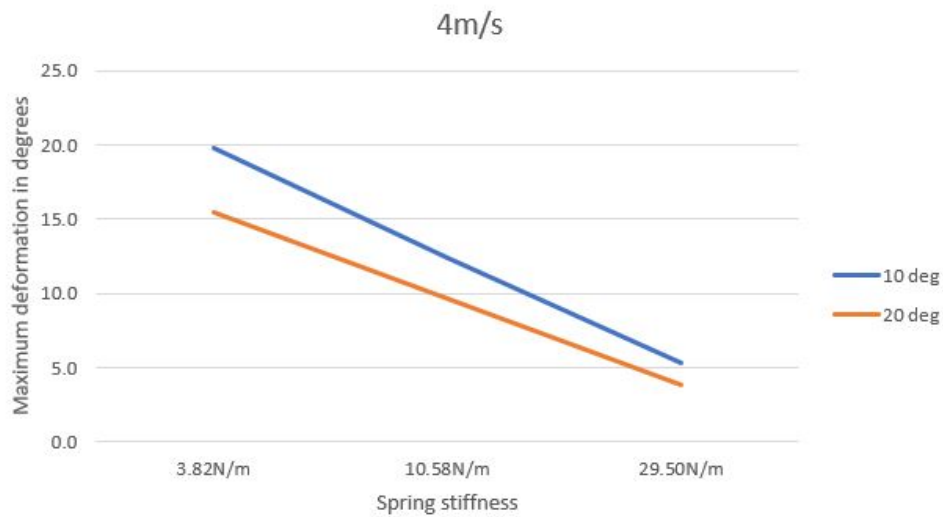


Figure 4.7: Progression of deformation with varying deadrise and spring stiffness.

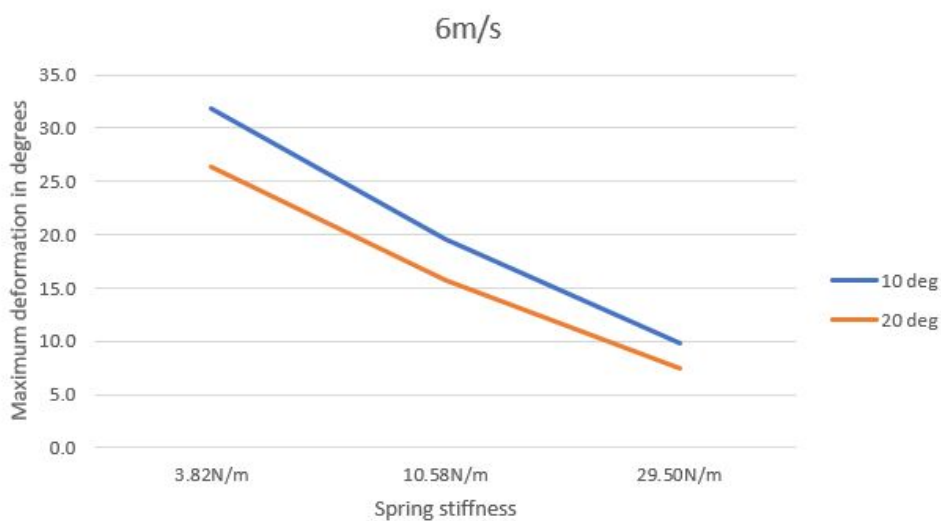


Figure 4.8: Progression of deformation with varying deadrise and spring stiffness, for constant impact velocity.

For low impact velocity impacts quasi-static response is visible. The plates rotate inward at first impact, then come down slightly after initial impact and then return to initial condition at the end of the run. Potentiometer 1 shows signs of a higher friction coefficient than potentiometer 2. This is determined due to lower amplitude response on all impacts. Since it is visible on all impacts it is ruled out that the difference is only due to the oblique wedge penetration. For a few impacts, fluttering effect is visible on the wedge plates during impact and post-impact penetration.

4.8. Comparison deformable and rigid impacts

The main goal of this research was to look for differences in pressure for a deformable wedge compared to a rigid wedge. In the previous sections various analyses were performed on rigid as well as deformable wedges. Since multiple setups of the deformable wedge are tested, multiple comparisons are made in the next chapter.

4.8.1. Rigid compared to deformable with 3.82N/mm spring and 10 degree dead-rise

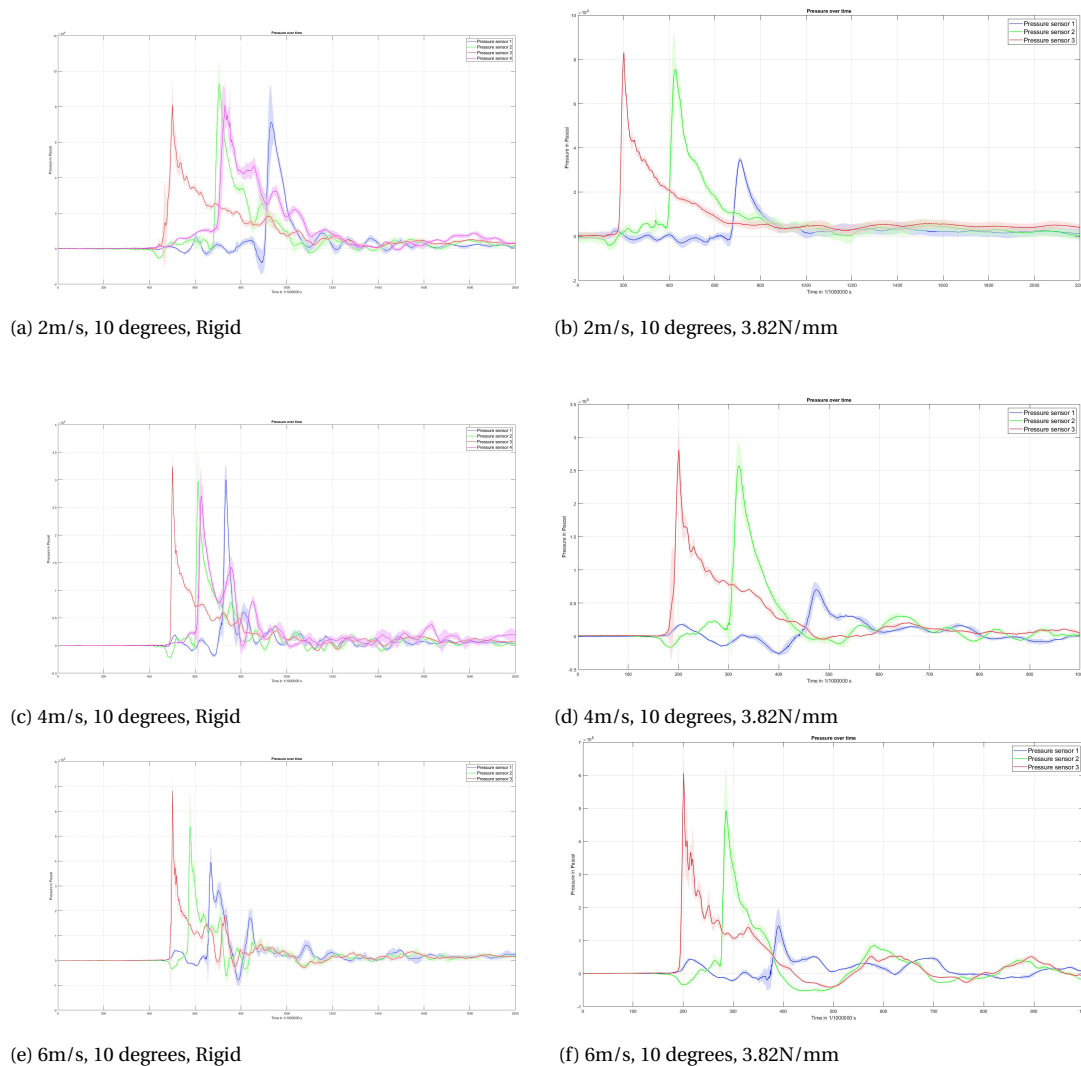


Figure 4.9: Overview of all pressure graphs from the rigid tests.

From the figures the following observations are made: The peak pressures recorded for P3 and P2 are slightly lower in the deformable experiments compared to the rigid experiments. Peak pressures are substantially lower for P1 during the deformable runs, sometimes up to 77%. The deformable pressure graphs show oscillations with higher amplitudes after the peak pressure in the 2m/s tests, whereas the rigid pressure graphs show oscillations with higher amplitudes after the peak pressure in the 4m/s and 6m/s tests. Finally, the area under the peak pressure seems higher for the deformable wedge impacts compared to the

rigid wedge indicating a higher average pressure.

To create a better perspective of the peak pressure difference on impact, the time histories of the individual pressure sensors from the rigid and deformable experiments are plotted in a single graph.

Figure 4.10, 4.11 and 4.12 show the time histories of pressure sensors 3, 2 and 1 respectively. The deformable run is performed with the 3.82N/mm spring.

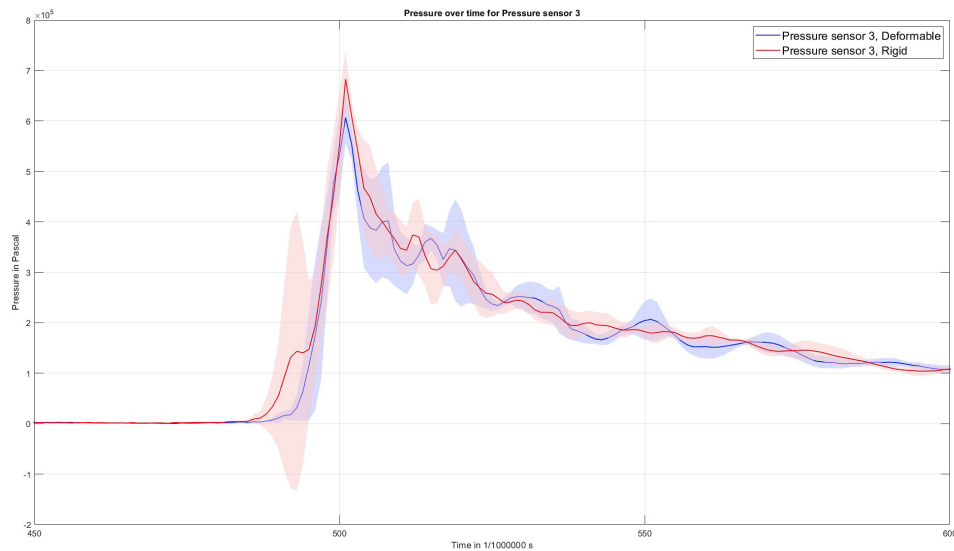


Figure 4.10: Pressure sensor 3 time-history for rigid and deformable impact.

In figure 4.10 it is clear to see that the deformable wedge shows a lower peak pressure. Generally, the shape of the graph is similar.

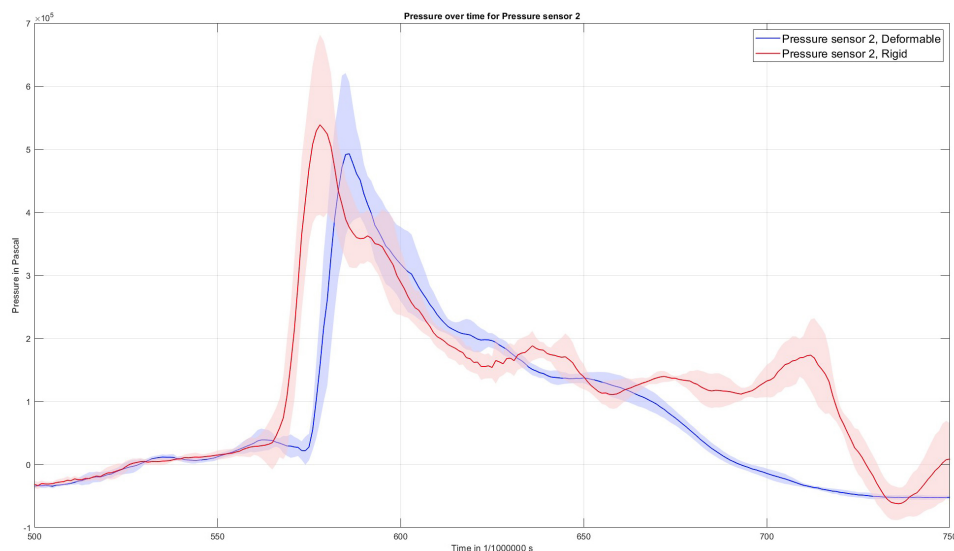


Figure 4.11: Pressure sensor 2 time history for rigid and deformable impact.

In figure 4.11, a similar peak pressure decrease is visible for the deformable runs. Again, the shape of the graph resembles the rigid run, only now there is a time delay visible for

the deformable peak pressure. Although unsure, it might have something to do with the fact that it takes longer for the pressure to reach the pressure sensor physically due to the rotation of the wedge. Finally, the pressure of the deformable wedge seems to be smoothed out slightly, the oscillations have a longer period and lower amplitudes post impact.

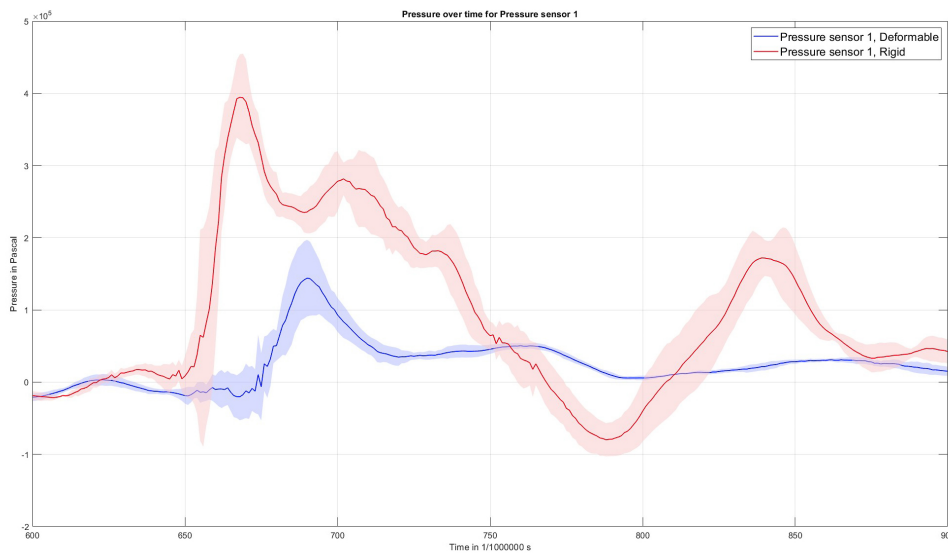


Figure 4.12: Pressure sensor 1 time history for rigid and deformable impact.

Finally, figure 4.12 shows the largest pressure decrease for pressure sensor 1. The shape of the pressure graph also does not resemble the rigid pressure graph any more. Again we see a delay in pressure, this time slightly larger than the delay visible in figure 4.11. Similarly to pressure sensor 2, the time history for pressure sensor 3 seems to have longer periodic oscillations and lower amplitudes post impact.

4.8.2. Rigid compared to deformable with 3.82N/mm spring and 20 degree dead-rise

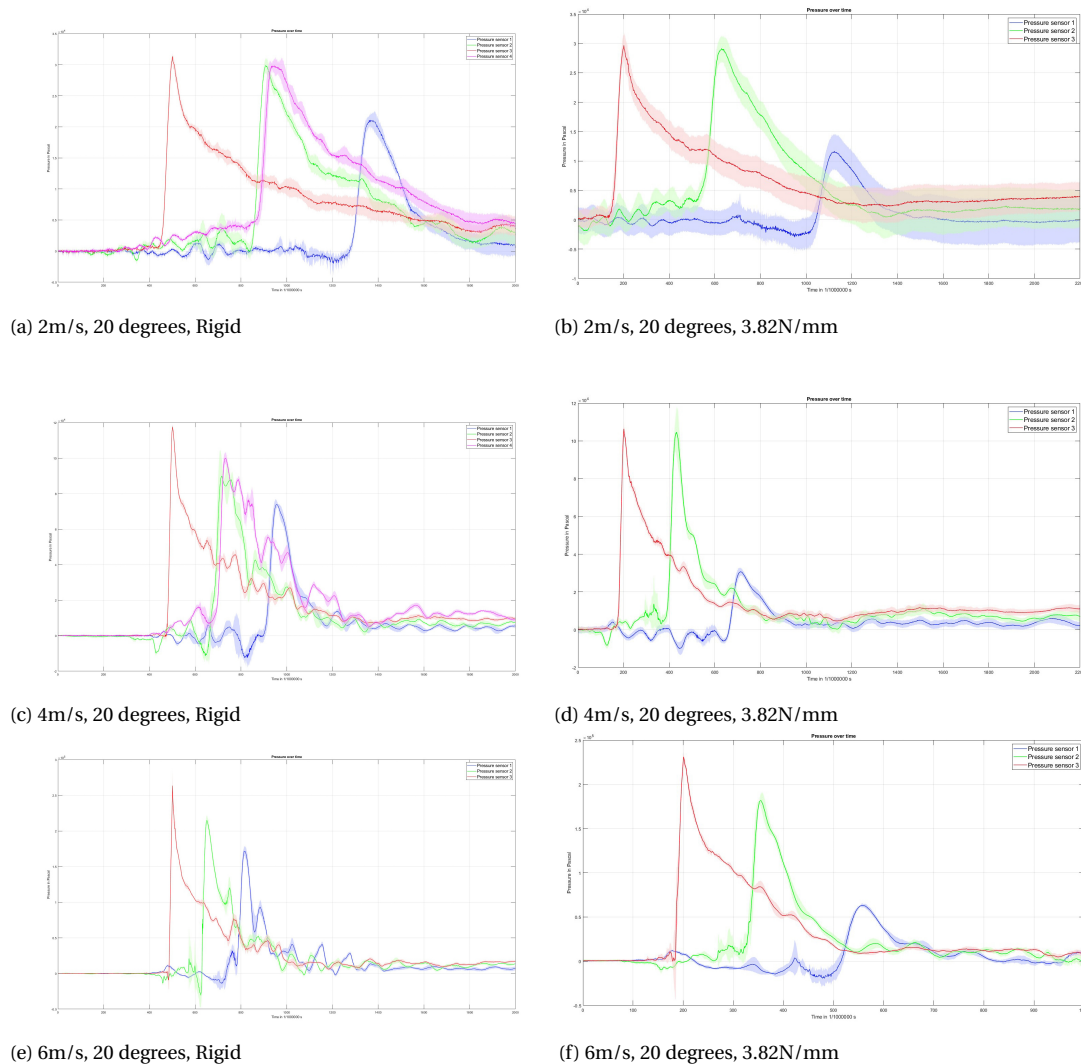


Figure 4.13: Overview of all pressure graphs from the rigid tests.

The main observation that was made is that all differences and similarities from the 20 degree deadrise impacts were also found in the 10 degree deadrise impacts. The maximum pressures of all rigid runs and the same runs performed with the 3.82N/mm spring are summarized in table 4.9.

Table 4.9: Rigid and deformable maximum pressures.

Expected velocity and deadrise	Final velocity in m/s	Maximum pressure in Pascal		
		P1	P2	P3
2m/s, 10deg Rigid	1.93	7.14E+04	9.27E+04	8.12E+04
2m/s, 20deg Rigid	1.93	2.12E+04	2.99E+04	3.13E+04
4m/s, 10deg Rigid	3.93	3.01E+05	2.97E+05	3.25E+05
4m/s, 20deg Rigid	3.94	7.40E+04	9.01E+04	1.18E+05
6m/s, 10deg Rigid	5.98	3.95E+05	5.39E+05	6.83E+05
6m/s, 20deg Rigid	5.86	1.72E+05	2.15E+05	2.64E+05
2m/s, 10deg, 3.82N/mm	1.94	3.46E+04	7.54E+04	8.32E+04
2m/s, 20deg, 3.82N/mm	1.94	1.17E+04	2.92E+04	2.89E+04
4m/s, 10deg, 3.82N/mm	3.93	7.03E+04	2.57E+05	2.81E+05
4m/s, 20deg, 3.82N/mm	3.92	3.07E+04	1.05E+05	1.06E+05
6m/s, 10deg, 3.82N/mm	5.96	1.44E+05	4.93E+05	6.06E+05
6m/s, 20deg, 3.82N/mm	5.75	6.32E+04	1.82E+05	2.31E+05

To provide a better overview of the difference in pressures the first six deformable maximum pressures are analyzed against the maximum pressures of the rigid impacts and their difference displayed in percentages in table 4.10. The main conclusion from the table 4.10 is that generally the pressure drops for most deformable runs. The largest drop is visible on pressure sensor 1, closest to the chine. The change in pressure for pressure sensors 2 and 3 show inconsistency.

Table 4.10: Pressure reduction percentage for a series of impacts.

	Pressure reduction percentage		
	P1	P2	P3
2m/s 10deg 4N/mm	-52%	-19%	+2%
2m/s 20deg 4N/mm	-45%	-3%	-8%
4m/s 10deg 4N/mm	-77%	-14%	-13%
4m/s 20deg 4N/mm	-59%	+16%	-10%
6m/s 10deg 4N/mm	-63%	-8%	-11%
6m/s 20deg 4N/mm	-63%	-15%	-12%

4.9. Free fall of all drops

Pressure analysis

During the free fall stage of the drop, no real pressure fluctuations are visible. The transition from tower to tank seems to show in some of the graphs but is not very pronounced.

4.9.1. Acceleration analysis

The first part of each test is the release of the wedge by shutting off the electromagnet, initiating the free fall of the wedge up to the impact with the free surface. In this section the time from release to impact is analyzed for each impact velocity increment.

Rigid, 2m/s, 10 and 20 degree deadrise

Figure 4.14 shows the acceleration measurements of the 2m/s, 20 degree, rigid impacts. Accelerometer 1 is calibrated to start at 0 and corrected for angle.

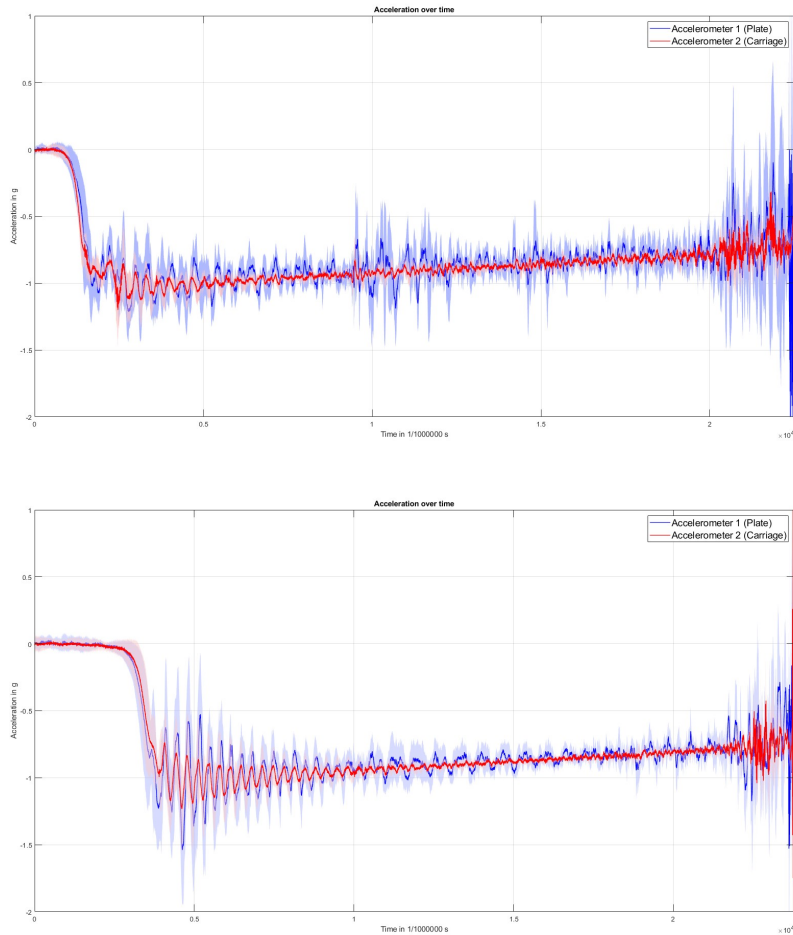


Figure 4.14: Rigid, 2m/s, 10(top) and 20(bottom) degree deadrise acceleration during free fall.

The following observations are made:

First of all, a 0g measurement is visible in the graph at the start of the graph. The 0g measurement at standstill means that the accelerometers used in this experiment only measure relative acceleration. Only when the accelerometers accelerate in space they measure an acceleration instead of showing 1 g of acceleration at standstill.

The accelerometer mounted on the plate shows larger amplitude acceleration peaks in the signal. The plate shows higher accelerations due to two reasons. The first one being play in the construction. All connections in the wedge have some form of play which causes slight vibrations to be amplified. Also, the accelerometer on the carriage is placed near the COG of the wedge. The accelerometer on the plate is located near the bottom and to the edge of the wedge which results in higher local accelerations due to rotations around the COG of the wedge.

For both accelerometers a $\pm 300\text{Hz}$ vibration is visible during free fall. The 300Hz vibrations can come from impacts with the tower. During the free fall the oscillations seem

to be damped. The dampening effect in the vibration is related to the energy lost on each impact.

The slow rise from $-1g$ towards $0g$ during free fall can be linked to slowly increasing resistance from air and moving parts, guiding the wedge down. Also, the acceleration downwards is constant at $-1g$. The sensors used have a discharge time which causes the signal to fade at constant acceleration. It is most likely that this discharge effect is the reason for the decreasing measured acceleration.

Right before impact with the free surface, an acceleration peak is visible. The high accelerations can be linked to the transition of the carriage from tower to tank. The transition is not perfectly smooth and causes slight impacts to occur. These impacts are recorded by both accelerometers.

Rigid, 4m/s, 10 and 20 degree deadrise

In figure C.1 in Appendix C not much differences can be indicated from the 2m/s impacts. It is clearly visible that the free fall happens over a longer time period. The accelerations near the end of the graph show slightly larger amplitudes which can be related to the higher velocity at the time of transition between tower and tank.

Rigid, 6m/s, 10 and 20 degree deadrise

Figure C.2 shows that the amount of time between release and impact is again slightly longer than the 4m/s tests, indicating a longer free fall period. The 300Hz vibrations are still visible but due to the larger amount of data points in the same width graph they are now less pronounced.

4.10. g-stickers

During the a few impact experiments, g-stickers were mounted on the carriage. A 50g and 25g sticker were placed to verify the measured accelerations of the accelerometer. While the 25g stickers broke on a few impacts in which the acceleration transcended 25g, the 50g sticker broke on none of the impacts even though the peak accelerations on the accelerometer recorded accelerations over 100g. This lead to the conclusion that the g-stickers did not encounter an acceleration that endured for more than 50ms.

4.11. Conclusions

Reviewing the measured pressures on all the deformable runs it can be concluded that increasing deadrise angle of the wedge during impact leads to a decrease in pressure. This difference can clearly be observed in the side by side comparisons of figure 4.9 and 4.13. [twijfel of dit klopt] Because a system under pressure has the ability to perform work on its surroundings, pressure is a measure of potential energy stored per unit volume. When the pressure results in a rotation of the wedge plate work is done and energy is partly stored (as potential energy in the springs) and part of the energy is lost as heat due to friction. The lost and stored energy results in a lower pressure on the plate.

The acceleration of the wedge plate as a result of the pressure on impact causes a decrease in pressure because the relative velocity between the pressure sensor and the fluid is lowered. From figure 4.4 it becomes clear that rotation of the plates of the wedge starts after the pressure peak in pressure sensor 3. This is due to inertia of the plates. At the peak

of pressure sensor 2 for all impacts, some deformation has already occurred. The slight deformation induced by the initial pressure at pressure sensor 3 already reduces the pressure for pressure sensor 2. The biggest difference is visible at pressure sensor 1. This sensor is placed closest to the chine of the wedge and therefore encounters the largest relative displacement and lowest relative velocity between the sensor and the incoming water.

Chapter 5

Conclusion and recommendations

5.1. Conclusions

The research question of this thesis was: *What is the effect of dynamic deformation of a structure on the maximum pressure at the wedge surface during impact?* This question can now be answered the following way: the dynamic deformation of the structure during impact results in an overall decrease in maximum pressure. From the results in this experiment, the conclusion can be made that larger deformations lead to larger decrease of pressure compared to a rigid structure. For specific combinations of stiffness, velocity and deadrise angle, a dynamic response of the structure is possible. A dynamic response seems to produce a pressure fluctuation, mainly after the initial impact of the fluid.

The deformable wedge impacts can be divided in three independent groups:

1. Constant spring stiffness with linearly increasing impact velocity
2. Constant impact velocity of 4m/s with quadraticly increasing spring stiffness
3. Constant impact velocity of 6m/s with quadraticly increasing spring stiffness

For the first group the spring with stiffness of 3.82N/mm was constant and the impact velocity was set at 2, 4 and 6m/s. At 2m/s an average deformation of 5.9 and 7.8 degrees was measured for 20 and 10 degrees deadrise angle respectively. Doubling the impact velocity to 4m/s resulted in an average deformation of 15.4 and 19.8 degrees for 20 and 10 degrees deadrise angle respectively. Finally, the 6m/s impact velocity resulted in an average deformation of 26.4 and 31.9 degrees for 20 and 10 degrees deadrise angle respectively. Doubling the impact velocity from 2 to 4m/s resulted in an increase in deformation with factor 2.6 and 2.5 for 20 and 10 degrees deadrise angle respectively. Tripling the impact velocity from 2 to 6m/s resulted in an increase of deformation with a factor of 4.5 and 4.1 for 20 and 10 degrees respectively.

In the second group the impact velocity was constant at 4m/s. The spring stiffness was increased quadraticly from 3.82N/mm to 10.58N/mm and finally 29.5N/mm. For 3.82N/mm a deformation of 15.4 and 19.8 degrees was recorded for 20 and 10 degrees deadrise angle respectively. Increasing the spring stiffness with a factor of almost 8 resulted in a decrease of 75% and 72% for 20 and 10 degrees respectively. The decrease of deformation resulted in an increase of pressure of 79% and 126% on pressure sensor 1 for deadrise angle 20 and 10 degrees respectively.

In the final group the impact velocity was constant at 6m/s. The spring stiffness was increased quadraticly from 3.82N/mm to 10.58N/mm and finally 29.5N/mm. For 3.82N/mm a deformation of 26.4 and 31.9 degrees was recorded for 20 and 10 degrees deadrise angle

respectively. Increasing the spring stiffness with a factor of almost 8 resulted in a decrease of 72% and 69% for 20 and 10 degrees respectively. The decrease of deformation resulted in an increase of pressure of 55% and 131% on pressure sensor 1 for deadrise angle 20 and 10 degrees respectively.

Summarizing, the relation between deformation and pressure is tried to put into a formula. To start off, the pressure using Von Karman [24] formula for wedge impacts, this is then scaled to adjust velocity for acceleration during impact. To incorporate the plate rotation on impact the Von Karman formula is multiplied by a function of $\beta_{(t)}$.

$$P_{max} \sim \frac{1}{2} \rho V_0^2 \frac{\pi^2 X^n}{4 \tan^2(\beta_0)} * (f_{(\beta_{(t)}, \dot{\beta}_{(t)})}), \quad (5.1)$$

with V_0 = impact velocity in m/s , X^n = correction on velocity for acceleration of the wedge, β_0 = initial deadrise angle in degrees.

In section 1.1.4, the conclusions of the most important papers were summarized in table 1.1. With the conclusions of our own research we now reflect on the conclusions drawn in earlier research to check if our conclusions match. The original table is copied to present findings in the third column of table 5.1.

Table 5.1: Results comparison with existing literature

Report/paper	Conclusion	Comparison own results
Faltinsen 1997	Maximum bending stress is proportional to the drop velocity.	In our research the stress on the plate was not measured specifically. However, it is clear to see that increasing impact velocity results in higher deformations which could be compared to bending stress in this case. The conclusions of Faltinsen (1997) therefore agree with our results.
Okada & Sumi 2000	Structural response can be estimated by using the average pressure at impact which leads to a new design approach for small impact angles.	The average impact pressure is not analyzed in depth in our research but over all there seems to be a relation between maximum pressure and deformation. A mathematical approach to this relation has yet to be determined.
Faltinsen 2000	The results show that it is misleading from a structural point of view to measure pressures when hydroelasticity is important	Misleading might not be the best choice of words since for our research the goal was specifically to find pressures in deforming situations.
Battley 2009	Increased impact pressure for decreasing panel stiffness did not result in increased panel deflection	Our research data does not agree with Battley 2009. Higher pressures for lower spring stiffness resulted in higher deflection.
Stenius et al. 2011	Where the hydroelastic interaction seems to have a significant effect, it is found both numerically and experimentally that the hydroelastic effects are amplifying the structural responses in comparison to the rigid/quasi-static solutions.	The data in our research shows similar findings. Overall our conclusions agree.
Wang & Guedes Soares 2018	The structural deflection is not affected by the maximum pressure.	Our data suggest that higher impact pressure leads to larger deformation of the wedge. Therefore our conclusions do not agree.
Mai 2020	The hydrodynamic impact loading of the dropped plates is influenced by the elasticity of the system of springs and plates.	Our findings agree with Mai except that we found an effect of deformation on pressure at lower impact velocities as well.

Section 3.1.5 describes the stages of a wedge impact. The first stage agrees with all our results from all sensors. The initial pressure peak on impact does not induce the majority of the total displacement of the plate. The second stage of Faltinsen's explanation does not completely agree with Faltinsen's findings. After initial peak pressure the plate starts

to deflect. For our data no large peak pressures were observed relative to the initial peak pressure on impact.

When closely analyzing what papers agreed with our findings and what papers did not, it was found that the papers that researched elastic deformation of plates did not show large deformation increase for higher peak pressure on impact. The reason for this might be that the initial peak pressure does not seem to contribute the biggest part into the elastic deflection for elastic deformation. In our research it becomes clear that the majority of the deflection happens after the peak pressure. What is clearly visible though is the level of "overshoot". The wedge plates seem to have a larger rotational deformation after a higher peak pressure occurred on impact. After the maximum deformation the wedge plates rotate back to a smaller angle but not all the way back to initial position. This could indicate that the impulse provided by the peak pressure does contribute to the maximum deformation.

The hypothesis for the difference in results lies in the increase in stiffness during bending. When a pinned pinned plate is bending, lateral forces counteract the bending. The larger the deformation in the plate, the larger the stiffness and therefore the force to bend back into its original shape.

Finally It can be concluded that the deformation of the structure leads to an overall decrease of impact pressure. Further research into plastic deformation and the resulting pressure decrease could lead to a better understanding of the dynamics of impacts on semi rigid structures. Improving our knowledge of this complex situation could help engineers design ships more efficiently. Less steel could be used in the structure of the ship which would lead to lower production costs and lower emissions for the production of a single ship.

5.2. Recommendations

Overall the experiment and its results were successful. However, some recommendations to the setup and execution of the experiment can be made. They are summed up below:

5.2.1. Recommendations for improved scientific results

- Redesign the spine of the wedge so the deadrise angle can be set to 5, 15 and 25 degrees.

During the experiment the accelerations during 0 degree deadrise exceeded the measuring limit of the sensors. Increasing all increments with 5 degrees will result in larger data set. Also, a direct comparison can be made with a previous rigid wedge with sharp keel. This comparison will help analyze the differences between the wedges with higher certainty.

- Rebuild the carriage for better fit inside the tower.

This will decrease data variation for all sensors.

- Use accelerometers with larger range so 0 degree deadrise angles can be tested without damaging the accelerometers

A 0 degree impact is hard to compare with wedges with a deadrise. Among other effects, there is a possibility an air cushion effect will appear. Allowing this effect to occur could change deflection pressure and acceleration results.

- reinforce the tank to reduce vibrations

Less vibrating parts in the experiment setup is desirable since it will result in a better representation (less noise) of the dynamics at play during impacts.

- Increase the length of the spine so a longer distance trough water can be traveled before the carriage impacts the end of the end of the track

A longer distance traveled trough the fluid might result in larger deceleration of the wedge before running into the emergency bumpers at the end of the tower tracks.

- Redesign the velocity measurement slots such that the velocity post-impact can also be measured

The acceleration during impact might be interesting to record and compare for impacts with and without deformation.

- Replace the potentiometers for deformation measurement and replace with a high resolution, high speed camera to analyse deformation of the wedge on impact to rule out damping factors from the potentiometers

The potentiometers turned out to have a dampening effect on the motion of the wedge plates. Elimination this dampening effect could show better results, especially in low impact velocity experiments.

- Increase plate stiffness

The wedge plates deformed slightly during the run of the entire experiment. Increasing plate stiffness should help prevent this, including possible side effects from this deformation.

- Redesign an experiment in which plastic deformation is measured in stead of rotational deformation.

The current research proved that rotational deformation resulted in decrease of pressure compared to a rigid wedge impact. To better simulate a plate section of a hull of a ship it is interesting to research the pressure response on elastic deformation.

- Review and improve R-ratio calculations

It seems as if the expected R-ratio's did not agree with the experiment results. Hence it would be of interest to improve the formula for this situation to better estimate the dynamics on impact.

5.2.2. Recommendations for improved comfort

- Use a rope with larger diagonal for more comfortable resetting of wedge
- Create an easily rolling carriage for the electromagnet to set it at varying release heights
- Use a clamp from sailing to quickly secure the rope that hoists the wedge and carriage

Bibliography

- [1] W. Amina et al. “Analysis of wave slam induced hull vibrations using continuous wavelet transforms”. In: *Ocean Engineering* 58 (2013), pp. 154–166. ISSN: 00298018. DOI: [10.1016/j.oceaneng.2012.10.011](https://doi.org/10.1016/j.oceaneng.2012.10.011).
- [2] M A Battley et al. *EFFECTS OF PANEL STIFFNESS ON SLAMMING RESPONSES OF COMPOSITE HULL PANELS*. 2009.
- [3] A Bereznitski. *SLAMMING: THE ROLE OF HYDROELASTICITY*. 2001, pp. 333–351.
- [4] R. Bishop and W. Price. *Hydroelasticity of Ships*. Cambridge University Press, 1979.
- [5] R L Bisplinghoff and C S Doherty. *SOME STUDIES OF THE IMPACT OF VEE WEDGES ON A WATER SURFACE*. 1952.
- [6] R W Bos and P R Wellens. “Fluid-structure interaction between a pendulum and monochromatic waves”. In: *Journal of Fluids and Structures* 100 (2021), p. 103191. DOI: [10.4121/13187594](https://doi.org/10.4121/13187594). URL: www.elsevier.com/locate/jfs.
- [7] R. W. Bos and P. R. Wellens. “Fluid structure interaction between a pendulum and focused breaking waves”. In: *Physics of Fluids* 33 (6 June 2021). ISSN: 10897666. DOI: [10.1063/5.0054426](https://doi.org/10.1063/5.0054426).
- [8] Sheng-Lun Chuang. *Experiments on Slamming of Wedge-Shaped Bodies'*. 1967. URL: <http://onepetro.org/JSR/article-pdf/11/03/190/2235620/sname-jsr-1967-11-3-190.pdf/1>.
- [9] Martin Van Der Eijk. *Experimental and numerical 2D wedge entry in water with entrained air*. 2022. URL: <https://www.researchgate.net/publication/359921552>.
- [10] Martin Van Der Eijk and Peter Wellens. *Experimental and numerical comparison of 2D buoyant falling emerging wedge*. 2022. URL: www.elsevier.com/locate/jfs.
- [11] O. M. Faltinsen. *Hydrodynamics of marine and offshore structures*. Jan. 2015. DOI: [10.1016/S1001-6058\(14\)60092-5](https://doi.org/10.1016/S1001-6058(14)60092-5).
- [12] O. M. Faltinsen. *The Effect of Hydroelasticity on Ship Slamming*. 1997, pp. 575–591.
- [13] O. M. Faltinsen, Maurizio Landrini, and Marilena Greco. *Slamming in marine applications*. 2004, pp. 187–217.
- [14] Odd M Faltinsen. *Hydroelastic slamming*. 2000.
- [15] Odd M Faltinsen, Maurizio Landrini, and Marilena Greco. *Slamming in marine applications*. 2004, pp. 187–217.
- [16] L E Fraenkel and G Keady. *On the entry of a wedge into water: The thin wedge and an all-purpose boundary-layer equation*. 2004, pp. 219–252.
- [17] *Free Fall with Air Resistance Calculator*. URL: <https://www.omnicalculator.com/physics/free-fall-air-resistance?advanced=1&c=EUR&v=g:9.807!mps2,ro:1.2041!kgm3,m:8!kg,A:52307!mm2,vel:6!ms,c:1.28>.

- [18] R. C. Hibbeler. *Engineering Mechanics: Statics*. Pearson, 2015. ISBN: 978-0133918922.
- [19] Bas Hofland, Mirek Kaminski, and Guido Wolters. "LARGE SCALE WAVE IMPACTS ON A VERTICAL WALL". In: *Coastal Engineering Proceedings* 1 (32 Feb. 2011), p. 15. ISSN: 0589-087X. DOI: [10.9753/icce.v32.structures.15](https://doi.org/10.9753/icce.v32.structures.15).
- [20] S. D. Howison, J. R. Ockendon, and S. K. Wilson. "Incompressible water-entry problems at small deadrise angles". In: *Journal of Fluid Mechanics* 222 (1991), pp. 215–230. ISSN: 14697645. DOI: [10.1017/S0022112091001076](https://doi.org/10.1017/S0022112091001076).
- [21] F. J. Huera-Huarte, D. Jeon, and M. Gharib. "Experimental investigation of water slamming loads on panels". In: *Ocean Engineering* 38 (11-12 Aug. 2011), pp. 1347–1355. ISSN: 00298018. DOI: [10.1016/j.oceaneng.2011.06.004](https://doi.org/10.1016/j.oceaneng.2011.06.004).
- [22] Raouf A. Ibrahim. *Assessment of breaking waves and liquid sloshing impact*. May 2020. DOI: [10.1007/s11071-020-05605-7](https://doi.org/10.1007/s11071-020-05605-7).
- [23] Norman Jones. "SLAMMING DAMAGE." In: *Journal of Ship Research* 17 (2 1973), pp. 80–86. ISSN: 00224502. DOI: [10.5957/jsr.1973.17.2.80](https://doi.org/10.5957/jsr.1973.17.2.80).
- [24] Von Karman. "The impact on seaplane floats during landing - CaltechAUTHORS". In: (1928). URL: <https://authors.library.caltech.edu/47898/>.
- [25] JA Keuning, S Toxopeus, and J Pinkster. "The effect of bowshape on the seakeeping performance of a fast monohull". Undefined/Unknown. In: *The 6th international conference on fast sea transportation, September 4-6*. null ; Conference date: 04-09-2001 Through 06-09-2001. Royal Institute of Naval Architects, 2001, pp. 197–212. ISBN: 0-903055-70-8.
- [26] A A Korobkin and V V Pukhnachov. *INITIAL STAGE OF WATER IMPACT*. 1988, pp. 159–85.
- [27] Alexander Korobkin. *ELASTIC RESPONSE OF CATAMARAN WETDECK TO LIQUID IMPACT*. 1998, pp. 687–714.
- [28] S.H. Kwon et al. *The proceedings of the Thirteenth (2003) International Offshore and Polar Engineering Conference : ISOPE : Honolulu, Hawaii, USA, May 25-30, 2003*. International Society of Offshore and Polar Engineers, 2003. ISBN: 1880653605.
- [29] Sun Hong Kwon, Young Jun Yang, and Hee Sung Lee. "Experimental and Numerical Study on Slamming Impact". In: *Journal of Ocean Engineering and Technology* 27 (1 Feb. 2013), pp. 1–8. ISSN: 1225-0767. DOI: [10.5574/ksae.2013.27.1.001](https://doi.org/10.5574/ksae.2013.27.1.001).
- [30] C. Lugni, M. Brocchini, and O. M. Faltinsen. "Wave impact loads: The role of the flip-through". In: vol. 18. American Institute of Physics Inc., 2006. DOI: [10.1063/1.2399077](https://doi.org/10.1063/1.2399077).
- [31] Hanbing Luo, Hui Wang, and C. Guedes Soares. "Numerical and experimental study of hydrodynamic impact and elastic response of one free-drop wedge with stiffened panels". In: *Ocean Engineering* 40 (Feb. 2012), pp. 1–14. ISSN: 00298018. DOI: [10.1016/j.oceaneng.2011.11.004](https://doi.org/10.1016/j.oceaneng.2011.11.004).
- [32] A G Mackie. *THE WATER ENTRY PROBLEM*. 1968. URL: <https://academic.oup.com/qjmam/article/22/1/1/1942341>.
- [33] T. Mai et al. "Hydroelasticity effects on water-structure impacts". In: *Experiments in Fluids* 61 (9 Sept. 2020). ISSN: 14321114. DOI: [10.1007/s00348-020-03024-3](https://doi.org/10.1007/s00348-020-03024-3).

- [34] Adolfo Maron and Geert Kapsenberg. “Design of a ship model for hydro-elastic experiments in waves”. In: *International Journal of Naval Architecture and Ocean Engineering* 6 (4 Dec. 2014), pp. 1130–1147. ISSN: 20926790. DOI: [10.2478/IJNAOE-2013-0235](https://doi.org/10.2478/IJNAOE-2013-0235).
- [35] Dr. M. Moore. *Introducing pre-impact air-cushioning effects into the Wagner model of impact theory*. Feb. 2021. URL: <https://www.youtube.com/watch?v=n7M2f0ektL4>.
- [36] NASA. *Shape Effects on Drag*. URL: <https://www.grc.nasa.gov/www/k-12/VirtualAero/BottleRocket/airplane/shaped.html>.
- [37] M. Nikfarjam et al. “Investigation of wedge water-entry under symmetric impact loads by experimental tests”. In: *Latin American Journal of Solids and Structures* 14 (5 2017), pp. 861–873. ISSN: 16797825. DOI: [10.1590/1679-78253315](https://doi.org/10.1590/1679-78253315).
- [38] Shinzo Okada and Yoichi Sumi. *Experimental Study on the Maximum Pressure and the Duration Time of the Horizontal Water Impact of Flat Plate*. 1995.
- [39] Shinzo Okada and Yoichi Sumi. *On the water impact and elastic response of a flat plate at small impact angles*. 2000.
- [40] Zhao R., Faltinsen O., and Aarsnes J. *Twenty-First Symposium on Naval Hydrodynamics - National Research Council, Division on Engineering and Physical Sciences, Commission on Physical Sciences, Mathematics, and Applications, Naval Studies Board*. 1996. URL: https://books.google.nl/books?hl=nl&lr=&id=q1PNZk1SKFMC&oi=fnd&pg=PA408&dq=zhao+%2B+faltinsen&ots=o5Q4Lv4N8n&sig=XX_470UcknpTSTYtuP1uDPJcQzk&redir_esc=y#v=onepage&q=zhao%20%2B%20faltinsen&f=false.
- [41] TMP Staff. *Ukrainian Cargo Ship Breaks and Sinks In Black Sea*. Jan. 2021. URL: <https://themaritimepost.com/2021/01/video-ukrainian-cargo-ship-breaks-and-sinks-in-black-sea/>.
- [42] I Stenius, Mark Battley, and Tom Allen. *Hydroelastic Effects in Slamming Loaded Panels Aspects of advanced marine vehicles design. View project Numerical Simulations-Computational Fluid Dynamics View project*. 2011. URL: <https://www.researchgate.net/publication/267556342>.
- [43] I Stenius, A Rosén, and J Kutteneuler. *Explicit FE-modelling of fluid-structure interaction in hull-water impacts*. 2006, pp. 103–121.
- [44] I Stenius, A Rosén, and J Kutteneuler. *Explicit FE-modelling of hydroelasticity in panel-water impacts*. 2007, pp. 111–127. URL: www.msy.se.
- [45] Van Der Zee T. *The Influence of Aeration and Deadrise Angle on Impact*. 2022.
- [46] T. Tveitnes, A. C. Fairlie-Clarke, and K. Varyani. “An experimental investigation into the constant velocity water entry of wedge-shaped sections”. In: *Ocean Engineering* 35 (14-15 Oct. 2008), pp. 1463–1478. ISSN: 00298018. DOI: [10.1016/j.oceaneng.2008.06.012](https://doi.org/10.1016/j.oceaneng.2008.06.012).
- [47] Carl Magnus Ullman. *Human impact exposure on fast boats*. URL: <https://ullmandynamics.com/wp-content/uploads/2015/08/Human-Impact-Exposure-on-Fast-Boats.pdf>.
- [48] J H G Verhagen. *Journal of SHIP RESEARCH The Impact of a Flat Plate on a Water Surface*. 1967. URL: <http://onepetro.org/JSR/article-pdf/11/04/211/2235646/sname-jsr-1967-11-4-211.pdf/1>.

- [49] Herbert Wagner. “Über Stoß- und Gleitvorgänge an der Oberfläche von Flüssigkeiten”. In: *ZAMM - Journal of Applied Mathematics and Mechanics / Zeitschrift für Angewandte Mathematik und Mechanik* 12 (4 Jan. 1932), pp. 193–215. ISSN: 1521-4001. DOI: [10.1002/ZAMM.19320120402](https://doi.org/10.1002/ZAMM.19320120402). URL: <https://onlinelibrary.wiley.com/doi/full/10.1002/zamm.19320120402>.
- [50] J Wang, O M Faltinsen, and C Lugni. *Unsteady hydrodynamic forces of solid objects vertically entering the water surface*. 2019.
- [51] Shan Wang and C. Guedes Soares. “Simplified approach to dynamic responses of elastic wedges impacting with water”. In: *Ocean Engineering* 150 (Feb. 2018), pp. 81–93. ISSN: 00298018. DOI: [10.1016/j.oceaneng.2017.12.043](https://doi.org/10.1016/j.oceaneng.2017.12.043).
- [52] Y. Yamamoto et al. “STRUCTURAL DAMAGE ANALYSIS OF A FAST SHIP DUE TO BOW FLARE SLAMMING.” In: *International Shipbuilding Progress* 32 (369 1985), pp. 124–136. ISSN: 0020868X. DOI: [10.3233/isp-1985-3236902](https://doi.org/10.3233/isp-1985-3236902).
- [53] Zhao R. Zhao and O. M. Faltinsen. “Water entry of two-dimensional bodies”. In: *Journal of Fluid Mechanics* 246 (4 1993), pp. 593–612. ISSN: 14697645. DOI: [10.1017/S002211209300028X](https://doi.org/10.1017/S002211209300028X).

Appendix A

Appendix A

A.1. Calculations

A.1.1. Accelerations on impact

$$v^2 = u^2 + 2as \quad (\text{A.1})$$

v = final velocity
 u = initial velocity
 a = acceleration
 s = displacement

$$0^2 = 7^2 + 2 * a * 0.2 \quad (\text{A.2})$$

$$\frac{-7^2}{2 * 0.2 * 9.81} = 12.5g \quad (\text{A.3})$$

$$\frac{-6.3^2}{2 * 0.05 * 9.81} = 40g \quad (\text{A.4})$$

A.1.2. Okada empirical formula for flat plate maximum pressure

$$P_{max} = \frac{M_w * K_m * V_0}{(B * \Delta t)} \quad (\text{A.5})$$

$$M_w = \frac{\rho_i}{8} * \rho_w * B^2 \quad (\text{A.6})$$

$$\Delta t = 6.94x10^{-3} * \left(\frac{B}{V_0}\right)^{0.673} \quad (\text{A.7})$$

M_w = added mass in kg
 M = mass wedge in kg
 K_m = dimensionless fraction
 Δt = impact duration in seconds
 B = breadth of the plate in m
 V_0 = impact velocity in m/s

Appendix B

Appendix B

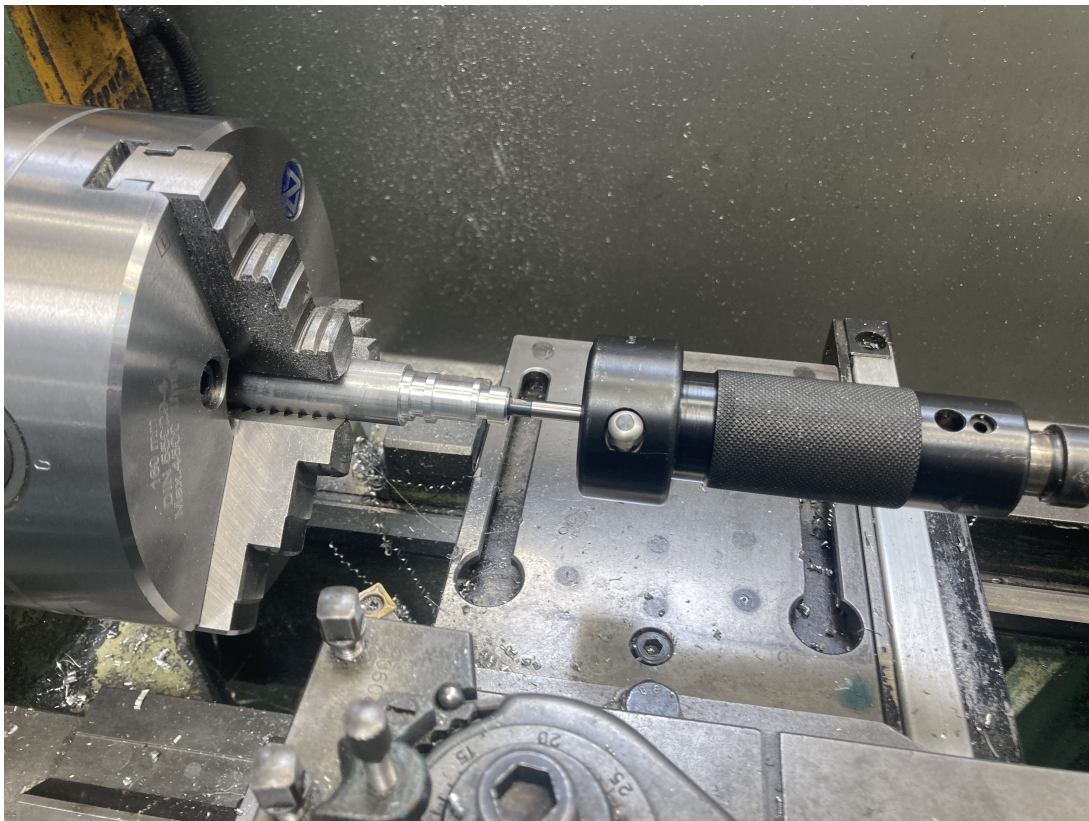


Figure B.1: Using a special tool to make sure tapping the thread in the part is exactly centered.



Figure B.2: Difference in outer diameter with thread cutting tool inside part.

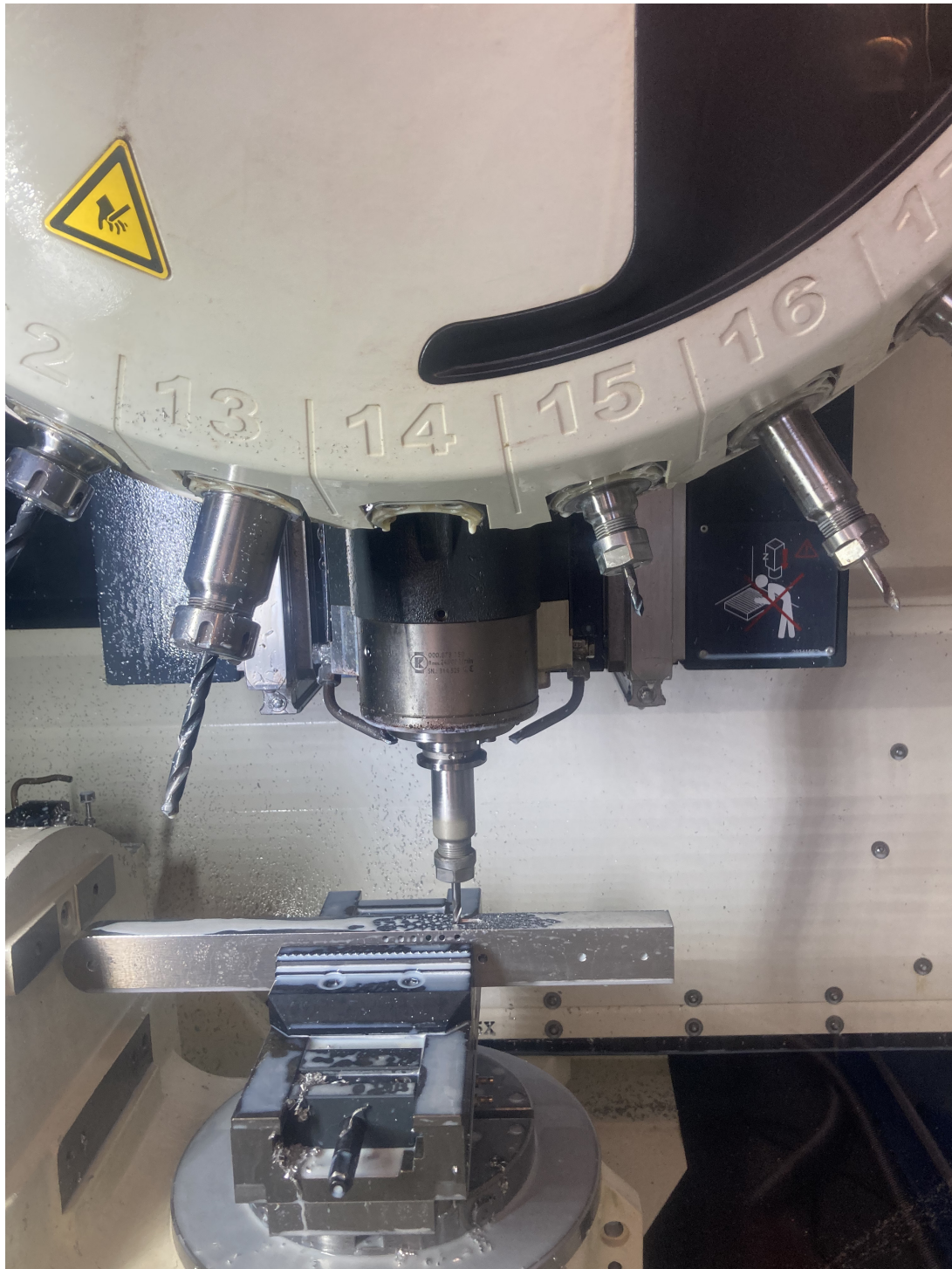


Figure B.3: CNC milling of spine in progress



Figure B.4: Four holes reamed and the other 4 still in their original shape in the cylinder of the shock absorber

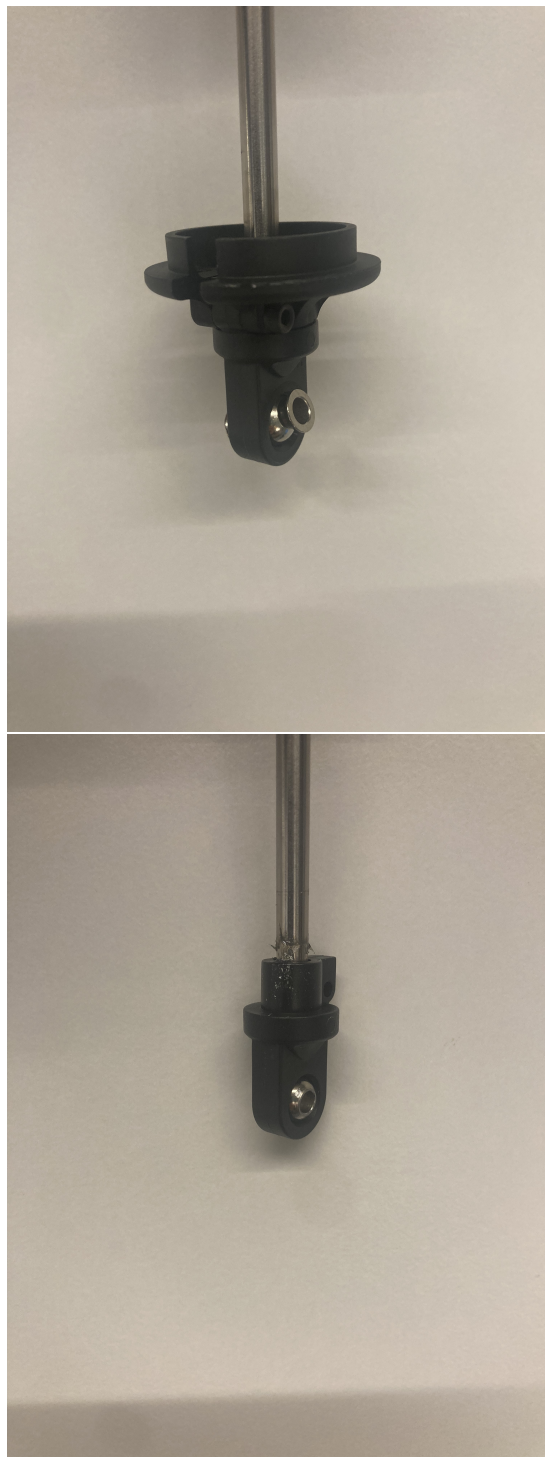


Figure B.5: Before and after of ball bearing joint.

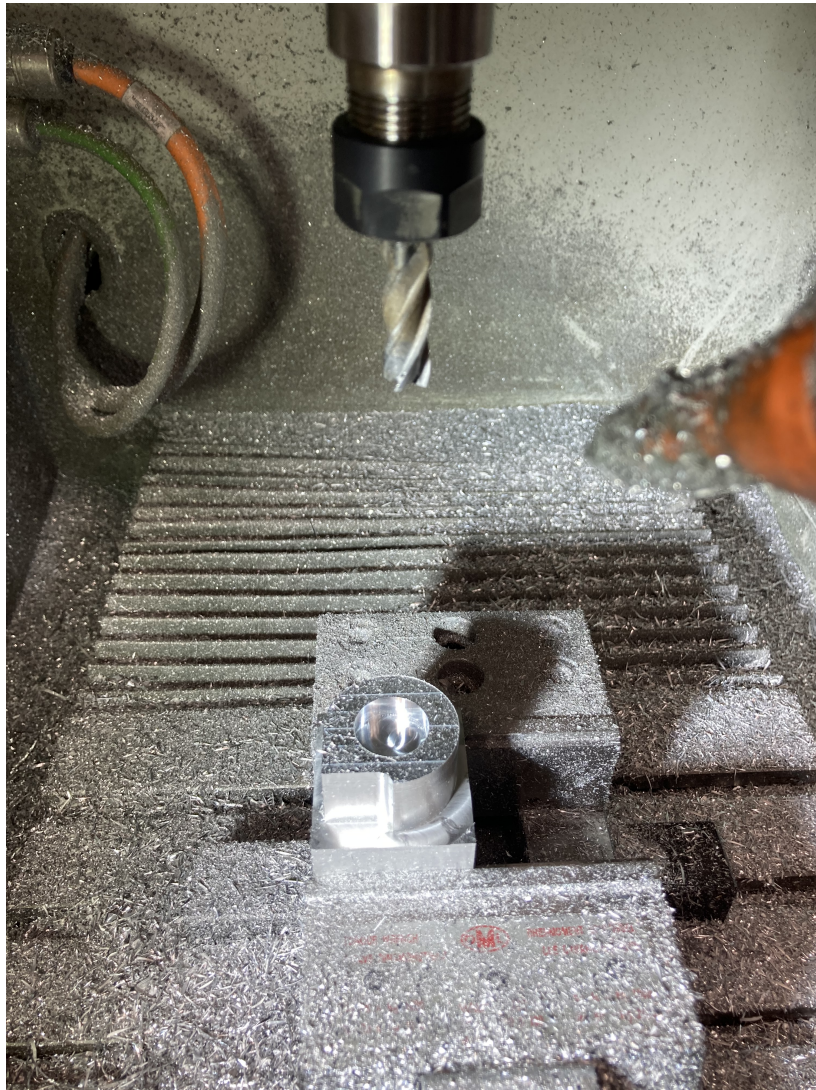


Figure B.6: Milling of hinge part



Figure B.7: Cutting of hinge part

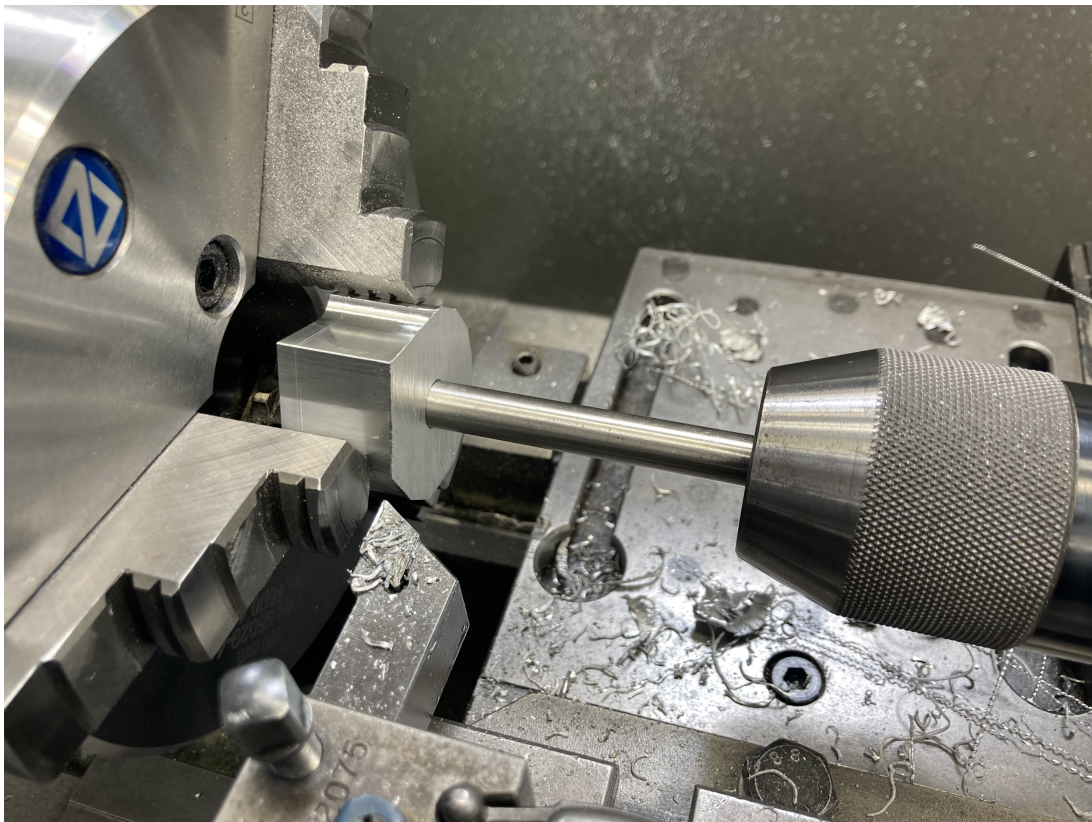


Figure B.8: Centering of hinge part to prepare for milling

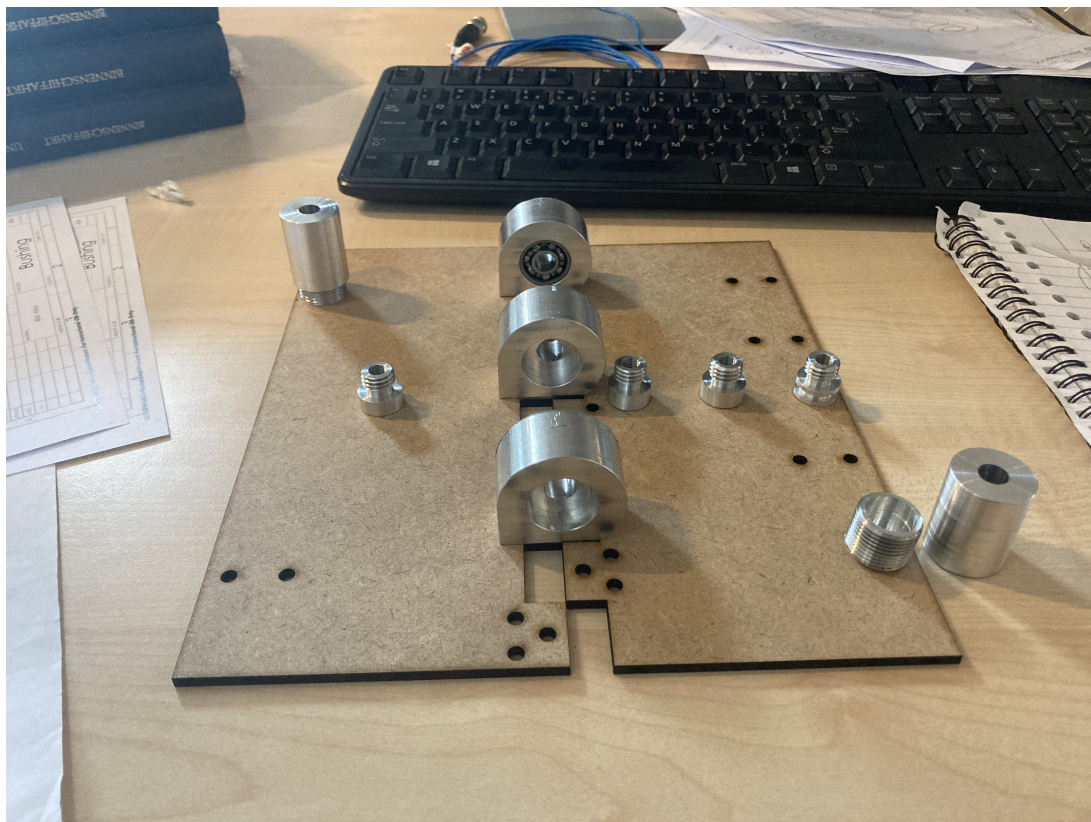


Figure B.9: Wedge plates cut out of wood with laser to check dimensions and placing of sensors

Appendix C

Appendix C - Experiment graphs

C.1. Acceleration

C.1.1. Free

fall

rigid

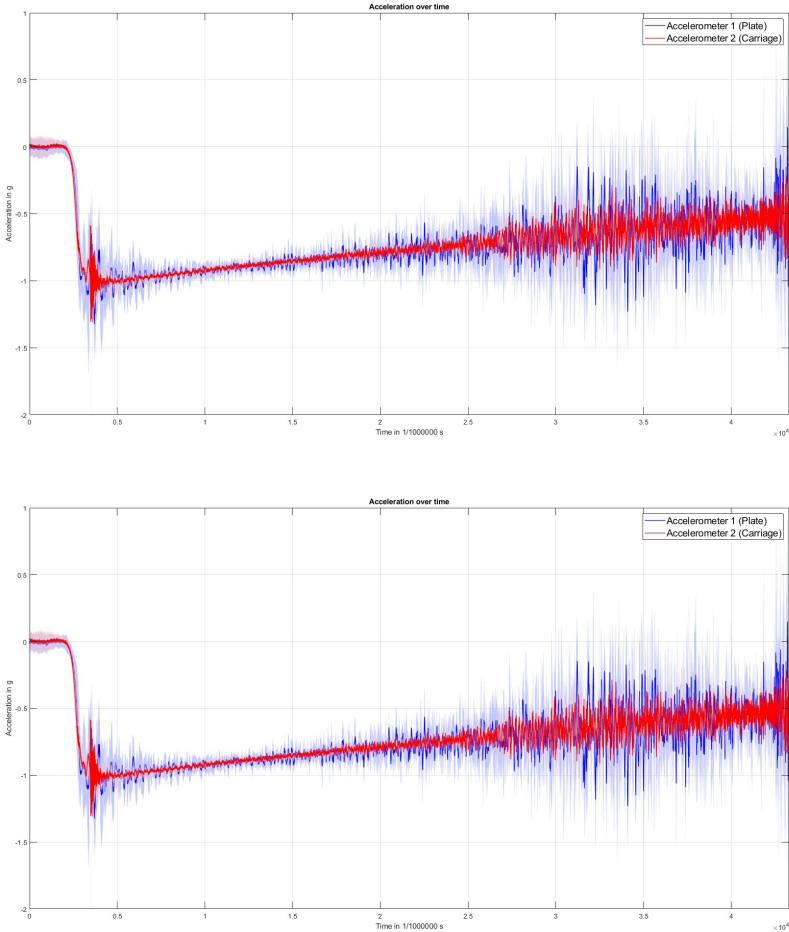


Figure C.1: Rigid, 4m/s, 10(top) and 20(bottom) degree deadrise acceleration during free fall

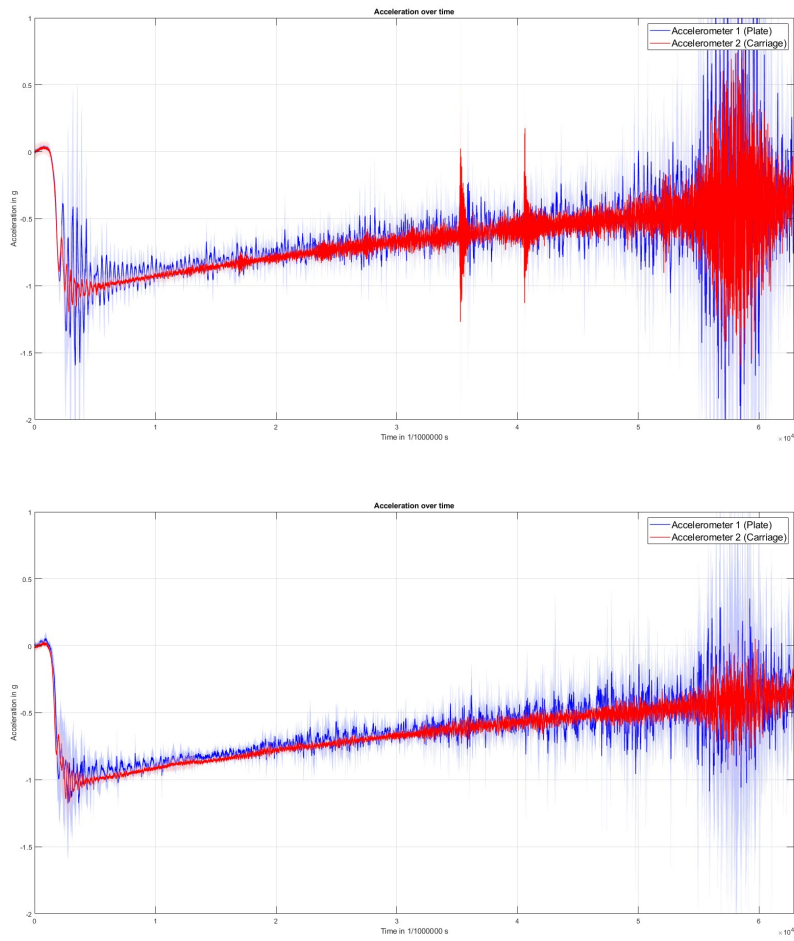
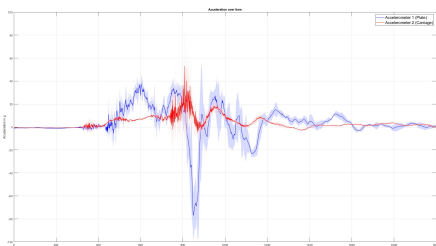


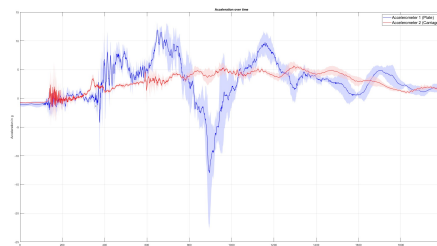
Figure C.2: Rigid, 6m/s, 10(top) and 20(bottom) degree deadrise acceleration during free fall

C.1.2. Impact

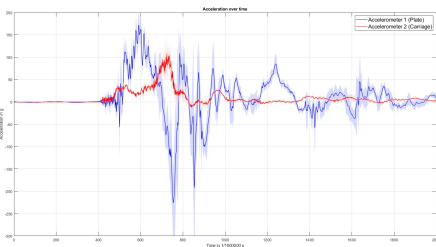
rigid



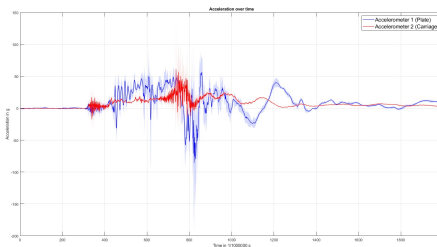
(a) 2m/s, 10 degrees



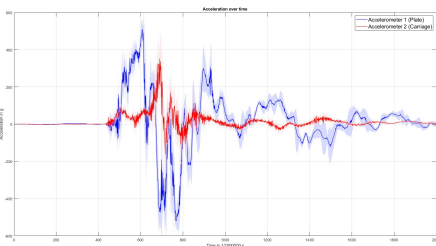
(b) 2m/s, 20 degrees



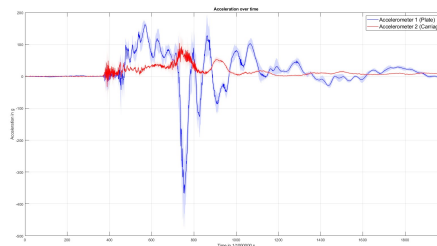
(c) 4m/s, 10 degrees



(d) 4m/s, 20 degrees



(e) 6m/s, 10 degrees



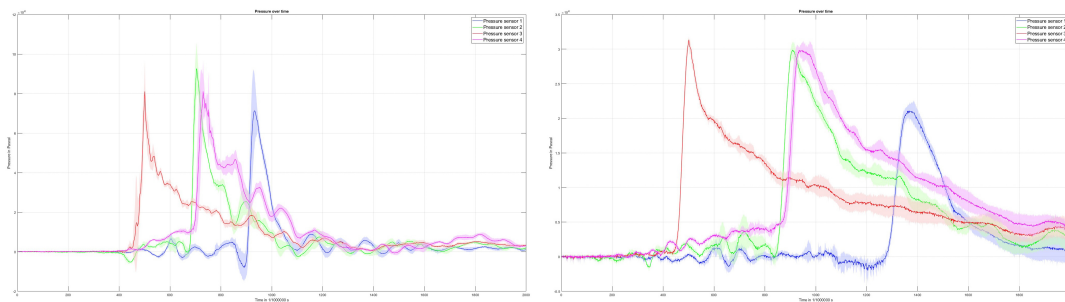
(f) 6m/s, 20 degrees

Figure C.3: Overview of all accelerometer graphs from the impact of the rigid tests

C.2. Pressure

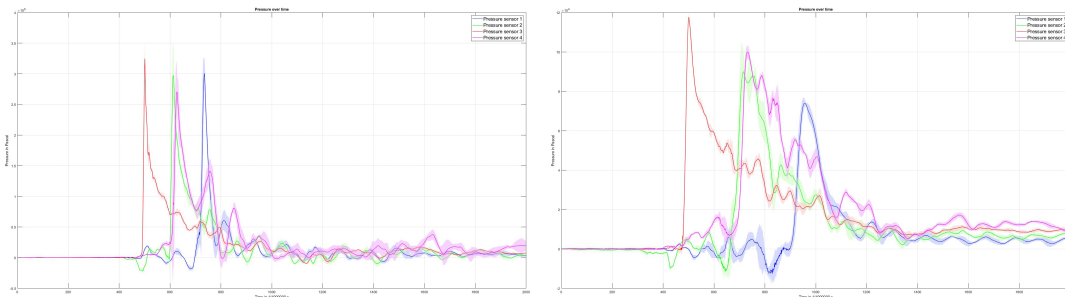
C.2.1. Impact

rigid



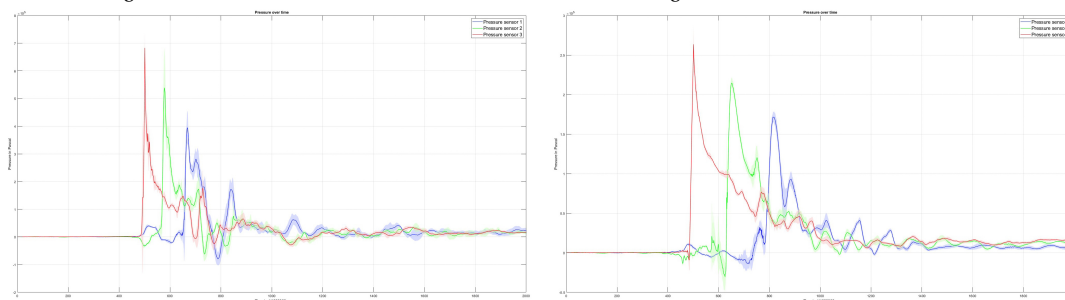
(a) 2m/s, 10 degrees

(b) 2m/s, 20 degrees



(c) 4m/s, 10 degrees

(d) 4m/s, 20 degrees



(e) 6m/s, 10 degrees

(f) 6m/s, 20 degrees

Figure C.4: Overview of all pressure graphs from the rigid tests

C.3. Deformation/Pressure

C.3.1. Post

impact

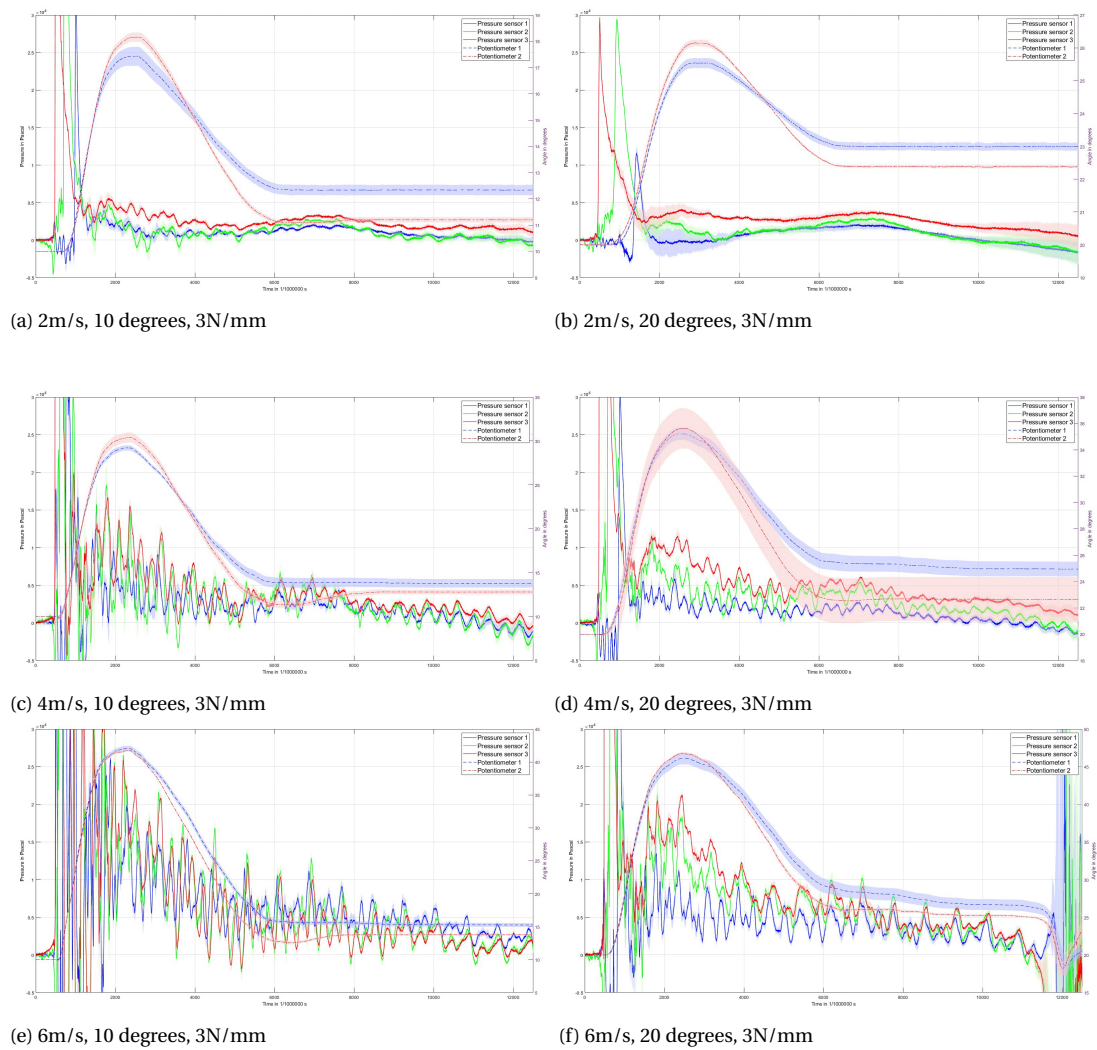
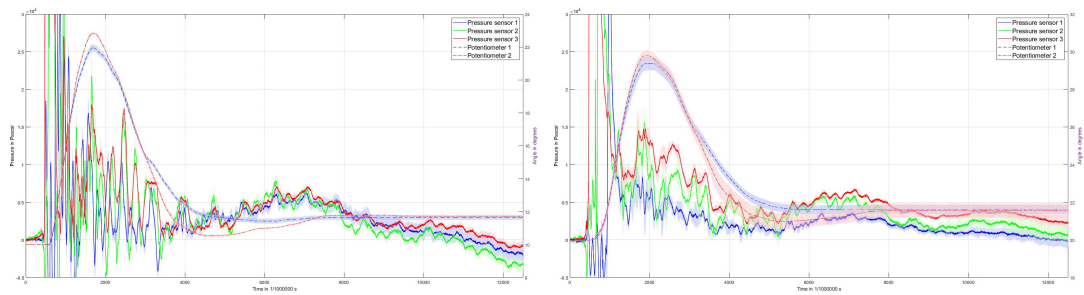
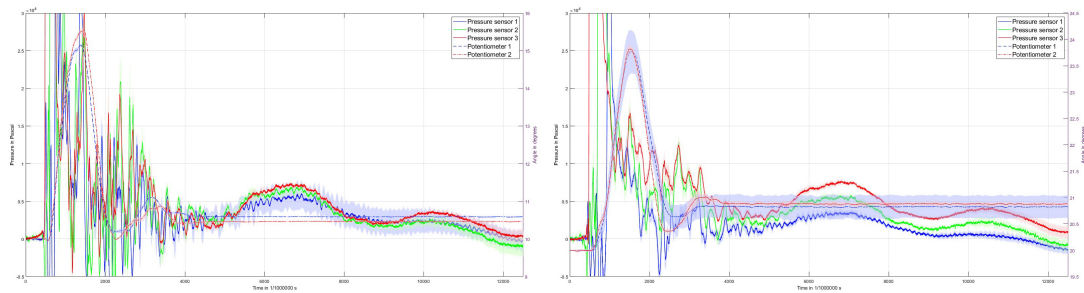


Figure C.5: Overview of all pressure and deformation graphs post for post impact analysis with the 3.82N/mm spring.



(a) 2m/s, 10 degrees, 10N/mm

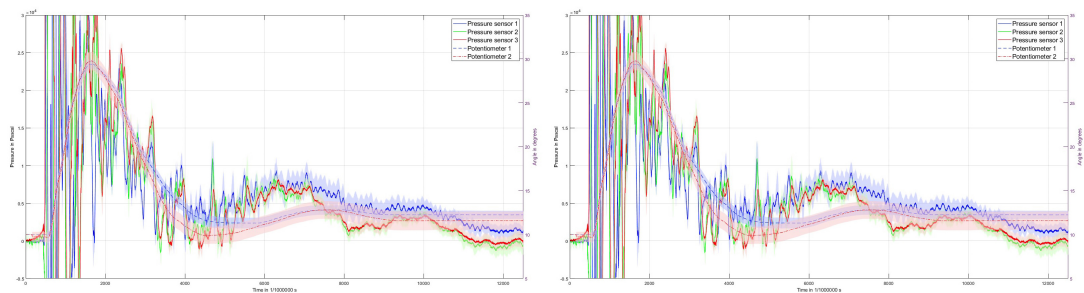
(b) 2m/s, 20 degrees, 10N/mm



(c) 4m/s, 10 degrees, 3N/mm

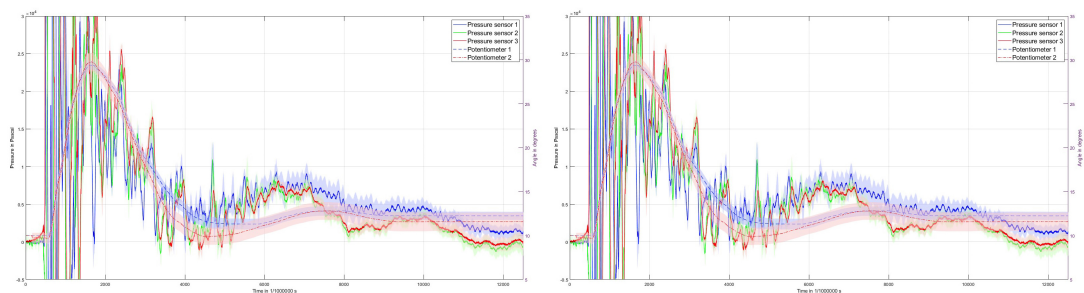
(d) 4m/s, 20 degrees, 3N/mm

Figure C.6: Overview of all pressure and deformation graphs post for post impact analysis with the remaining 4m/s impacts for 10.58 and 29.5N/mm spring.



(a) 2m/s, 10 degrees, 10N/mm

(b) 2m/s, 20 degrees, 10N/mm



(c) 4m/s, 10 degrees, 3N/mm

(d) 4m/s, 20 degrees, 3N/mm

Figure C.7: Overview of all pressure and deformation graphs post for post impact analysis with the remaining 6m/s impacts for 10.58 and 29.5N/mm spring.